Hillslope Scale Hydrologic Spatial Patterns in a Patchy Ponderosa Pine Landscape: Insights from Distributed Hydrologic Modeling

by

Taufique Hasan Mahmood

A Dissertation Presented in Partial Fulfillment
Of the Requirements for the Degree
Doctor of Philosophy

Approved April 2012 by the
Graduate Supervisory Committee:

Enrique R. Vivoni, Chair
Kelin X. Whipple
Everett Shock
Arjun M. Heimsath
Benjamin Ruddell

ARIZONA STATE UNIVERSITY

May 2012

ABSTRACT

Ponderosa pine forests are a dominant land cover type in semiarid montane areas. Water supplies in major rivers of the southwestern United States depend on ponderosa pine forests since these ecosystems: (1) receive a significant amount of rainfall and snowfall, (2) intercept precipitation and transpire water, and (3) indirectly influence runoff by impacting the infiltration rate. However, the hydrologic patterns in these ecosystems with strong seasonality are poorly understood. In this study, we used a distributed hydrologic model evaluated against field observations to improve our understandings on spatial controls of hydrologic patterns, appropriate model resolution to simulate ponderosa pine ecosystems and hydrologic responses in the context of contrasting winter to summer transitions. Our modeling effort is focused on the hydrologic responses during the North American Monsoon (NAM), winter and spring periods.

In Chapter 2, we utilized a distributed model explore the spatial controls on simulated soil moisture and temporal evolution of these spatial controls as a function of seasonal wetness. Our findings indicate that vegetation and topographic curvature are spatial controls. Vegetation controlled patterns during dry summer period switch to fine-scale terrain curvature controlled patterns during persistently wet NAM period. Thus, a climatic threshold involving rainfall and weather conditions during the NAM is identified when high rainfall amount (such as 146 mm rain in August, 1997) activates lateral flux of soil moisture and

frequent cloudy cover (such as 42% cloud cover during daytime of August, 1997) lowers evapotranspiration.

In Chapter 3, we investigate the impacts of model coarsening on simulated soil moisture patterns during the NAM. Results indicate that model aggregation quickly eradicates curvature features and its spatial control on hydrologic patterns. A threshold resolution of ~10% of the original terrain is identified through analyses of homogeneity indices, correlation coefficients and spatial errors beyond which the fidelity of simulated soil moisture is no longer reliable. Based on spatial error analyses, we detected that the concave areas (~28% of hillslope) are very sensitive to model coarsening and root mean square error (RMSE) is higher than residual soil moisture content (~0.07 m^3/m^3 soil moisture) for concave areas. Thus, concave areas need to be sampled for capturing appropriate hillslope response for this hillslope.

In Chapter 4, we investigate the impacts of contrasting winter to summer transitions on hillslope hydrologic responses. We use a distributed hydrologic model to generate a consistent set of high-resolution hydrologic estimates. Our model is evaluated against the snow depth, soil moisture and runoff observations over two water years yielding reliable spatial distributions during the winter to summer transitions. We find that a wet winter followed by a dry summer promotes evapotranspiration losses (spatial averaged ~193 mm spring ET and ~ 600 mm summer ET) that dry the soil and disconnect lateral fluxes in the forested hillslope, leading to soil moisture patterns resembling vegetation patches. Conversely, a dry winter prior to a wet summer results in soil moisture increases

due to high rainfall and low ET during the spring (spatially averaged 78 mm ET and 232 mm rainfall) and summer period (spatially averaged 147 mm ET and 247 mm rainfall) which promote lateral connectivity and soil moisture patterns with the signature of terrain curvature. An opposing temporal switch between infiltration and saturation excess runoff is also identified. These contrasting responses indicate that the inverse relation has significant consequences on hillslope water availability and its spatial distribution with implications on other ecohydrological processes including vegetation phenology, groundwater recharge and geomorphic development.

Results from this work have implications on the design of hillslope experiments, the resolution of hillslope scale models, and the prediction of hydrologic conditions in ponderosa pine ecosystems. In addition, our findings can be used to select future hillslope sites for detailed ecohydrological investigations. Further, the proposed methodology can be useful for predicting responses to climate and land cover changes that are anticipated for the southwestern United States.

ACKNOWLEDGEMENT

First of all, I would like to thank almighty God for the successful completion of the dissertation. This dissertation is a compilation and culmination of research works collaborated with faculties, scientists, graduate students and different agencies whose helps and supports are very useful. First off, I would like to thank my advisor Dr. Enrique R. Vivoni for his inspiration, cordial and perceptive guidance and constructive criticism and suggestions during my research work in doctoral program. I would also like to thank my committee members: Professor Kelin Whipple, Professor Arjun Heimsath, Professor Everett Shock and Dr. Benjamin Ruddell for their advices and suggestions. Special thanks to SAHRA (Sustainability of semi-Arid Hydrology and Riparian Areas), Jemez-Santa Catalina CZO (Critical Zone Observatory) for funding my research. Likewise, I would also like to thank scientists of Los Alamos National Laboratory (LANL), particularly, Dr. Everett Springer, Dr. David Moulton, Dr. Marvin Grad and Dr. Gary Langhorst for providing valuable hydrometeorological and land surface dataset.

I would like to thank my wife Nessa, my late father A.S.M. Mahbubur Rahman and my mother Quemrunnessa for their support, esteem cooperation and sacrifice during my study. Finally, I would like to thank my fellow group members and graduate students of New Mexico Tech and Arizona State University for their help at multiple stages of my research.

TABLE OF CONTENTS

Page

CHAPTER Page

LIST OF FIGURES

Figure Page

Figure Page

Figure Page

Figure Page

LIST OF TABLES

Table Page

Table Page

Table Page

1. Introduction

1.1. Motivation

Ponderosa pine forest is an important ecosystem in the semiarid southwestern U.S. (New Mexico, Colorado, Arizona, Nevada and Utah), due to its extensive spatial occurrence at mid altitude elevation both in the form of continuous and patchy park-like forest and its spatiotemporal dynamics due to deforestation [e.g. *Wallace et al.,* 1997], forest regeneration [e.g. *Balmat, 2004*], and long term forest encroachment [e.g. *Coop and Jivnish,* 2007]. It receives significant amount rainfall and snowfall and exerts strong controls on hydrology via interception [e.g. *Crockford and Richardson,* 2000; *Hedstrom and Pomeroy,* 1998], unloading and evaporation of intercepted precipitation, strong seasonal transpiration, indirectly influencing infiltration by controlling soil moisture seasonality, controlling macro-pore induced preferential lateral transport [e.g. *Newman et al.,* 1998; *Newman et al.,* 2004], and controlling evapotranspiration on neighboring grassland areas by shading on it. These processes are very important in semiarid landscapes covered by ponderosa pine forest, yet are poorly understood due to lack of detailed studies.

The hydrologic processes in ponderosa pine ecosystems are interconnected through soil moisture such that some processes (e.g. evapotranspiration) depletes moisture from soil [e.g. *Brandes and Wilcox*, 2000] and other processes (e.g. infiltration of precipitation and snow melt water) recharge moisture to soil [e.g. *Wilcox et al.,*1997]. As a result, the soil moisture pattern and seasonality encode a detailed story about the competition between these vertical and horizontal fluxes.

Thus, a detailed decoding of spatiotemporal soil moisture pattern can be useful to understand the hydrologic processes. Seasonality in weather condition is also another major driver controlling the soil moisture pattern. The major seasons impacting soil moisture dynamics are the North American Monsoon (NAM), winter, and spring (winter-summer transitional period) periods. The NAM is a summer (July-September) high energy season that brings intense, short duration localized convective storms to the southwest U.S. affecting hydrologic processes in the semiarid region. On the other hand, the winter season is a low energy season causing significant snow fall with subsequent snowmelt and rainfall impacting hydrologic processes. In addition to NAM and winter, there is a spring period (transitional period between winter and NAM) in which the low energy season transition into the high energy season resulting in dynamic hydrologic patterns. In this dissertation, we have focused on all these seasons and explored the soil moisture temporal dynamics using a distributed hydrologic model with a coupled distributed snow model.

Current knowledge on hydrologic processes in the ponderosa pine ecosystem at hillslope scale is limited and based on measuring fluxes and hydrologic state variables at distributed locations [e.g. *Wilcox et al.*, 1997] and modeling hillslopes using a simple model lacking incorporation of spatially detailed ponderosa pine characteristics [e.g. *Guan et al*., 2010]. As a result, spatially and temporally detailed hydrologic responses are not well understood from these studies. In addition, it is time consuming and expensive to sample observation at each location. A distributed model evaluated against multiple

hydrologic variables is an alternate approach to simulate hydrologic processes with high spatial and temporal resolutions. Therefore, we used a distributed model to advance our understandings on hydrology underneath a ponderosa pine ecosystem. Current knowledge on ponderosa pine hydrology at the hillslope scale lacks (1) detailed understanding about spatial controls on hydrologic patterns and temporal evolution of these spatial controls with seasonality, (2) knowledge about an appropriate spatial model resolution and its threshold to simulate this system and finally (3) understandings about hydrologic responses due to contrasting winter to summer seasons. Several studies addressed and investigated these issues in past at regional and watershed scale which were unable to provide hillslope scale spatially detailed hydrologic information [e.g. Seth et al., 1999; *Vivoni et al.,* 2005; *Mahmood and Vivoni,* 2008]. In this dissertation, we advanced our standings on these subjects listed above using a distributed model tested against multiple hydrologic state variables.

Distributed hydrologic models have the potential to reproduce soil moisture patterns over distributed locations and a range of time scales, allowing the spatiotemporal investigations of physical mechanisms. Physically-based distributed models account for the spatial variability of topography, vegetation (both in space and time), soils and meteorological forcing (both in space and time) [e.g., *Anderson et al.,* 2001; *Ivanov et al.,* 2004a; *Vivoni et al.,* 2007]. Representations of hillslope characteristics such as topography and vegetation in distributed models significantly impact soil moisture simulations as these exert strong controls on the processes of soil infiltration, evapotranspiration and lateral

water redistributions. Building confidence in distributed hydrologic models is a real challenge as these require detailed observations of numerous hydrological states and fluxes at multiple locations [e.g. *Beven*, 1993]. In addition, comparisons to soil moisture observations are necessary, in particular at very fine resolution under each vegetation type, to make significant progress for hillslope scale water balance predictions. Unfortunately, very few investigations have attempted to compare distributed simulations with observations over a range of hillslope locations [e.g. *Motovilov et al.*, 1999; *Western et al.*, 1999b; *Anderson et al.*, 2001], especially in the ponderosa pine ecosystems. The application of these models to hillslope scales has been rare due to the lack of coordinated, high-resolution data required for model evaluation. Since a new generation of hillslope experiments is underway in the Critical Zone Observatories (CZOs) [*Anderson et al*., 2008], the evaluation of existing distributed hydrologic models at the hillslope scale is a timely pursuit. Building model confidence through testing with data at distributed locations allows characterizing hydrologic dynamics and their spatial controls by tracking all relevant fields resulting from internally-consistent processes. In addition to conventional hydrologic simulations, it is important to simulate snow processes to understand the winter to summer transitory hydrologic responses. Snow processes simulations also require the high spatial and temporal resolution datasets for building confidence on the model physics and capturing spatial variation of snow accumulation, sublimation and melt.

In this study, we used a distributed model applied to a ponderosa pine field site to study hillslope hydrologic behavior occurring during the NAM, winter

snow accumulation and spring period. In particular, we inspect the spatiotemporal patterns in surface and root zone soil moisture, snow depth, sublimation, evapotranspiration and runoff generation and identify the underlying processes responsible for the temporal evolution in hillslope response. In addition to exploring underlying hydrologic processes, we have investigated the model coarsening impacts on distributed hydrologic responses and land surface characteristics and its implications on future hillslope studies. Since the study site is representative of ponderosa pine areas in Arizona, New Mexico and Colorado [*Brandes and Wilcox*, 2000], the findings of this study using the distributed model are relevant to forests throughout the region. Studying the hydrologic dynamics in these semiarid forests is of particular importance since these areas are highly susceptible to climate change [e.g., *Woodhouse et al*., 2010].

A summary of Chapters (2-4) is given in the next section. Each Chapter is independently prepared for publication.

1.2. Overview of chapters

Chapter 2 investigates the spatial controls and its temporal evolution on distributed soil moisture simulation during NAM under uniform soil condition using a field tested distributed model. Science questions for Chapter 2 are given below:

1. What are the spatial controls on hydrologic patterns during the NAM?

2. Are these controls static or evolve with seasonality? What are the processes and physical mechanisms responsible for the temporal evolutions of the spatial controls?

To answer these questions, we use a distributed model simultaneously evaluated against the soil moisture and runoff to explore the local (vegetation) and nonlocal (topography) spatial controls and switching between the local (vegetative) and nonlocal (topographic) controls. Our modeling effort is focused on identifying the threshold behavior in the hillslope response due to wetting during the North American monsoon (NAM). We calibrate the model to the distributed surface soil moisture data for one summer and then test the model against a broader range of observations over multiple seasons. Model simulations are then used to identify the vegetation and topographic controls on the spatial patterns in soil moisture and runoff generation. Vegetation patterns primarily influence the hydrologic response during the dry summer periods leading to patchiness related to the ponderosa pine stands. The spatial response switches to fine-scale terrain curvature controls during persistently the wet NAM periods. Thus, a climatic threshold involving rainfall and weather conditions during the NAM is identified in the hillslope response when sufficient lateral soil moisture fluxes are activated by the high rainfall amounts and the lower evapotranspiration induced by cloud cover. The spatial variability of the hillslope soil moisture and runoff generation also increases due to the crossing of this threshold in the seasonal rainfall distribution.

Chapter 3 investigates the impacts of model coarsening on distributed hydrologic simulations, detects a threshold model resolutions beyond which the fidelity of the simulated soil moisture pattern is no longer reliable and comments on the impacts of simulating at coarser resolutions and it implications on future hillslope instrumentations. Science questions for Chapter 3 are given below:

1. What are the impacts of model coarsening on land surface characteristics and simulated hydrologic patterns?
2. Is there any threshold model resolution beyond which the reliability of simulated hydrologic patterns is no longer reliable?
3. What are implications for selecting future sampling site if the finest resolution model simulations are representations of real world hydrologic patterns?

To answer these questions, we utilize the Triangulated Irregular Network (TIN)-based Real-time Integrated Basin Simulator (tRIBS) to investigate how model aggregation leads to the breakdown of spatial hydrologic patterns in a ponderosa pine hillslope parameterized at fine-resolution (~0.3 m). Results indicate that spatial patterns in soil moisture are controlled by small-scale curvature features at fine resolutions and by larger-scale vegetation patches at coarser resolutions. Model aggregation quickly eradicates curvature features and its spatial control on hydrologic patterns, while the level of coarsening possible in the hillslope still preserves vegetation patchiness. A threshold resolution of ~10% of the original topographic field is identified through analyses of homogeneity indices, correlation coefficients and spatial errors. Below this resolution, model

aggregation leads to unrealistic patterns in soil moisture and a transition from curvature-controlled lateral fluxes to vegetation-mediated vertical fluxes. Based on spatial error analyses, we evaluate the use of the distributed hydrologic model to identify sampling sites that represent the hillslope behavior and minimize the sensitivity to model resolution. Our findings demonstrate that spatial sensitivity occurs within hillslope domains depending on the characteristics of the spatial features that control the hydrologic response.

Chapter 4 investigates the impacts of inverse relationship between winter and summer wetness on the winter to summer transitional hydrologic response. Thus, we examine the winter to summer hydrologic responses during a sequence of the winter and summer season having significant wetness contrast. Science questions for Chapter 4 are given below:

1. What are impacts on hydrologic responses during contrasting winter to summer transitions (spring season)?

In this Chapter, we use a distributed model evaluated concurrently against the distributed snow depth, soil moisture and runoff for two water years having contrasting winter and summer wetness to answer above question. During a water year with a sequence containing wet winter and dry summer, evapotranspiration induced losses dry the hillslope soil and disengage the hillslope lateral connectivity. Our findings suggest that wet winter results thick snow pack in inter-patch grassland areas and abundant moisture infiltrates into the soil underneath grasses from initial melt resulting soil saturation, soil dries out during the spring period due to increase in evapotranspiration and decrease in

precipitation and the soil moisture finally recess to near residual moisture content due to the high evapotranspiration during the dry summer season. In contrast, during a water year having seasons with an order of the dry winter and wet summer, generally hillslope soil wetting is observed. Soil is extremely dry with no snow cover during winter period, soil wets up due to sparse snow events with subsequent melts and rainfall during the spring period and the summer rainfall events continue soil wetting during wet summer period resulting both vegetation and topographic controlled soil moisture pattern. Our findings also suggest temporal switch from the saturation excess to the infiltration excess mechanisms during wet winter followed by dry summer and vice versa during dry winter prior to wet summer. Overall, we find that the impacts of contrary winter and summer wetness in a water year have significant influences on hillslope ecohydrological processes, wetness, lateral connectivity and soil moisture spatial patterns.

2. A Climate-Induced Threshold in Hydrologic Response in a Semiarid Ponderosa Pine Hillslope

2.1. Introduction

Vegetation, soil and topography have been recognized to exert spatial controls on hydrologic responses across a range of different climates [e.g., *Teuling and Troch*, 2005; *Lawrence and Hornberger*, 2007; *Mahmood and Vivoni*, 2008; *Vivoni et al*., 2010]. Vegetation exerts controls via evapotranspiration (*ET*) and interception, soil properties influence directly the infiltration and subsurface flow, and topography has effects on lateral fluxes and runoff [e.g., *Carey and Woo*, 2001; *Caylor et al*., 2005; *Burt and Butcher*, 2006; *Zou et al*., 2007; *Ivanov et al*., 2008; *Bi et al*., 2008; *Vivoni et al*., 2008a; *Litaor et al*., 2008]. However, the temporal evolution of these spatial controls is poorly understood, in particular for hydrologic systems with a strong seasonality in water availability, such as those in the North American monsoon (NAM) region [e.g., *Goodrich et al*., 2008; *Vivoni et al*., 2010].

The NAM is a summer (July-September) climate system that brings intense, short duration storms to the southwest U.S. affecting hydrologic processes in the semiarid region. We hypothesize that the seasonal evolution of soil moisture leads to a transition in the dominant spatial controls on the hydrologic response as the NAM progresses. This hypothesis follows *Grayson et al*. [1997] who found, in a different climate setting, that "local" vertical fluxes influenced hydrologic patterns during dry states, while "nonlocal" lateral fluxes

controlled patterns during wet states. To our knowledge, this hypothesis has not been tested in semiarid regions with seasonal wetting. It is also unclear how vegetation patches in forested mountain areas may affect the transition between local and nonlocal factors.

Water-limited forests in the NAM region present an interesting case for understanding the temporal switching of spatial controls. Several studies have characterized the hydrologic dynamics of ponderosa pine areas in New Mexico [*Newman et al*., 1997; *Wilcox et al*., 1997; *Brandes and Wilcox*, 2000; *Zou et al*., 2008; *McDowell et al*., 2008]. From these studies, a conceptual framework for runoff production at the hillslope scale has emerged [see *Wilcox et al*., 1997; *Newman et al*., 2004 for a discussion]. In this framework, lateral subsurface flow through macropores is the principle mechanism during snowmelt, while infiltration-excess runoff is the main source during the NAM. Today, however, this framework has not: (1) recognized the role of progressive wetting during the NAM; (2) identified landscape features that control hydrologic patterns, or (3) accounted for contrasts between ponderosa pine stands and interstand grasses.

Identifying whether a transition in hillslope behavior exists due to local and nonlocal factors requires spatial datasets that are difficult to obtain in field studies. Distributed models, however, could be used to evaluate conceptual frameworks since these account for physical processes and surface properties that impact the hillslope response. The application of these models to hillslope scales has been rare due to the lack of coordinated, high-resolution data required for model evaluation. Since a new generation of hillslope experiments is underway in

the Critical Zone Observatories (CZOs) [*Anderson et al*., 2008], the evaluation of existing hydrologic models is a timely pursuit. After building model confidence through testing with spatial data, distributed models should allow characterizing hydrologic dynamics and their spatial controls by tracking all relevant fields resulting from internally-consistent processes.

In this study, we use a distributed model applied to a ponderosa pine field site to study the hillslope hydrologic behavior occurring during the NAM. In particular, we inspect the spatiotemporal patterns in surface and root zone soil moisture and runoff generation and identify the underlying processes responsible for the temporal evolution in hillslope response. Since the study site is representative of ponderosa pine areas in Arizona, New Mexico and Colorado [*Brandes and Wilcox*, 2000], the hydrologic insights gained from the distributed model are relevant to forests throughout the region. Studying the hydrologic dynamics in these semiarid forests is of particular importance since these areas are highly susceptible to climate change [e.g., *Woodhouse et al*., 2010]. Our goal in this study is to identify the spatial controls on hydrologic patterns and their transition in semiarid regions with strong seasonality in water availability. This investigation is intended to shed light upon the threshold behavior of semiarid, forested hillslopes and provide guidance for future field experiments and hillslope characterizations.

2.2. Methods

2.2.1. Study area

The study area is a ponderosa pine (*Pinus ponderosa*) hillslope (~1280 m^2) located in the Los Alamos National Laboratory (LANL) in New Mexico, USA (Figure 2.1). At the site, an intensive set of hydrologic studies were carried out from 1993 to 1998 [*Wilcox et al*., 1997]. Spatial data characterizing the hillslope include: (1) a LIght Detection And Ranging (LIDAR)-based digital elevation model (DEM) at 0.305 m resolution, and (2) a LIDAR-based vegetation height map (Figure 2.2). The hillslope is gently sloping from west to east with low relief (~6 m) and an average elevation of ~2315 m. Vegetation consists of open ponderosa pines with intercanopy grasses. Soil stratigraphy is characterized as: A and Bw horizons (loess deposit, sandy loam texture), a Bt horizon (alluvium), a clay-rich CB horizon (weathered tuff, clay texture), and an R horizon of Bandelier Tuff. Soil hydraulic properties were only available at one location [*Wilcox et al.*, 1997], limiting our ability to resolve spatial patterns in soil properties or depth.

2.2.2. Field observations

The field dataset collected at the site included precipitation, air temperature, relative humidity, incoming solar radiation, volumetric soil moisture at fourteen locations, and runoff estimates from a trench in the eastern boundary. While the meteorological and runoff data was obtained at 15 min to hourly

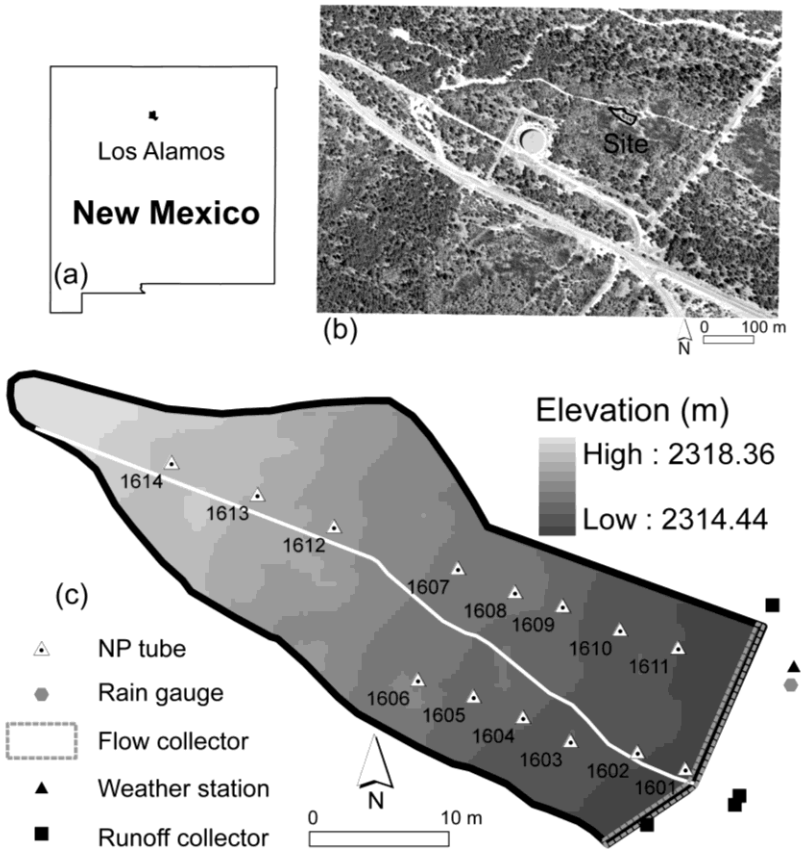

Figure 2.1. Location of the study site. (a) Los Alamos county in the northern New Mexico, USA. (b) Panchromatic high-resolution aerial photograph of study area (polygon with black line). (c) Digital elevation model (DEM at 0.305 m resolution from LIDAR) and the boundary of the ponderosa pine hillslope. This figure also shows the neutron probe (NP) locations for soil moisture measurements, runoff collectors, PVC flow collectors, rain gauge and weather station.

resolution, soil moisture sampling occurred at weekly intervals or greater. Due to significant data gaps, we did not consider the summers from 1993 to 1995 in our simulations. Instead, we focused on summers of 1996, 1997 and the early part of 1998. Summer 1996 was included despite the paucity of soil moisture data to expand the range of conditions.

Soil moisture was measured via a hand-held neutron probe (NP) placed at different soil depths (10, 25, 40, 55, 70, 85 and 100 cm) through access tubes

(sites 1601 to 1614) and converted to volumetric soil moisture via two calibrations for the A/B and CB/R horizons [*Brandes and Wilcox*, 2000]. Only one sampling location is completely within a ponderosa pine stand (site 1608), six access tubes are at stand edges, and the remaining are in grass patches. We used soil moisture at 10 cm for model calibration due to its responsiveness to competing processes such as infiltration, evaporation and transpiration. As a result, these observations are useful for inferring the hillslope hydrologic response, despite the potential limitations of neutron probe measurements in shallow soils [*Evett et al*., 2003]. Runoff and subsurface lateral transport were measured using a polyvinyl chloride collection system in the trench with separate runoff collectors for "north" and "south" hillslope sections, aggregated here as the outlet runoff.

Figure 2.3 summarizes the field dataset used in this study, including hourly incoming solar radiation and precipitation, spatially-averaged soil moisture ($<\theta>$) (from 14 locations) at 10 cm depth and averaged over the top 1 m, and hourly outlet runoff. The spatial variability of soil moisture (± 1 standard deviation) is also depicted as vertical bars. Spatially-averaged soil moisture at both depths decreases during interstorm periods in the summer and increases in response to large storms. As the summer progresses, incoming solar radiation decreases due to the presence of cloud cover, affecting the soil moisture recession, Runoff is discontinuous during the summer as a consequence of the infiltration-excess mechanism [*Wilcox et al.,* 1997].

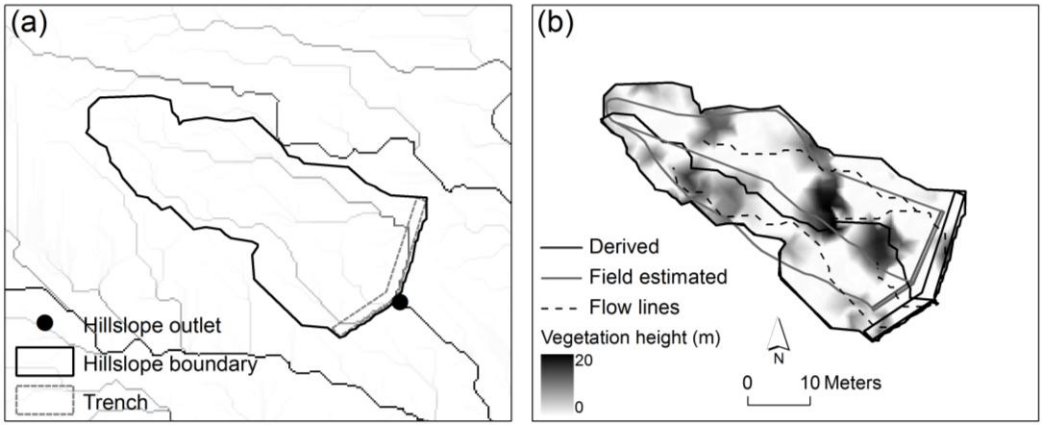

Figure 2.2. (a) Location of hillslope outlet and delineated boundary. (b) Flow lines in the hillslope and comparison of the field-estimated and derived hillslope boundary and divide. Note that the background represents LIDAR-based vegetation canopy height vegetation canopy height.

2.2.3. Distributed hydrologic simulations

We used the Triangulated Irregular Network (TIN)-based Real-time Integrated Basin Simulator (tRIBS) for the hillslope simulations. tRIBS is a distributed model with physically-based processes [*Ivanov et al*., 2004a,b; *Vivoni et al*., 2007], including rainfall interception, infiltration, evapotranspiration, water table fluctuations, lateral subsurface transport and runoff production and routing. tRIBS incorporates available hillslope descriptors in the simulation. The use of LIDAR data allowed an opportunity to depict small-scale topographic features and the distribution of vegetation patches within a hillslope. The model estimates the spatiotemporal variation of runoff production and soil moisture at different depths, among other variables such as *ET* and soil temperature, which can be

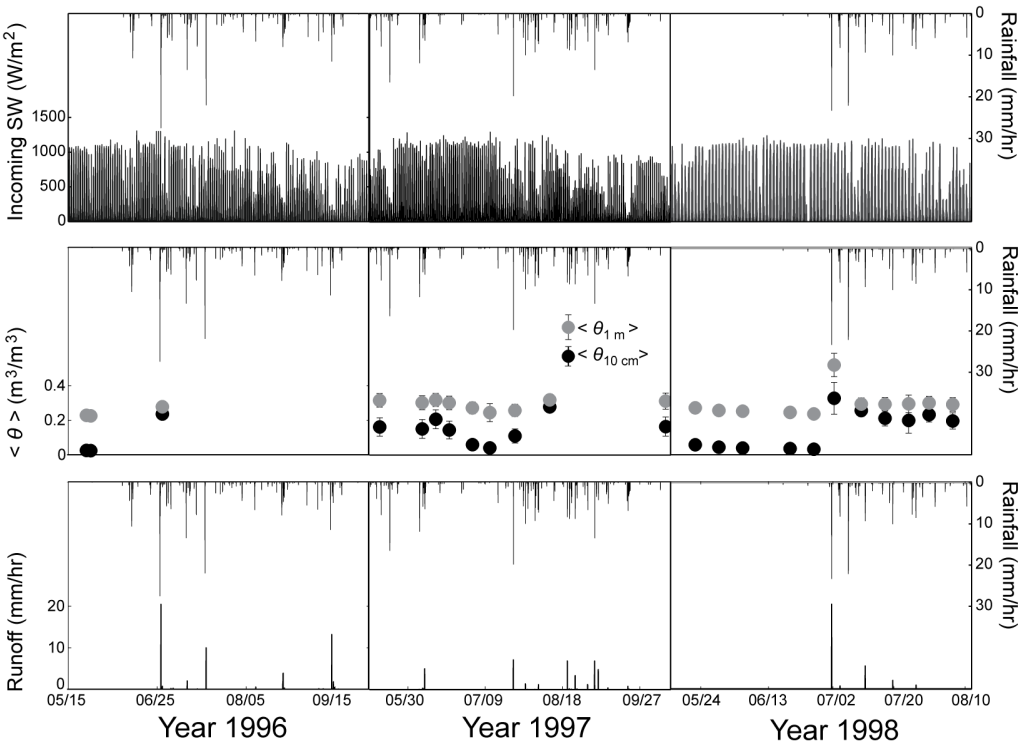

Figure 2.3. Hydrometeorological variables during study periods. Hourly rainfall shown as inverted axis. (top row) Hourly incoming solar radiation. (middle row) Soil moisture data averaged over 14 locations at the available sampling times (black circles are 10 cm depth and gray circles are 1 m depth-averaged). Vertical bars are ±1 spatial standard deviation. (bottom row) Hourly runoff at hillslope outlet estimated by summing observations at north and south parts of the hillslope**.**

compared to available observations. The reader is referred to *Ivanov et al.* [2004a,b] and *Vivoni et al*. [2007, 2010] for details on the model physics.

Briefly, the soil moisture dynamics are controlled by infiltration, lateral transport, rainfall interception, soil evaporation and plant transpiration. A kinematic model of unsaturated flow in heterogeneous, sloping, anisotropic soil is used to estimate infiltration [*Cabral et al*., 1992]. The evolution of the top and bottom wetting fronts and soil properties determine the infiltration rate and runoff production, including infiltration-excess, saturation-excess, perched return flow

and groundwater exfiltration. A simple approach is used for enhanced lateral subsurface flow based on an anisotropy ratio of the saturated hydraulic conductivity. Rainfall interception is estimated using a canopy water balance [*Rutter et al*., 1971]. Bare soil evaporation and plant transpiration are based on the Penman-Monteith equation and soil moisture availability [*Ivanov et al*., 2004a].

2.2.3.1. Hillslope representation

Hillslopes can be represented in tRIBS using a TIN constructed from a grid-based DEM [*Vivoni et al*., 2004]. To obtain a hillslope boundary, we create a ~1 m deep trench in the LIDAR DEM, consistent with *Wilcox et al*. [1997]. We set the hillslope outlet at the location of highest upstream area that drained the north and south portions (Figure 2.2a). We then derived a hillslope boundary similar to the field estimates of *Wilcox et al*. [1997] (Figure 2.2b). However, the derived area in the model is 1280 m^2, as compared to the 870 m^2 field estimate. The discrepancy is due to the difficulty in determining the boundary in the gently sloping terrain in both the field observations and in the LIDAR data. We also split our hillslope into north and south parts to mimic the field maps of *Wilcox et al*. [1997], finding good agreement between both estimates.

We represented the hillslope at the highest possible resolution to preserve all LIDAR cells. The tRIBS domain consists of N_v = 12,755 Voronoi polygons (nearest neighborhood of a TIN node) at a resolution of 0.305 m. This domain has a horizontal point density, $d^{'} = (n_t - n_b)/(n_g - n_b) = 1$, where n_t is the number of TIN nodes, n_g is the number of DEM cells and n_b is the number of nodes in the

boundary and flow network. Each Voronoi polygon is characterized by the elevation, slope (degrees), and curvature (dimensionless) at each location (Figure 2.4). Note the curvature distribution has areas of flow convergence (negative curvature) and divergence (positive curvature). The model assigns vegetation and soil parameters to each polygon based on its spatial location. In addition, we added a flow network to transport runoff from the hillslope into the trench. The network was derived using an upslope area threshold of 37 m^2 to ensure proper routing of the hillslope runoff from the northern and southern portions into the trench.

2.2.3.2. Model forcing, parameterization and initialization

Spatially-uniform forcing consisted of hourly precipitation, air temperature, relative humidity, wind speed and incoming solar radiation. Since sub-hourly data was unavailable for most variables, we restricted simulations to an hourly resolution. Summer rainfall, accounting for >50% of the annual precipitation [*Brandes and Wilcox*, 2000], exhibits a few, high intensity pulses during the early summer (May and June) and frequent, but lower intensity, events during the NAM (July to September). As a result, incoming solar radiation remains high during May and June, but is affected by cloud cover later in the summer. As shown in Table 2.1, the three summer periods have different rainfall distributions, with the wettest summer in 1997. Clearly, the 1997 summer also appears to be wetter than the long-term average, in particular during September. The other two summers are drier and more consistent with the average conditions.

	Precipitation (mm)					
Year	**May**	**June**	**July**	**August**	**September**	**Total**
Average (1965-90)	29.7	34.5	82.8	89.4	53.8	290.2
1993	–	17.4	84.8	136.5	28.6	267.3
1994	76.5	45.2	102.2	72.3	27.2	323.4
1995	59.2	65.0	33.4	105.2	56.0	318.8
1996	0.1	100.0	109.0	83.0	66.0	358.1
1997	58.0	69.0	57.0	146.0	93.0	423.0
1998	0.0	1.9	165.1	42*	20.6*	167.0

Table 2.1. Monthly precipitation at the study site for 1993 to 1998 (field study period) and long-term spatial averages (1965-1990) for stations in Los Alamos [*Bowen*, 1996]. Periods with no data are indicated by a dash (-) and months with large data gaps by an asterisk (*).

Initial soil parameters for a spatially-uniform sandy loam were assumed based on *Wilcox et al*. [1997]. This is consistent with *Newman et al*. [1997] who found similar vertical fluxes (and thus homogeneous soil) in a set of hillslope locations. We used the depth variation of hydraulic conductivity from *Wilcox et al.* [1997] to estimate the saturated hydraulic conductivity at the surface (K_o) and its decay parameter (f) (Table 2.2). Conductivity values are consistent with the

Soil Parameter							
K_o (mm/hr)	θ_s (m^3/m^3)	θ_r (m^3/m^3)	θ^* (m^3/m^3)	λ (-)	Ψ (mm)	f (mm^{-1})	A_s (-)
0.29*	0.45*	0.01%	0.18+	1.9+	-250+	0.0067*	40+

Table 2.2. Soil parameter values from field observations (indicated by *), literature (%), or manual calibration (+), including saturated hydraulic conductivity at surface (K_o), saturated (θ_s) and residual (θ_r) soil moisture [*Rawls et al.,* 1983], soil mo moisture stress threshold (θ^*), pore size distribution index (λ), air entry bubbling pressure (ψ), conductivity decay parameter (f), and soil anisotropy ratio ($A_s = K_l/K_v$). K_l and K_v are the lateral and vertical conductivities, respectively.

Vegetation Units	Vegetation Parameter									
	Area (%)	*p* (-)	*S* (mm)	*K* (mm/hr)	*g* (mm^{-1})	*A* (-)	H_v (m)	K_t (-)	r_s (s/m)	*v* (-)
Grassland (0-1 m)	52	0.9%	1.0%	0.12%	4.7%	0.28%	1*	0.9%	40%	0.8+
Short ponderosa pine (1-5 m)	20	0.4%	1.5%	0.12%	4.7%	0.2%	5*	0.5%	10%	0.85+
Medium ponderosa pine (6-10 m)	15	0.4%	1.5%	0.12%	4.7%	0.1%	10*	0.5%	10%	0.95+
Tall ponderosa pine (10-20 m)	13	0.4%	1.5%	0.12%	4.7%	0.1%	20*	0.5%	10%	0.95+

Table 2.3. Vegetation parameter values from field observations (*), literature (%), or manual calibration (+), including percentage of hillslope area (*Area*), throughfall coefficient (p), albedo (A) [*Iziomon and Mayer,* 2002], canopy water storage capacity(S), drainage rate from canopy (K), drainage exponential parameter (g) [*Rutter et al.,* 1971], vegetation height (H_v), optical transmission coefficient (K_t) [*Zou et al.,* 2007], minimum stomatal resistance (r_s) [*Karlson and Assmann,* 1990; *McDowell et al.,* 2008] and vegetation fraction (v).

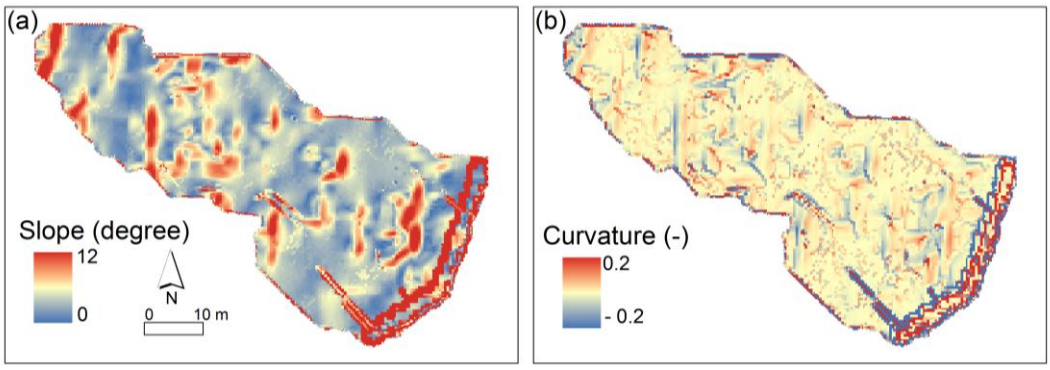

Figure 2.4. Terrain characteristics including (a) slope field in degrees and (b) dimensionless curvature field.

infiltration map of *Kwicklis et al*. [2005] and estimates of *Guan et al*. [2010]. Soil moisture at saturation (θ_s) was inferred from porosity data of *Wilcox et al*. [1997], while the residual soil moisture content (θ_r) was obtained from literature values (Table 2.2). Other soil parameters were varied within reasonable ranges for a sandy loam during a calibration exercise. In addition, we used soil anisotropy ratio (A_s) as a calibration parameter to allow lateral moisture transfer that mimicked the effect of root macropores [*Newman et al*., 2004; *Guan et al*., 2010]. We used a uniform soil depth of 1.06 m to be consistent with the uniform soil properties in the hillslope.

The canopy heights derived from LIDAR provided a way to vary the vegetation within the hillslope. We classified vegetation into four units based on height (Table 2.3): (1) grassland: 0 to 1 m, (2) short ponderosa pine: 1 to 5 m, (3) medium ponderosa pine: 5 to 10 m, and (4) tall ponderosa pine: 10 to 20 m. Here, we assume that vegetation classes can be mapped to the domain (~0.305 m resolution) such that elements within a patch have uniform properties and behave in a similar fashion. We incorporated the vegetation height directly into the model

as H_v, but the model currently neglects the effect of canopy height on shading of surrounding areas. We also varied other vegetation parameters using this classification and based values on results from prior studies in forested areas (Table 2.3). Following *Laio et al.* [2001], we treated the soil moisture stress threshold (θ^*) as a soil parameter and applied it uniformly in the hillslope. The use of the LIDAR canopy height provides structured spatial variability in the hillslope model that closely follows the characteristics of the ponderosa pine stands and interstand grasslands.

Model initialization was carried out by varying the initial level of perched saturation. Perched saturation occurs in the hillslope above the CB horizon and expands concentrically around root macropores in the Bt horizon [*Newman et al*., 2004]. We mimic this by imposing an initial depth to saturation such that soil moisture at 10 cm and 1 m depths are consistent with the first observation of each summer. The initial depth to perched saturation above the impermeable bottom was interpolated from the sampling locations using Ordinary Kriging. The assumption of an impermeable bottom is appropriate based on site observations [e.g., *Newman et al*., 1998]. This approach is consistent with the establishment of a saturated zone at the Bt-CB boundary during the winter snowmelt period [*Brandes and Wilcox*, 2000; *Newman et al*., 2004; *Guan et al*., 2010] and leads to the carryover of winter moisture for utilization by the ponderosa pine stands. Note that the initial condition is wetter in 1997 as compared to other summers (Figure 2.3).

2.2.3.3. Model calibration and confidence building

We used the soil moisture data at 10 cm depth during 1997 to manually calibrate a selected number of soil and vegetation parameters (Tables 2 and 3). This selection was based on a few important criteria: (1) the availability and quality of the soil moisture and runoff data, (2) the large dynamic range of soil moisture, including a wet initial condition and a long dry-down, and (3) the ability to fine-tune *ET* during the dry-down period to circumvent the lack of direct observations. Since neutron probe data are obtained at 10 cm, we depth-averaged the model soil moisture between 8 and 12 cm in each element that was co-located with a sampling location. Further, to account for geospatial uncertainty (i.e., spatial mismatch between model element and sampling location), we considered the standard deviation of the neighboring Voronoi polygons around each site in the calibration. This was deemed important since the majority of the sampling locations are located at the boundaries between ponderosa pine and grassland patches.

Our calibration strategy followed the descriptions of *Ivanov et al.* [2004b] in terms of the relative importance of each parameter. For each calibrated parameter (indicated by + in Tables 2 and 3), we sampled acceptable ranges based on the soil and vegetation classification. As in prior studies [e.g., *Ivanov et al*., 2004b; *Vivoni et al*., 2005, 2010], within-class parameter variations were not allowed. Model calibration was performed in a systematic fashion for the parameters where field-based estimates or literature values were not available. For example, soil moisture recession dynamics allowed estimation of the vegetation

fraction (v) controlling ET. Performance of the manually-calibrated model was assessed by comparing the simulated soil moisture and runoff response with the 1996 and 1998 observations. As a result, these two seasons and the runoff from the hillslope during all seasons serve as independent tests of the model performance.

2.3. Results and Discussion

In the following, we describe the model application, including comparisons to soil moisture and runoff observations. An initial contrast in the summer periods is shown through the simulated, time-averaged spatial patterns. A more detailed analysis is then used to explore dynamic differences between ponderosa pine and grassland sites. Finally, a threshold in the hillslope response is revealed for progressively wet summer conditions using a set of distributed and lumped metrics and their relation to the underlying physical processes.

2.3.1. Distributed soil moisture simulations in the surface and root zones

Figure 2.5 shows the simulated and observed volumetric soil moisture (θ in m^3/m^3) at 10 cm depth for one site in each vegetation unit. Model performance is similar at the other sampling locations (Table 2.4). During the 1997 calibration period, the simulated θ is in excellent agreement with observations (average RMSE of 0.03 and 0.07 m^3/m^3 at 10 cm and 1 m). A comparison of spatial patterns of θ at 10 cm using correlation lengths also revealed agreement for wet days in 1997 (~20 m in averaged correlation length for 6 wet days), while

differences were larger for three dry days (~16 m for model and ~31 m for data). Note the two temporal regimes: (1) a dry period from May 10 to July 22, with infrequent rains and carryover moisture receding toward $\theta_r \sim 0.05$ m^3/m^3, and (2) a wet period from July 23 to October 12, with frequent, small rainfall events and soil moisture rising toward $\theta_s \sim 0.4$ m^3/m^3. The model captures the soil moisture recession well during the drying period. Since this period is primarily controlled by *ET*, the good match suggests that vegetation parameters are appropriate. Seasonal *ET* also agrees well with *Brandes and Wilcox* [2000] (seasonal average of 401 mm as compared to 385 mm in this study).

Independent testing for 1996 and 1998 shows good agreement between simulated and observed soil moisture in the vegetation units. As in 1997, early summers are characterized by dry conditions. Differences, however, are observed in the later part of the season, depending on the timing and distribution of precipitation. In 1996 and 1998, the simulated θ did not increase significantly after the first high intensity (~20-30 mm/hr) rainfall, as observed at the sampling locations (June 29, 1996 and July 1, 1998). In each case, dry conditions prior to the event resulted in infiltration-excess runoff in the model that matched the observations [*Wilcox et al*., 1997], but that prevented rapid surface wetting. This is due to an initial dryness reducing the unsaturated hydraulic conductivity at the surface, limiting infiltration and promoting runoff [*Ivanov et al*., 2004a]. Despite this discrepancy, simulated soil moisture matched fairly well the observations for the testing period. As shown in Table 2.4, the average RMSE for 1998 was 0.10

m^3/m^3 at 10 cm and 0.08 m^3/m^3 at 1 m, with individual sites ranging from 0.05 to 0.14 m^3/m^3.

A careful inspection of the soil moisture dynamics reveals similarities and contrasts between grassland and ponderosa pine locations. Greater differences are observed for the dry period prior to the NAM, with drier surface soils and more subdued responses to rainfall with increasing tree height in the ponderosa sites (Figure 2.5, top to bottom). This is also observed during the 1996 season since the infrequent, low intensity rainfall events prevented the development of sustained saturation. Grassland soil moisture exhibits a faster increase after storms, but a slower recession as compared to the progressively taller ponderosa pines. However, during the wet periods of 1997 and 1998, there is little contrast in surface soil moisture timing and magnitude between the vegetation types. The variation of soil moisture dynamics among the types provides a first indication of the importance of plant characteristics, primarily during the dry period.

We compare the spatially-averaged θ at 10 cm ($<\theta_{10\ cm}>$ in m^3/m^3) and the depth-averaged soil moisture in the top 1 m or root zone ($<\theta_{1\ m}>$ in m^3/m^3) to corresponding data in Figure 2.6. Simulated soil moistures are in good agreement with the observed values at the two depths, except for the rapid wetting on June 29, 1996 and July 1, 1998. A slight underestimation of root zone soil moisture is also observed in 1996 and 1998. Note that high values of $<\theta_{1\ m}>$ on July 1, 1998 (~0.55 m^3/m^3) and its rapid recession suggest a potential measurement error in this period. As shown in Table 2.4, the RMSE between the spatially-averaged observed and simulated θ (labeled as All Sites) are low for 10 cm at 0.04 and 0.05

m^3/m^3. At 1-m, the outlier on July 1, 1998 leads to a high RMSE of 0.09 and 0.11 m^3/m^3. In addition, the RMSE averaged over each vegetation unit indicates that better performance is present for grasses in 1997, followed by grassland/short pine, and ponderosa pine sites. Nearly equal RMSE performance for each unit is obtained in 1998. These lines of evidence suggest that the hillslope-scale hydrologic model is reproducing both the distributed and aggregated soil moisture conditions at multiple depths.

We also investigated the temporal average and variance of surface soil moisture (Figure 2.7). These maps provide a first indication of the spatial controls on the hillslope response. Vegetation patterns clearly affect the θ distribution during 1996 and 1998, with drier ponderosa pines and wetter grass areas. This is supported by probability density functions (PDFs) of θ that exhibit bimodality related to vegetation contrasts [e.g., *Vivoni et al*., 2008a]. In addition, the soil moisture variance in ponderosa pines is lower, a result of more modest responses to rainfall and higher *ET*. For 1997, however, both vegetation and terrain curvature leave an imprint on soil moisture, with the variance exhibiting higher values in areas of flow convergence. Interestingly, the PDF is characterized by a single mode when the terrain features exhibit some controls.

Sampling Locations		Temporal RMSE (m^3/m^3)			
		1997		1998	
	Vegetation Unit	10 cm	1 m	10 cm	1 m
1601	Grassland	0.01	0.06	0.08	0.05
1602	Grassland/Short Pine	0.04	0.07	0.10	0.07
1603	Grassland/Short Pine	0.02	0.08	0.11	0.07
1604	Grassland	0.03	0.06	0.09	0.06
1605	Grassland/Short Pine	0.05	0.07	0.09	0.06
1606	Short Pine	0.02	0.06	0.11	0.06
1607	Medium Pine	0.07	0.08	0.08	0.08
1608	Tall Pine	0.03	0.12	0.12	0.07
1609	Grassland/Short Pine	0.05	0.05	0.14	0.11
1610	Grassland	0.02	0.05	0.14	0.10
1611	Grassland	0.02	0.05	0.14	0.09
1612	Grassland/Short Pine	0.03	0.09	0.09	0.07
1613	Grassland	0.02	0.07	0.14	0.09
1614	Grassland	0.02	0.03	0.09	0.08
Average		0.031	0.067	0.109	0.076
Standard Deviation		0.016	0.02	0.024	0.017
All Sites		0.04	0.05	0.11	0.09
All Grassland		0.02	0.05	0.11	0.08
All sites		0.04	0.07	0.11	0.08
All Pine		0.04	0.09	0.10	0.07

Table 2.4. Temporal root mean square error (*RMSE* in m^3/m^3) between simulated (Voronoi polygon average) and observed soil moisture at 10 cm depth and averaged over the top 1 m for 1997 and 1998. The year 1996 was excluded due to the few observations. The average and standard deviation of the individual RMSE at each site are shown. All Sites refers to the RMSE of the simulated site-averaged soil moisture. Spatial averages are also provided for All Grassland, All Grassland/Short Pine and All Pine sites. Vegetation classifications for each site are shown with two units when located on a boundary.

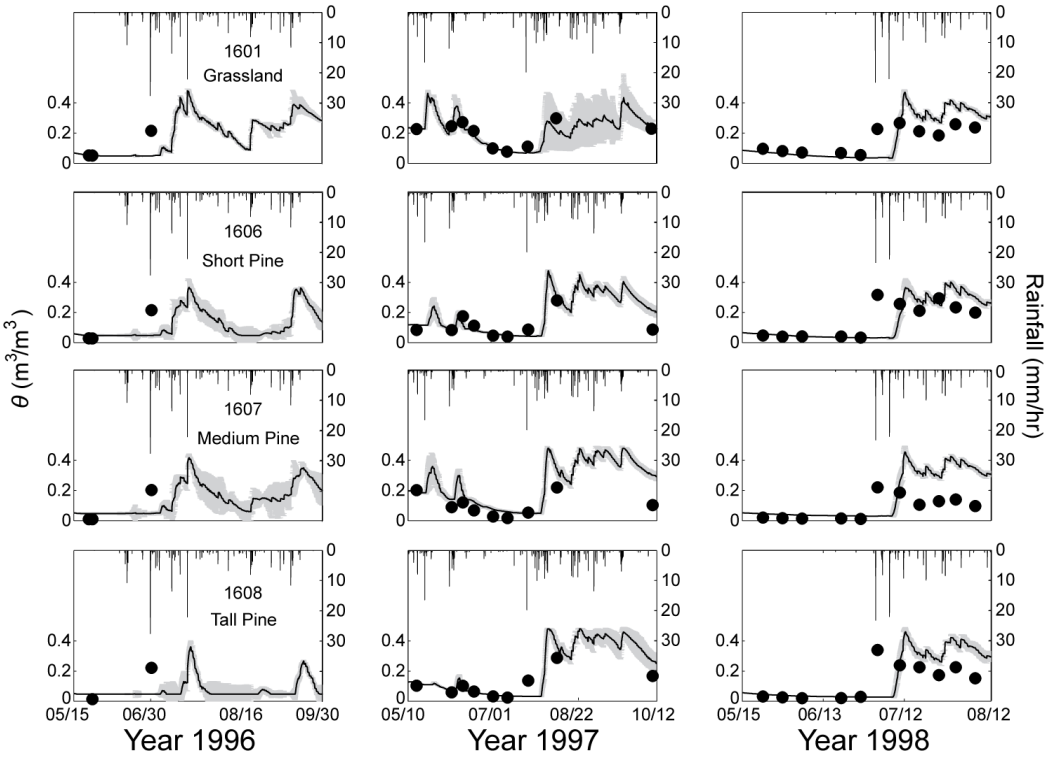

Figure 2.5. Comparisons between simulated and observed volumetric soil moisture (θ in m^3/m^3) at 10 cm depth. Rows represent sites in the grassland, short, medium and tall ponderosa pine units. Columns depict 1996, 1997 and 1998 years. Simulated values are spatial averages of the Voronoi polygon co-located with the sampling location and its neighboring elements (black lines). Spatial uncertainties are shown as ±1 standard deviation (gray shading).

2.3.2. Simulated runoff generation and its spatial pattern

We compare the simulated hillslope runoff to the trench observations as an additional model test. Note that calibration for 1997 did not include runoff as a consideration. Figure 2.8 presents an hourly comparison of the total runoff, along with the spatially-averaged surface θ. While sub-hourly runoff data are available [*Wilcox et al*., 1997], meteorological forcing only allow comparisons at hourly intervals. Simulations capture most of the observations, particularly during the early (dry) part of the summer season and for the first NAM runoff event (e.g.,

June 29, 1996 and July 1, 1998). Table 2.5 presents the runoff RMSE for the hillslope outlet and the north and south collectors. The model performance yields a low RMSE (0.20 to 0.34 mm/hr) during the summer. However, the model overestimated some events during the wetter portions of the NAM, in particular for 1997. This was identified as due to the evolution of the net infiltration rate, which increases as the wetting front penetrates into the soil and raises the hydraulic conductivity [*Ivanov et al*., 2004a], resulting in less infiltration-excess runoff. For all events, infiltration-excess runoff is the major simulated mechanism, in agreement with *Wilcox et al*. [1997]. A small degree of saturation-excess runoff also occurred in 1997 (<0.6% of total runoff) along flow convergence areas. While this mechanism was not observed in the field study, it is deemed possible given the concave regions that saturate infrequently in the hillslope.

We also explored the spatial patterns in runoff rates and frequency of runoff occurrence. Figure 2.9 shows maps of the time-averaged runoff rate conditioned on occurrence (R_I in mm/hr) and the percentage of the simulation that R_I occurs (T_{Ri} in %). This type of spatial analysis has been used to identify preferential runoff sites previously [*Vivoni et al*., 2008b]. Note the relatively infrequent occurrences of runoff (T_{Ri} is 0 to 4% of time), but the possibility of high rates (R_I is 0 to 17.8 mm/hr). The spatial fields suggest that vegetation patterns control R_I in 1996 and 1998. Lower runoff rates with a slightly higher frequency (T_{Ri}) appear in ponderosa pine stands, while the opposite is observed

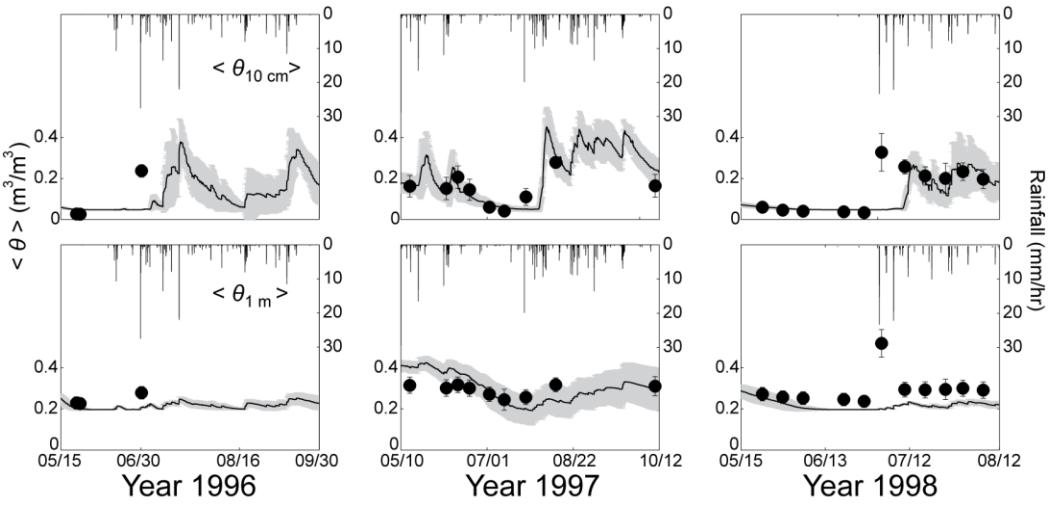

Figure 2.6. Comparison between simulated and observed spatially-averaged soil moisture at the fourteen sampling locations for 1996-1998. (top row) Surface soil moisture at 10 cm depth. (bottom row) Root zone soil moisture at 1 m depth-averaged. Spatial variations are represented by vertical bars for the observations and gray shading for the simulations.

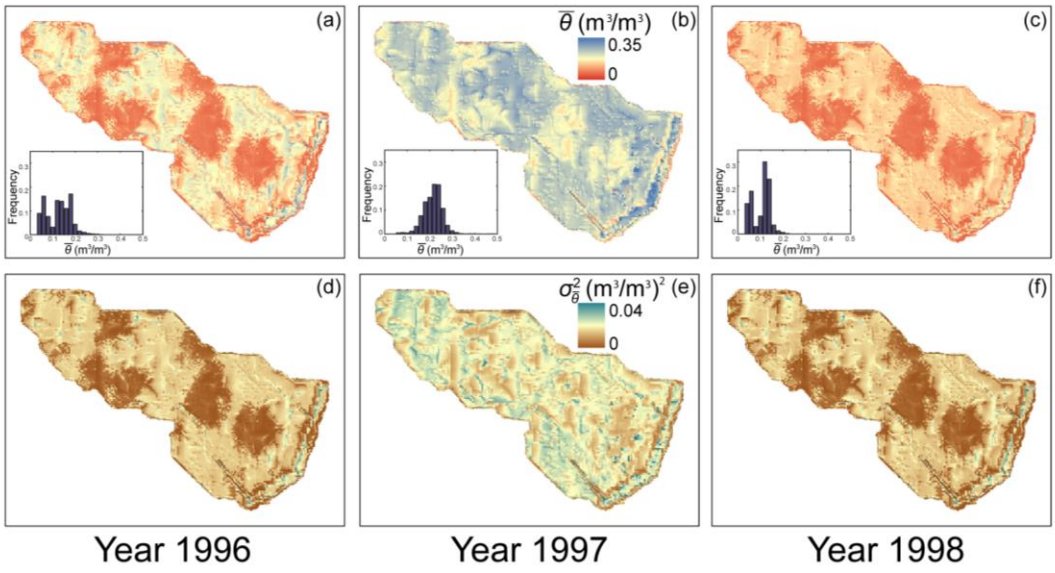

Figure 2.7. Spatial patterns of simulated temporal statistics of soil moisture at 10 cm depth. Time-averaged soil moisture during 1996-1998 (a-c), and the temporal soil moisture variance during 1996-1998 (d-f). Probability density functions (PDFs) of soil moisture are shown in the insets.

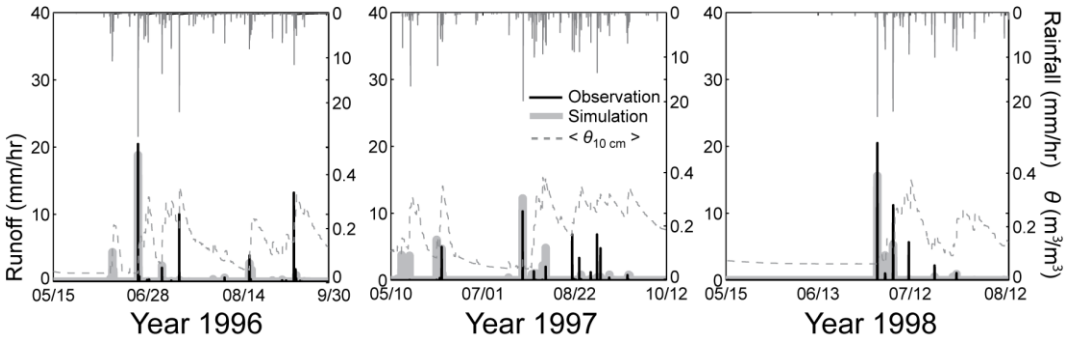

Figure 2.8. Comparison between observed (black line) and simulated runoff (gray line) at the hillslope outlet in mm/hr during 1996-1998. The spatially-averaged soil moisture at 10 cm is shown for reference using dashed gray line.

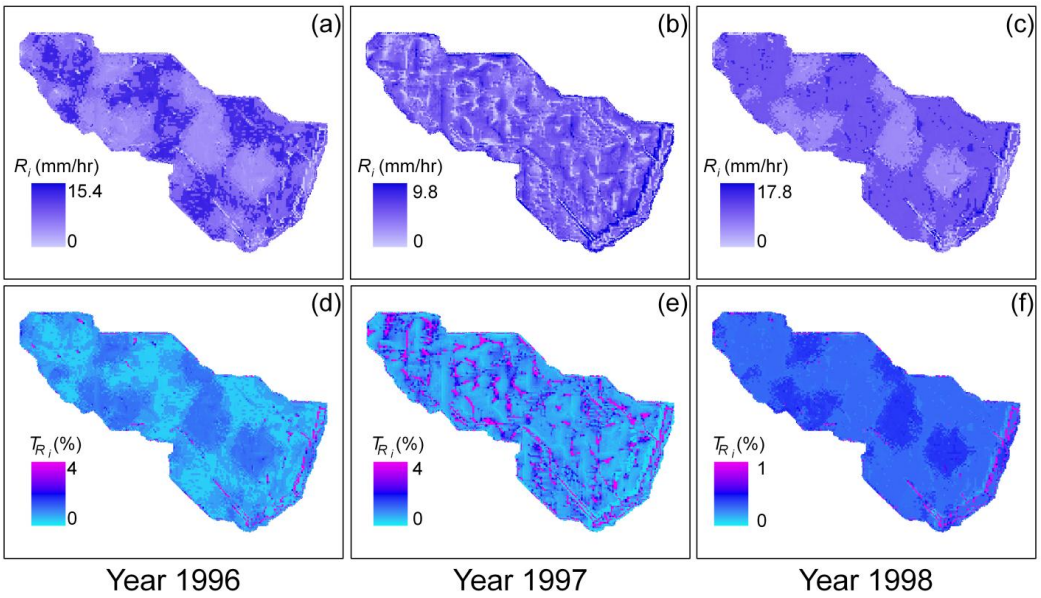

Figure 2.9. Distributed runoff responses for each simulation period. Time-averaged infiltration-excess runoff rate for 1996-1998 conditioned on its occurrence, R_I in mm/hr (a-c), and the percentage of the simulation time with the runoff occurrence, T_{Ri} in % (d-f).

for grass areas. In contrast, for 1997, the terrain curvature exerts a strong control on the spatial pattern of runoff generation. Note the regions of flow convergence that produce runoff frequently, but at relatively low rates, and that delineate a discontinuous and ephemeral flow network. Clearly, the imprint of the vegetation

patterns in 1997 is overwhelmed by the terrain curvature controls on runoff occurring during the wetter portions of the NAM.

2.3.3. Hydrologic contrasts between ponderosa pine and grassland sites

We used the model next to explore vegetation differences by comparing a grass (1604) and a tall ponderosa pine (1608) site in Figure 2.10. Surface θ is more responsive to precipitation (*P*) for the grassland due to its lower interception (*I*), exhibiting a maximum difference of 1.5 mm/hr between the sites. In general, surface and root zone θ are also higher in the grass site due to lower *ET*, though there are periods in the late season where the ponderosa pine retains high θ not observed in the grassland. Infiltration fronts are similar for both sites until the onset of the NAM, after which there is a more frequent development of a saturated moisture wedge and perched saturation in the ponderosa pine. A deeper wetting front is also observed in the ponderosa pine site, a condition that increases the surface infiltration in the model [*Ivanov et al*., 2004a]. Infiltration dynamics also lead to a small R_I runoff event due to surface saturation in late September not observed in the grass area, resulting in a slightly higher T_{Ri}. Nevertheless, the time-averaged runoff rate in the ponderosa pine is lower, due to interception effects in mid July.

Another important contrast is the net radiation (R_n) and its influence on *ET*. Ponderosa pines receive a lower R_n due an increased light absorption (K_t). This difference and the higher vegetation fraction lead to lower soil evaporation from ponderosa pines (15% of total *ET*) as compared to grasses (30% of *ET*).

Ponderosa pines transpire at a higher rate than grasses due to: (1) lower aerodynamic resistance due to greater height (H_v), (2) larger vegetation fraction (v), (3) lower minimum stomatal resistance (r_s), and (4) lower amounts of soil moisture stress due to the deeper root zone, despite the lower R_n. These factors lead to a greater total *ET* from ponderosa pines that reduces θ and decreases the perched saturation depth (N_{wt}) during the early, dry summer. As the NAM progresses, cloud cover reduces R_n, leading to a decrease in *ET* for both sites. This is consistent with the daily-averaged estimates of *Brandes and Wilcox* [2000] who found an *ET* decrease for the wet NAM season in 1995. With the small, frequent rainfall events and lower *ET* rates, θ increases after early August and reaches saturation in the ponderosa pine. Since transpiration is the dominant form of *ET*, 70% and 85% in the grass and ponderosa pine sites, the variation in this process structures the hydrologic patterns of during dry periods.

The differences between ponderosa pine and grass sites are further explored in Figure 2.11 through the water balance for all polygons in each unit. This analysis is based on climographs that depict the monthly precipitation and temperature conditions at a site. We adapted the modified climographs of *Yildiz and Barros* [2007] that capture normalized relations between the water balance components in a basin. In the top row, the relation between runoff (Q/P) and evapotranspiration (ET/P) ratios is presented, whereas the bottom row depicts the change in storage ($\Delta S/P$) versus ET/P.

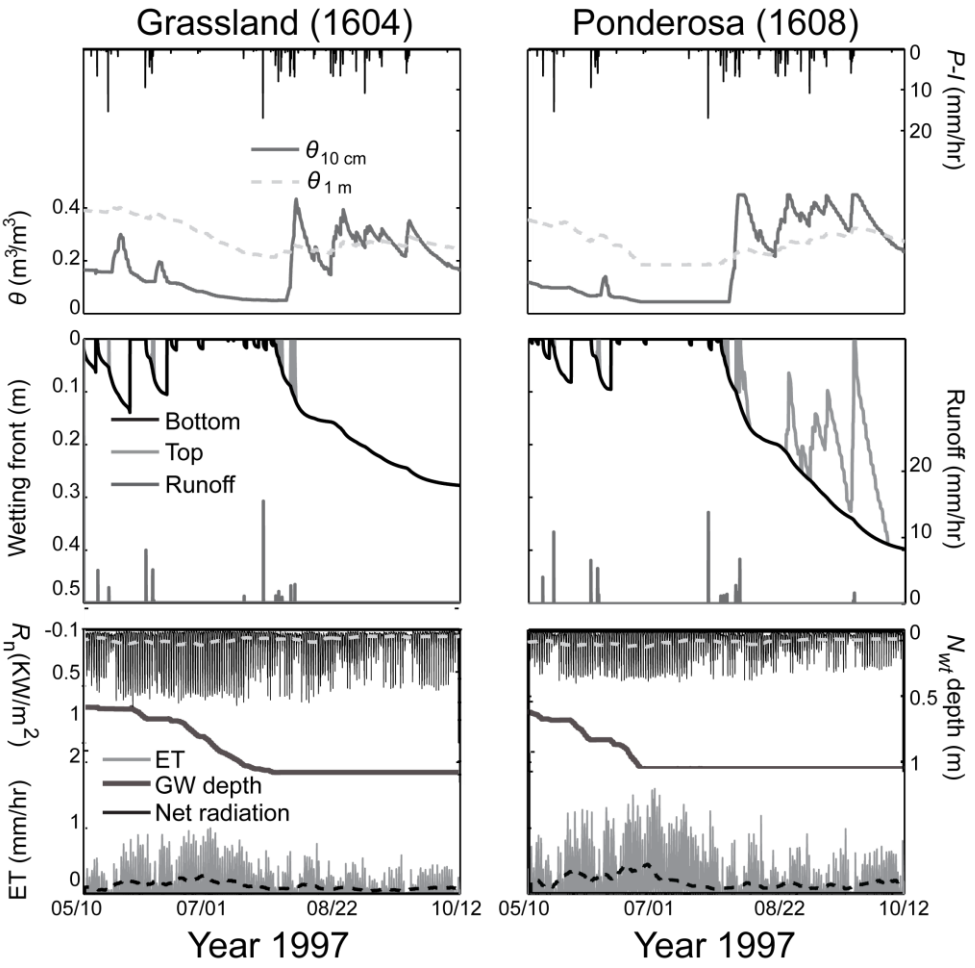

Figure 2.10. Hydrologic processes in grassland and tall ponderosa pine sites, including 10 cm and 1 m depth-average soil moisture, wetting front depths (top and bottom), runoff production, evapotranspiration (*ET*), net radiation (R_n) and depth to perched saturation layer (N_{wt} or GW depth). The inverted axis of the top row is the difference between precipitation (*P*) and interception (*I*). Dashed lines represent 7-day moving averages for R_n and *ET*.

ΔS is estimated in the model from the total hillslope moisture above the impermeable bottom and was comparable to estimates in *Brandes and Wilcox* [2000]. To help guide the interpretations, solid lines representing $Q/P = ET/P$ and $-\Delta S/P = ET/P$ are shown. The position of each symbol relative to the lines indicates the major water balance component, while their sequence from May (M) to September (S) measures the seasonal progression.

Climographs indicate that both vegetation types have high ET/P relative to Q/P and that ET/P leads to a decrease in storage (negative $\Delta S/P$). In addition, there is strong seasonality in the water balance, grouped as: (1) May to July, and (2) August to September. The early summer has high Q/P and ET/P with a decrease in $\Delta S/P$, while the later summer has a $ET/P < 1$, minimal Q/P and an increase in $\Delta S/P$. These analyses indicate that significant water losses occur due to *ET* and runoff during May to July, while the hillslope gains water in August and September due to frequent, low intensity storms and low *ET* (due to cloudy conditions). The climographs also reveal that the change in hillslope water storage ($\Delta S/P$) is linearly related to ET/P, while a nonlinear relation is apparent between Q/P and ET/P. This indicates that storage changes and *ET* are strongly linked over all conditions, while runoff and *ET* are decoupled when infiltration-excess runoff is the primary mechanism and depends less on hillslope storage conditions.

In addition to seasonality, the climographs demonstrate strong vegetation controls on the hillslope water balance. Over all months, the ET/P of ponderosa pine stands are higher than grass areas. This is reinforced in Table 2.6 by presenting the seasonal ET/P and Q/P for both vegetation types and the hillslope. Increased vertical fluxes from ET/P result in greater storage extractions (more negative $\Delta S/P$) for ponderosa pine stands. $ET/P > 1$ indicates that soil moisture storage is used by *ET*. A less clear distinction is present between grass and ponderosa pine areas for runoff (Q/P), indicating that a combination of opposing factors is in operation (Table 2.6).

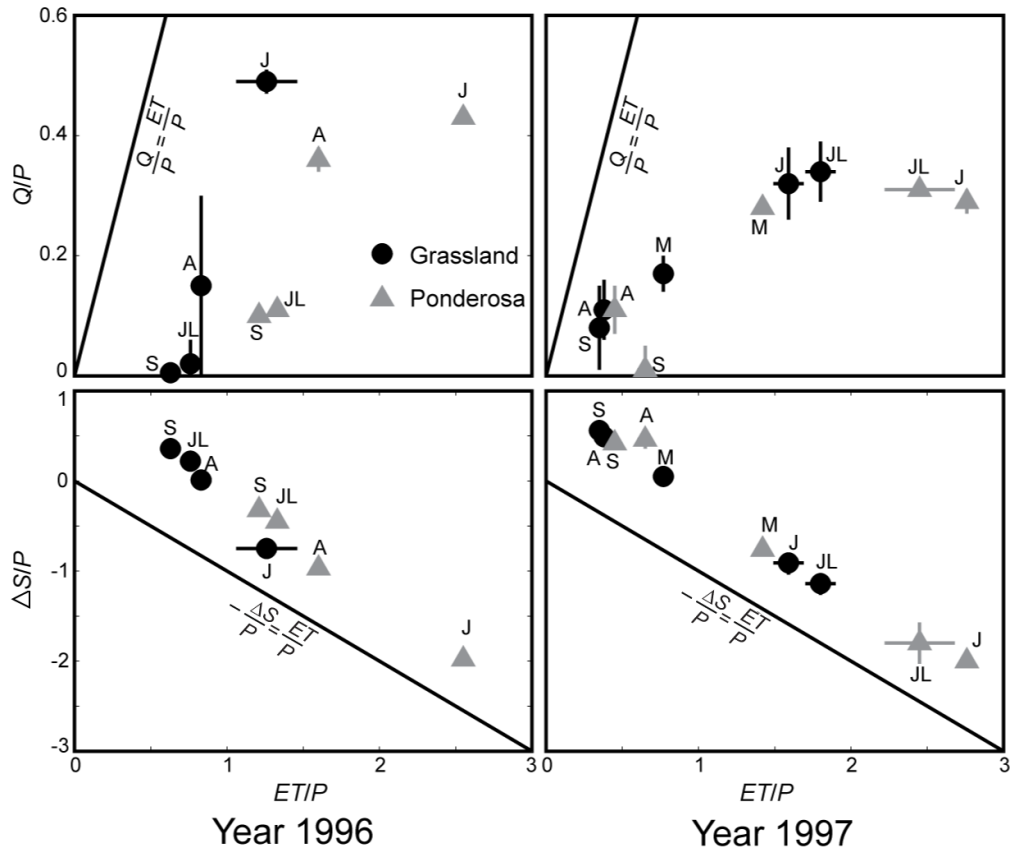

Figure 2.11. Monthly climographs for *Q/P* (top row) and *ΔS/P* (bottom row) as a function of ET/P for grassland and tall ponderosa pine sites during 1996 and 1997. Black circles and gray triangles represent the spatial mean of grassland and tall ponderosa pine sites, respectively, with the vertical and horizontal bars capturing the ±1 spatial standard deviation. For reference, solid lines depicting the 1:1 relations in the climographs (*Q/P = ET/P* and *-ΔS/P = ET/P*) are included.

Ponderosa pine stands reduce infiltration-excess runoff by intercepting more rainfall in the early summer, but their surface saturation dynamics in the later summer lead to higher runoff.

2.3.4. Temporal switching of spatial controls on hydrologic response

To identify the seasonality of spatial controls, we explore the monthly storage dynamics (Δ*S*) in Figure 2.12. Note the strong vegetation imprint on the storage

change during June and July, with ponderosa pines losing more water (negative ΔS) than grasslands. As the hillslope wets up, vegetation-induced patterns in ΔS are observed during August and September of 1996. However, during August in 1997, storage dynamics exhibit strong water gains (positive ΔS) and the imprint of terrain curvature emerges. In September 1997, most of the hillslope gains water, though flow convergence areas have negative ΔS due to runoff production. This transition is clear and occurs due to the high rainfall and the low *ET* induced by cloud cover. High soil moisture storage during August 1997 leads to a temporal switch between *ET*-dominated vertical (local) fluxes to terrain-controlled (nonlocal) lateral transport. A detailed inspection of the hourly storage dynamics (not shown) revealed that the transition began on August 8 and was completed by September 11, 1997. This suggests that the full transition from vertical to lateral fluxes can take up to one month with sufficient rainfall. This transition is not observed during 1996 or 1998 due to the lower soil moisture resulting from less frequent and lower rainfall in August and September.

To identify the underlying causes for the threshold behavior, we present the spatial coefficient of variation ($<CV_{1\ m}>$) of the root zone θ and the spatially-averaged subsurface lateral transport ($<q_l>$) in Figure 2.13. $<q_l>$ represents the internal lateral transfers in the hillslope and not the downstream lateral flow in the trench. For reference, cumulative rainfall, *ET* and runoff are included. Based on the storage dynamics, we identified periods as "drying" or "wetting" during each summer.

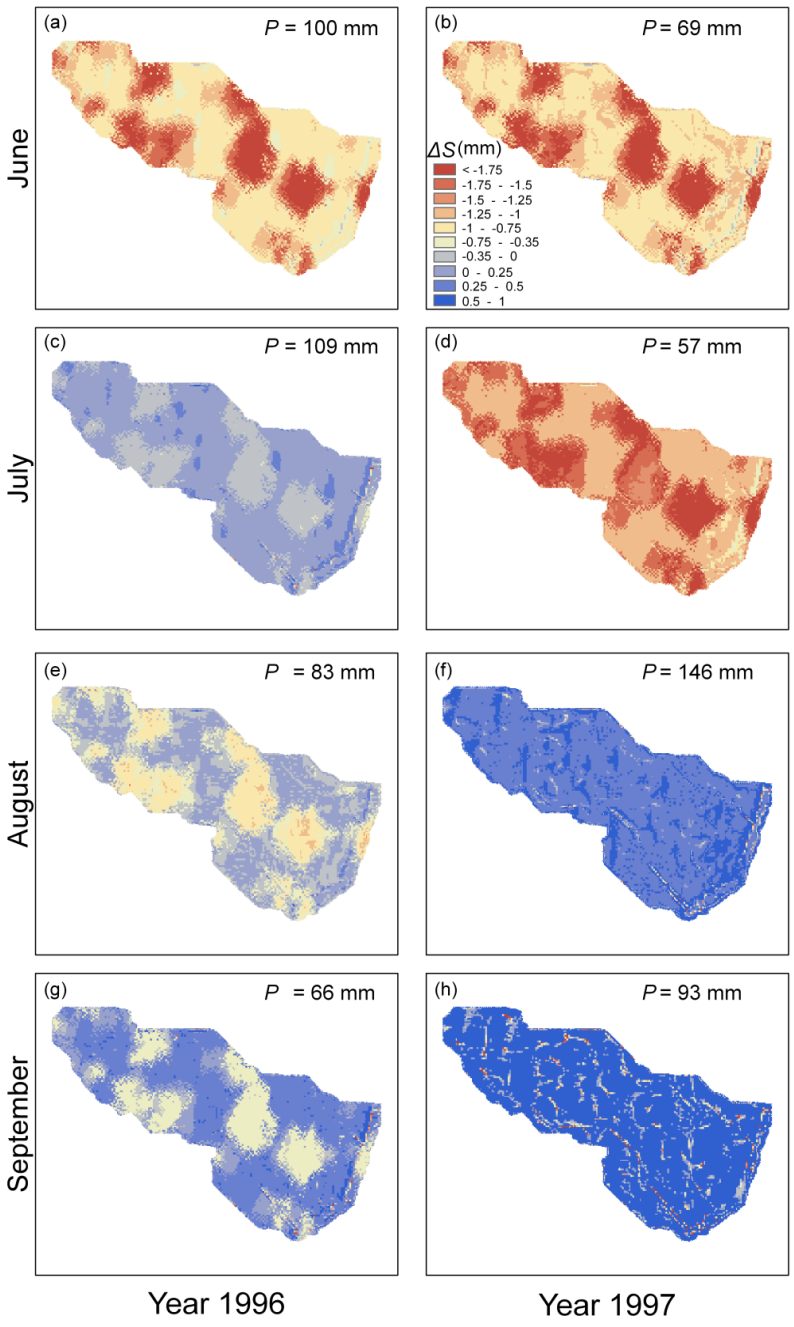

Figure 2.12. Spatial maps of the monthly storage change (ΔS in mm) for June through September during 1996 and 1997. Red colors indicate a decrease in storage, while blue colors depict a storage increase. The monthly precipitation (P in mm) is indicated for each map.

In 1997, a short drying period occurs in the early summer during which $<CV_{1\,m}>$

increases gradually until the rainfall onset. This is due to the increasing disparity

between grass and ponderosa pine areas. When the hillslope wets up, the $<CV_{1\,m}>$ decreases, an indication of the homogenization effect of the first rainfall. This is followed by another wetting sequence with frequent storms at low to moderate intensities. $<CV_{1\,m}>$ increases once again, due to the lateral redistribution of soil moisture controlled by terrain curvature, in particular for the later part of the NAM (September 1997), where $<q_l>$ frequently occurs (dashed lines). The rising importance of terrain on the spatial variability of θ is due to the large and frequent amounts of lateral transport in the hillslope. In contrast, hillslope dynamics during 1996 are impacted by a lower rainfall and a different distribution of drying and wetting periods. Note that the $<CV_{1\,m}>$ is much lower than in 1997 and that the lateral transport is subdued. As a result, a temporal switch in spatial controls from vertical to lateral fluxes is only observed under wet conditions in 1997.

2.4. Synthesis and Conclusions

Distributed model evaluations at hillslope scales are challenging. In this study, we present a hillslope model application based on: (1) high-resolution LIDAR data to describe topography and vegetation, (2) spatially-uniform soil properties and meteorological forcing, and (3) a distributed initialization of the perched saturation layer. More importantly, a set of spatial soil moisture observations at multiple depths and runoff collectors from different portions of the hillslope were available for model testing. We calibrated the distributed model during the 1997 summer season only against soil moisture data at 10 cm, and then independently evaluated the model with other observations in the same season

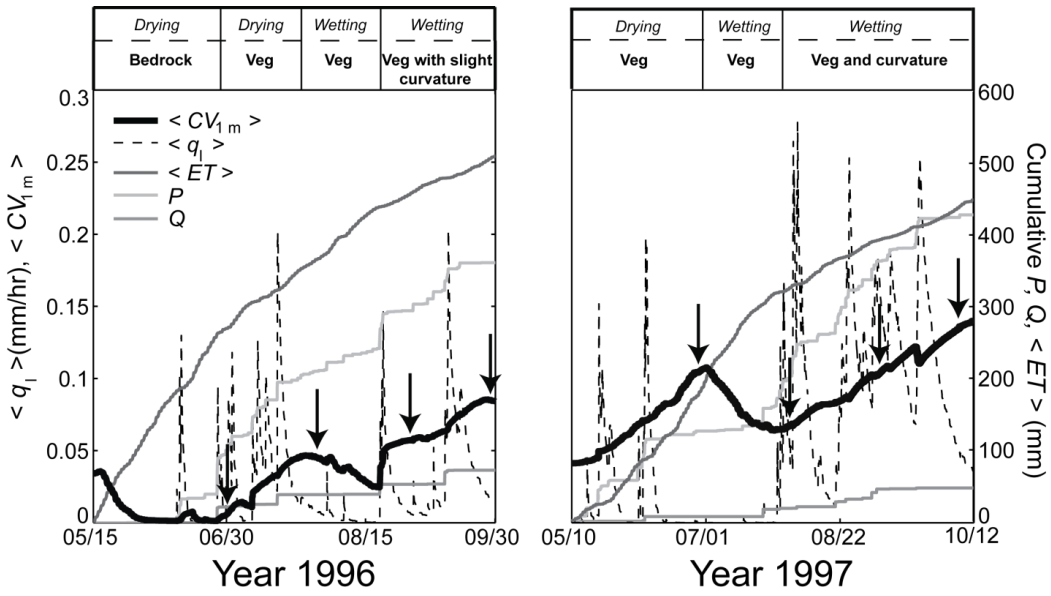

Figure 2.13. Seasonal dynamics of the coefficient of variation of soil moisture averaged over 1 m depth (<$CV_{1\,m}$>, dimensionless) and the spatially-averaged lateral transport (<q_l>, mm/hr) during 1996 and 1997. Cumulative rainfall, runoff and ET are plotted on the right hand side for reference. The arrows depict the time periods of the spatial maps shown in Figure 2.12. Drying and wetting periods along with the dominant spatial controls are labeled on the top of the graphs.

Year	Temporal RMSE (mm/hr)		
	Hillslope	**North**	**South**
1996	0.34	0.21	0.29
1997	0.25	0.21	0.26
1998	0.29	0.16	0.20

Table 2.5. Temporal root mean square error (RMSE in mm/hr) between simulated and observed hillslope outlet runoff, north slope runoff and south slope runoff.

and with the available soil moisture and runoff datasets in two other seasons. The distributed model performed well with respect to the soil moisture distributions and runoff dynamics in the ponderosa pine hillslope.

A comparison of model simulations with inferences from field observations of *Wilcox et al*. [1997] and *Newman et al*. [1997] is also instructive. The model exhibited a strong difference in soil moisture between ponderosa pine and grassland areas, due to varying interception, *ET* and infiltration dynamics. These results are consistent with the chloride concentrations of soil cores collected in summer 1993 by *Newman et al.* [1997]. Chloride concentrations at 10 cm depth beneath ponderosa pine were much higher than in the grassland, suggesting lower θ and higher *ET*. The model also produced runoff primarily through the infiltration-excess mechanism during the summer, consistent with *Wilcox et al*. [1997]. In the model, R_I can be produced either when the rainfall intensity is greater than the unsaturated hydraulic conductivity, or when a shallow layer of saturation occurs near the surface and impedes infiltration. The first case occurred in the early (dry) part of the season with a preference toward grass areas, while the second case was more common in the later (wet) period within the ponderosa pine. This distinction was not possible to identify in the field experiments due to the lack of runoff estimates within patches.

Locations	***Q*/*P***		***ET*/*P***	
	1996	**1997**	**1996**	**1997**
Hillslope	0.20	0.21	1.58	1.04
Tall ponderosa pine	0.24	0.20	1.97	1.27
Grassland	0.18	0.21	1.26	0.86

Table 2.6. Runoff (Q/P) and evapotranspiration (ET/P) ratios averaged over entire hillslope, tall ponderosa pine areas and grassland areas for 1996 and 1997.

During the wetter part of the 1997 season, the model exhibited a clear impact of lateral transport on the spatial variability of soil moisture, runoff response and storage dynamics. This response was found to be due to the high wetness during this period, induced by frequent rainfall events and relatively low *ET*. This near-saturated hillslope condition is comparable to snowmelt-driven saturation discussed in the *Newman et al*. [2004]. These authors inferred that the Bt horizon was the most conductive layer for lateral transport based on root density, soil moisture data and lateral flows in the trench. Due to the decrease in hydraulic conductivity with depth and high anisotropy ratio (Table 2.2), the model simulations also exhibit greater lateral flow above the Bt-CB boundary, consistent with *Newman et al*. [2004]. Our simple approach to mimic the effect of root macropore flow was through the use of a soil anisotropy ratio (A_s) that was in agreement with the range of root conductivity values presented by *Guan et al.* [2010].

The simulations also allowed identifying the mechanisms underlying the hillslope response. We focused attention on the landscape features responsible for

the spatial patterns in soil moisture and runoff generation. For all summer seasons, vegetation and terrain curvature imparted varying levels of control on the hillslope response under the assumption of spatially-uniform soils and meteorological forcing. During the early (dry) part of the summer, vertical fluxes, in particular transpiration accounting for 70 to 85% of *ET*, are responsible for the spatial patterns. The dominance of transpiration is consistent with evidence of *Newman et al.* [1998] suggesting a rapid bypassing of infiltration from the near-surface evaporation zone. In the dry period, infiltration-excess runoff is infrequent, of short duration, and related to the rainfall rate exceeding the surface hydraulic conductivity. Vegetation controls persist if relatively low rainfall occurs during the wetter part of the NAM or if long interstorm periods reduce soil moisture.

A climatic threshold in the hillslope response is crossed during periods of frequent rainfall and high soil moisture that are aided by lower *ET* resulting from high cloud cover in the 1997 season. Although there is high rainfall during the early summer in 1996, the threshold is not surpassed due to the infrequent nature of rainfall and cloud cover in the subsequent periods. As a result, the NAM conditions of 1996 fail to establish sustained lateral soil moisture fluxes. On the other hand, as the NAM progresses during 1997, the wetting of the hillslope can increase the lateral transport during and after rainfall events when near saturation conditions occur. Lateral transport resulted in spatial patterns that reflect the fine-scale details of surface topography, in particular the terrain curvature, rather than the patchiness of ponderosa pine and grass areas. It is important to note that this

transition is closely related to the switching of the dominance of vertical fluxes (*ET*) in the early (dry) season to terrain-mediated lateral fluxes (subsurface lateral transport) during the later (wet) period. The full transition between the two states occurred over a one-month period (August 8 to September 11, 1997) with frequent rainfall events and cloudy conditions. This model-based evidence suggests that a transition from local to nonlocal controls is possible in seasonally-wet, forested systems in semiarid regions, a finding that has not been previously made through field or modeling studies.

Temporal transitions of spatial controls due to wetting or drying have been discussed previously, particularly in modeling studies [e.g., *Grayson et al*., 1997; *Western et al*., 1999; *Loague*, 1988; *Kalma et al*., 1995; *Chamran et al*., 2002; *Teuling et al.*, 2007]. This transition is difficult to observe in nature due to the requirements of distributed measurements. *Western et al.* (1999) discussed the transition in observed soil moisture from terrain (wet state) to vegetation (dry state) controls in a different setting. In this study, we identified through modeling that semiarid forests have vegetation-controlled vertical fluxes that can easily prevent the generation of high soil moisture conditions conducive to terrain-mediated lateral transport. This is particularly true in the NAM region where the annual cycle of radiation and precipitation are in-phase [*Vivoni et al*., 2010], such that high soil moisture occurs along with high *ET* demand. As a result, we expect that crossing the hillslope response threshold is restricted to wetter-than-average NAM seasons, those exceeding ~400 mm from May through October. The sequencing of precipitation pulses during the NAM is also important for inducing

the transition. As shown in 1997, a series of frequent and intense storms and the reduction in *ET* due to cloudiness triggers sustained lateral fluxes. Based on long-term records, these conditions may currently occur at decadal intervals, but their likelihood could increase under greater NAM rainfall amounts induced by climate change (see *Woodhouse et al.* [2010] for a discussion). As a result, a useful avenue for future research would be to identify the seasonal rainfall properties (duration, intensity, frequency) and associated weather conditions leading to the transition in spatial controls. This could be achieved by linking a distributed hydrologic model with a stochastic weather generator tailored to the local climate data, as illustrated by *Ivanov et al.* [2008].

Our findings also have implications for the design of hillslope experiments, such as those through Critical Zone Observatories (CZOs). For example, to identify hillslope thresholds when lateral (nonlocal) fluxes become more critical than vertical (local) fluxes, multi-year studies able to sample across interannual variations are preferable. The ponderosa pine study afforded this opportunity due to its long period and thus provides an excellent, but rarely used, benchmark for hillslope-scale distributed models. Our results also point to the need for additional observations to further constrain modeling efforts, including: (1) continuous soil moisture data that samples different vegetation patches and fine-scale terrain features, (2) direct estimates of *ET* along with runoff and soil moisture data, and (3) direct or inferred runoff estimates within the hillslope. Other desirable data include the partitioning of rainfall into throughfall and stemflow; the partitioning of *ET* into soil evaporation and transpiration; and field-

based estimates of vegetation and soil property patterns. We found the LIDAR-derived topography and canopy heights and the trench system for runoff and lateral flow collection to be invaluable and encourage their full use in future hillslope studies to improve the spatial representations of internal conditions.

The application of a distributed model can also help determine optimal sensor locations that can track hydrologic fluxes and states leading to the crossing of the hillslope threshold. Existing or planned sensor sites in a hillslope experiment can be evaluated with respect to their ability to capture transitions between local and non-local controls given the sparse nature of the observational network. For example, the simulations of *Ivanov et al.* [2010] for an experimental semiarid hillslope designed for Biosphere 2 would allow the selection of sensor locations that best capture the spatial heterogeneity in soil moisture and its temporal variations. The authors also found that lateral fluxes impacted soil moisture patterns, albeit under a set of different conditions (steeper slopes, more conductive soil, shrub vegetation). Our study indicates that terrain-mediated lateral fluxes are possible in the more restrictive case of forested hillslopes of gentle relief with less conductive soils. This finding has implications on field and modeling studies in semiarid systems concerned with water transit times, biogeochemical fluxes or weathering rates. Further, the joint use of distributed field and modeling studies at the hillslope scale can help predict important climate and land cover change impacts that are anticipated for the southwestern United States [e.g. *Woodhouse et al*., 2010; *Williams et al*., 2010].

3. Breakdown of Hydrologic Patterns upon Model Coarsening at Hillslope Scales and Implications for Experimental Design

3.1. Introduction

Simulating reliable spatial hydrologic patterns is critical for: (1) understanding the connections between the biosphere, atmosphere and lithosphere [e.g. *Bertoldi et al.*, 2010; *Vivoni et al.*, 2008, 2010], (2) identifying the spatiotemporal controls of land surface properties [e.g. *Teuling and Troch*, 2005; *Minet et al.*, 2011], (3) predicting the hydrologic response arising from changes in land cover or climate [e.g. *Cuo et al.*, 2008; *Cayan et al.*, 2010] and (4) enhancing the understanding of hydrologic processes by policy makers and resource managers [e.g. *Georgakakos and Carpenter*, 2006]. Fine-resolution (<1 to 10 m) simulations are considered to be essential for reproducing realistic spatial patterns, as the actual representations of topography, soil and vegetation characteristics are important when evaluating models with data [*Grayson et al.*, 2002; *Rößler and Löffler,* 2010]. Current practice is to use coarse resolution domains (~30 to 100 m) due to the computational burden of simulations and the lack of adequate fine-resolution data sets to capture small-scale features in a landscape. In coarse models, hillslopes are typically not depicted at high resolution and, as a result, the impact of coarsening on hillslope-scale patterns is poorly understood [e.g. *Weschsler*, 2007]. Is there a particular model resolution threshold beyond which the fidelity of simulated soil moisture patterns is lost?

Considering the effects of model resolution on hydrologic responses is essential for reliable predictions [*Famiglietti and Wood,* 1994]. Thus, significant attention has been placed in prior studies on identifying the influence of model resolution in grid-based models [e.g. *Vieux,* 1991; *Kuo et al.,* 1999; *Molnar and Julien,* 2000; *Vázquez et al.,* 2002; *Haddeland et al.,* 2002; *Chaubey et al.,* 2005; *Cochrane and Flanagan,* 2005; *Cho and Lee,* 2007; *Dixon and Earls,* 2009; *Zhao et al.,* 2009], in distribution-function models [e.g. *Zhang and Montgomery,* 1994; *Wolock and Price,* 1994; *Bruneau et al.,* 1995; *Higy and Musy,* 2000] and in distributed models using irregular discretizations [*Vivoni et al.,* 2005]. In general, prior studies have focused on the integrated basin response such as the outlet discharge, without considering spatial patterns. Since distributed models offer the potential to predict internal basin states, it is important to evaluate the spatial sensitivity to coarsening across a range of scales, from hillslopes to large river basins.

At the hillslope scale, *Mahmood and Vivoni* [2011a] conducted a set of fine-resolution (~0.3 m) simulations that revealed the controls of terrain and vegetation features on the spatial patterns in soil moisture and runoff production. For this ponderosa pine hillslope, topographic attributes, in particular curvature, varied at smaller scales than the patchy forest stands. These simulations provide an excellent opportunity to test the impact of model coarsening through alternative domain representations. We hypothesize that decreasing the resolution modifies hillslope characteristics, such as topography and vegetation cover, in ways that depend on the spatial scale of each feature [see *Kavvas,* 1999]. These

modifications, in turn, will impact the spatial controls on soil moisture and runoff patterns. The lack of spatially-distributed data on subsurface properties (soil hydraulic parameters and depth) limits our ability to analyze the model resolution sensitivity to soil patterns. Thus, we seek to identify a threshold resolution beyond which the simulations no longer resemble the finest resolution case and to explore the impacts of aggregation of the small-scale (terrain) and large-scale (vegetation) features.

In the following, we present the study site and briefly review the model application of *Mahmood and Vivoni* [2011a]. We then discuss the gradual resolution coarsening and the model setup for the different simulations. Differences in the soil moisture and runoff spatial patterns among model resolutions are quantified using probability density functions, an index of spatial homogeneity, correlation coefficients, and error fields. Our objective is to use a range of metrics to quantify the threshold resolution (or break-point) for simulating reliable spatial patterns. We also examine the implications of model coarsening on the design of hillslope experiments. By using the finest resolution model, we identify the errors introduced by coarser models when sampling is allowed at a subset of locations. Since field experiments are often limited in their spatial sampling, we provide guidance to help determine sampling sites that either minimize spatial errors or reduce the sensitivity to model resolution.

3.2. Methods

3.2.1. Study area and field observations

The study area is a ponderosa pine (*Pinus ponderosa*) hillslope (~1280 m^2) at the Los Alamos National Laboratory (LANL), New Mexico, USA (Figure 3.1). At the site, soil moisture and runoff observations are available from extensive field studies [e.g. *Wilcox et al.*, 1997; *Newman et al.*, 1998; *Brandes and Wilcox*, 2000]. In addition, spatial datasets describing topography and forest cover are available from a LIght Detection And Ranging (LIDAR)-based digital elevation model (DEM) and vegetation height model, each at 0.305 m resolution. The LIDAR products were derived as part of repeat airborne surveys at LANL using techniques for bare-earth and canopy detection [e.g. *Canfield et al.*, 2005]. As with other topographic products, inaccuracies in the LIDAR data could propagate to derived terrain attributes. The hillslope is gently sloping and low in relief (~6 m), with an average elevation of 2315 m, decreasing from west to east. The vegetation is characterized as open ponderosa pines with intercanopy grasses. Available field data include volumetric soil moisture estimates (m^3/m^3) at 14 sampling locations using a neutron probe (NP) placed at different depths through access tubes. In this study, we used soil moisture at 10 cm and averaged over the top 1 m during the summer periods in 1996, 1997 and 1998, with a focus on May through October, 1997 (Figure 3.2). Additional datasets include hourly weather forcing and hillslope runoff estimates (mm/hr) from a trench along the eastern

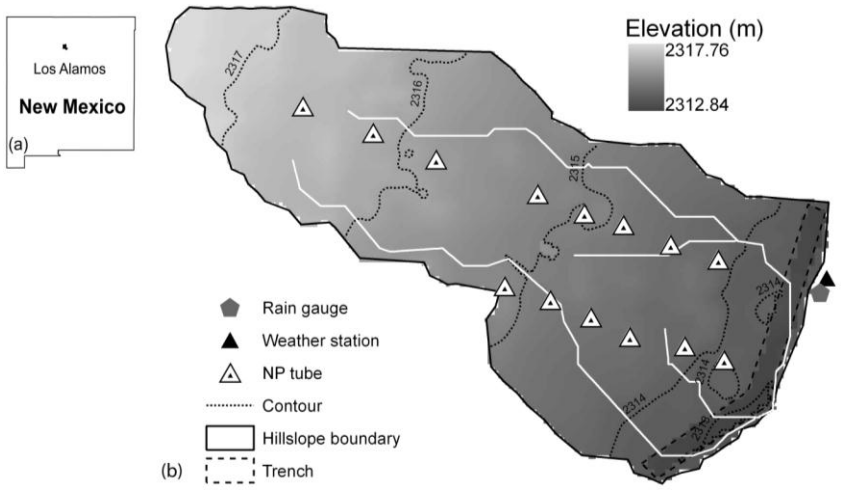

Figure 3.1. Study site. (a) Los Alamos county in New Mexico, USA. (b) Ponderosa pine hillslope modeling domain including locations of neutron probes (NP), rain gauge and weather station. White lines represent the flow lines in the hillslope domain.

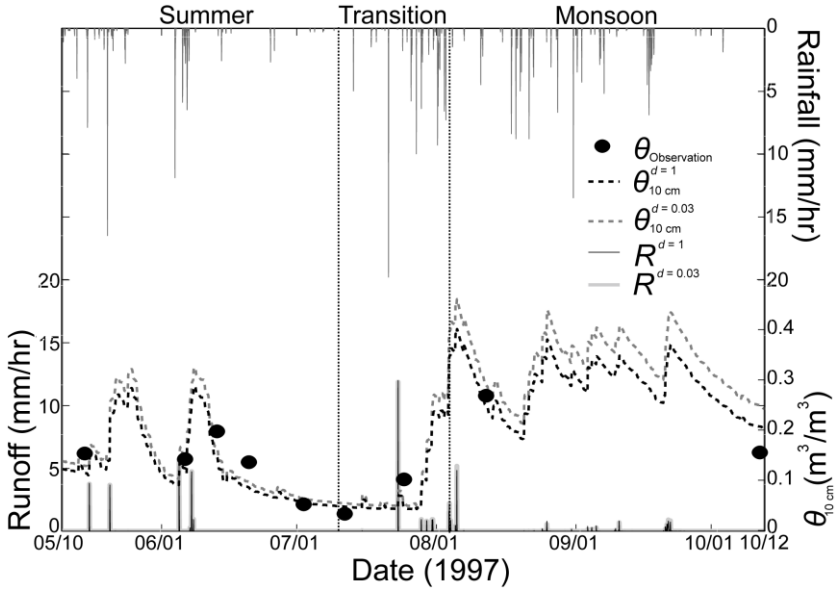

Figure 3.2. Simulated soil moisture and runoff using the finest (d = 1) and coarsest (d = 0.03) model resolutions for 1997. Black circles represent observed spatially-averaged soil moisture at 10 cm depth from 14 sampling locations. Dashed lines depict simulated spatial average at the sampling locations. The durations of summer (May 10 to July 9), transition (July 10 to August 6) and monsoon (August 6 to October 12) periods are shown.

boundary. The reader is referred to *Mahmood and Vivoni* [2011a] for additional details on the field observations.

3.2.2. Distributed hydrologic model

We used the Triangulated Irregular Network (TIN)-based Real-time Integrated Basin Simulator (tRIBS) to study the impacts of model coarsening on hillslope simulations. tRIBS is a spatially-distributed model with physically-based processes [*Ivanov et al.,* 2004a,b; *Vivoni et al.,* 2007] used in a wide range of applications. At the hillslope scale, the model simulates vertical and lateral dynamics in the unsaturated and saturated zones within a spatially-connected system of Voronoi polygons derived from the TIN [*Vivoni et al.,* 2004; *Noto et al.,* 2008]. Hydrologic processes include rainfall interception, infiltration, evapotranspiration, water table fluctuations, lateral subsurface transport and runoff production and routing. Relevant outputs for this study are the spatiotemporal patterns of soil moisture and infiltration-excess runoff as well as the hillslope outlet runoff. Model calibration and testing using a fine-resolution TIN (d = 1, as explained in the following section) was conducted by *Mahmood and Vivoni* [2011a] through a comparison of distributed soil moisture and outlet runoff simulations to field data. These comparisons assumed a uniform soil depth (i.e. thickness above the Bandelier Tuff horizon) of 1.06 m derived from site observations (see *Mahmood and Vivoni*, [2011a] for a discussion). Figure 3.2 illustrates the model performance in the 1997 summer season at the finest resolution (black lines) for soil moisture at 10-cm depth ($\bar{\theta}_{10cm}$) and the outlet

runoff (R). Good model performance is achieved with a root mean square error (RMSE) in $\bar{\theta}_{10cm}$ of 0.040 m^3/m^3 and R of 0.25 mm/hr. For more details on the model calibration and evaluation, the reader is referred to *Mahmood and Vivoni* [2011a].

3.2.3. Model coarsening and aggregated fields

We coarsened the hillslope domain by reducing the number of TIN nodes derived from the LIDAR DEM, as shown by *Vivoni et al.* [2005]. We define the model resolution (d) using the ratio of the number of TIN nodes (n_t) to the number of grid cells in the DEM (n_g = 13,181). For a fair comparison across resolutions, we retain the same number of nodes along flow lines (n_{fl} = 507) and the trench area (n_{tr} = 451), as shown in Figure 3.1. Thus, the resolution is computed as:

$$d = \frac{n_t - n_{fl} - n_{tr}}{n_g - n_{fl} - n_{tr}} \quad . \qquad (1)$$

We varied d from 0.03 to 1 to generate six different model domains, where d = 1 indicates the fine-resolution case used by *Mahmood and Vivoni* [2011a]. A useful metric for comparison is the equivalent cell size (r_e) for each domain, defined by *Vivoni et al.* [2005] as $r_e = r/\sqrt{d}$, where r is the DEM cell size (r = 0.305 m here). Table 3.1 reports r_e for all domains, ranging from 0.305 m (d = 1) to 1.76 m (d = 0.03). Further reductions in d are possible, but the number of Voronoi polygons retained between flow lines is essentially unchanged.

Property (unit)	Metric	d = 1	d = 0.5	d = 0.25	d = 0.1	d = 0.05	d = 0.03
Equivalent cell size (m)	r_e	0.305	0.431	0.610	0.964	1.36	1.76
Elevation (m)	μ	2315.17	2315.06	2314.88	2314.62	2314.27	2314.17
	σ	1.18	1.29	1.33	1.34	1.28	1.26
Curvature (dimensionless)	μ	$2.54\text{x}10^{-4}$	$-1.77\text{x}10^{-5}$	$-2.82\text{x}10^{-5}$	$5.35\text{x}10^{-6}$	$2.07\text{x}10^{-3}$	$2.32\text{x}10^{-3}$
	σ	3.71	36.44	41.44	55.78	0.44	10.99
Slope (radians)	μ	0.12	0.16	0.19	0.21	0.19	0.19
	σ	0.14	0.22	0.24	0.24	0.22	0.22
Vegetation height (m)	μ	5.43	5.86	5.68	5.21	4.90	4.82
	σ	6.27	6.48	6.32	6.05	5.83	5.77

Table 3.1. Variation of hillslope properties as a function of model resolution, including the spatial mean (μ) and standard deviation (σ) of the fields.

Figure 3.3 illustrates the impact of model coarsening on the Voronoi polygon discretization. The Voronoi Polygon Network (VPN) is the dual diagram of the TIN and polygons constitute the control-volumes for mass balance and flux computations in tRIBS [*Ivanov et al.*, 2004a]. As the model is coarsened, spatial aggregation occurs for all properties assigned to each polygon. Table 3.1 reports the spatial mean (μ) and standard deviation (σ) of terrain properties (elevation, slope, curvature) and vegetation height, derived from the model aggregation of the LIDAR DEM and vegetation heights. Note that soil properties and weather forcing are spatially-uniform in these simulations. As shown by *Mahmood and Vivoni* [2011a], curvature and vegetation exert spatial controls on the modeled response. As a result, Figure 3.3 also shows the aggregation of these two

properties. Clearly, the spatial pattern of small-scale curvature features deteriorate quickly with model coarsening (by d = 0.25), while the large-scale vegetation patches persist. By design, the six simulations (d = 1 to 0.03) only differ in the domain discretization and sampling of terrain and vegetation properties. As in *Vivoni et al.* [2005], we retained the same soil, vegetation and routing parameters across all simulations reflecting the calibration effort for d = 1 [*Mahmood and Vivoni*, 2011a]. We also used the same initial conditions for all resolutions for several reasons: (1) seasonal simulations do not allow dynamic equilibration through periodic forcing, and (2) early summer dry-downs quickly reduce the impact of initial conditions. Model initialization consists of specifying the distributed depth to perched saturation by matching the modeled soil moisture (at d =1) to the sampling location data for the first observation date. Figure 3.2 presents an example of the initial conditions for fine (d = 1) and coarse (d = 0.03) resolutions. Differences of $\bar{\theta}_{10cm}$ ~ 0.02 m^3/m^3 in the summer period are dissipated in the transition period. As a result, the wetter conditions in d = 0.03 during the monsoon period (by $\bar{\theta}_{10cm}$ ~ 0.05 m^3/m^3) are no longer related to differences in initial state. Note the RMSEs with respect to observations increase slightly in $\bar{\theta}_{10cm}$ to 0.043 m^3/m^3 and in R to 0.28 mm/hr for d = 0.03, indicating that the calibration at d = 1 is also adequate for coarse resolutions for these integrated measures.

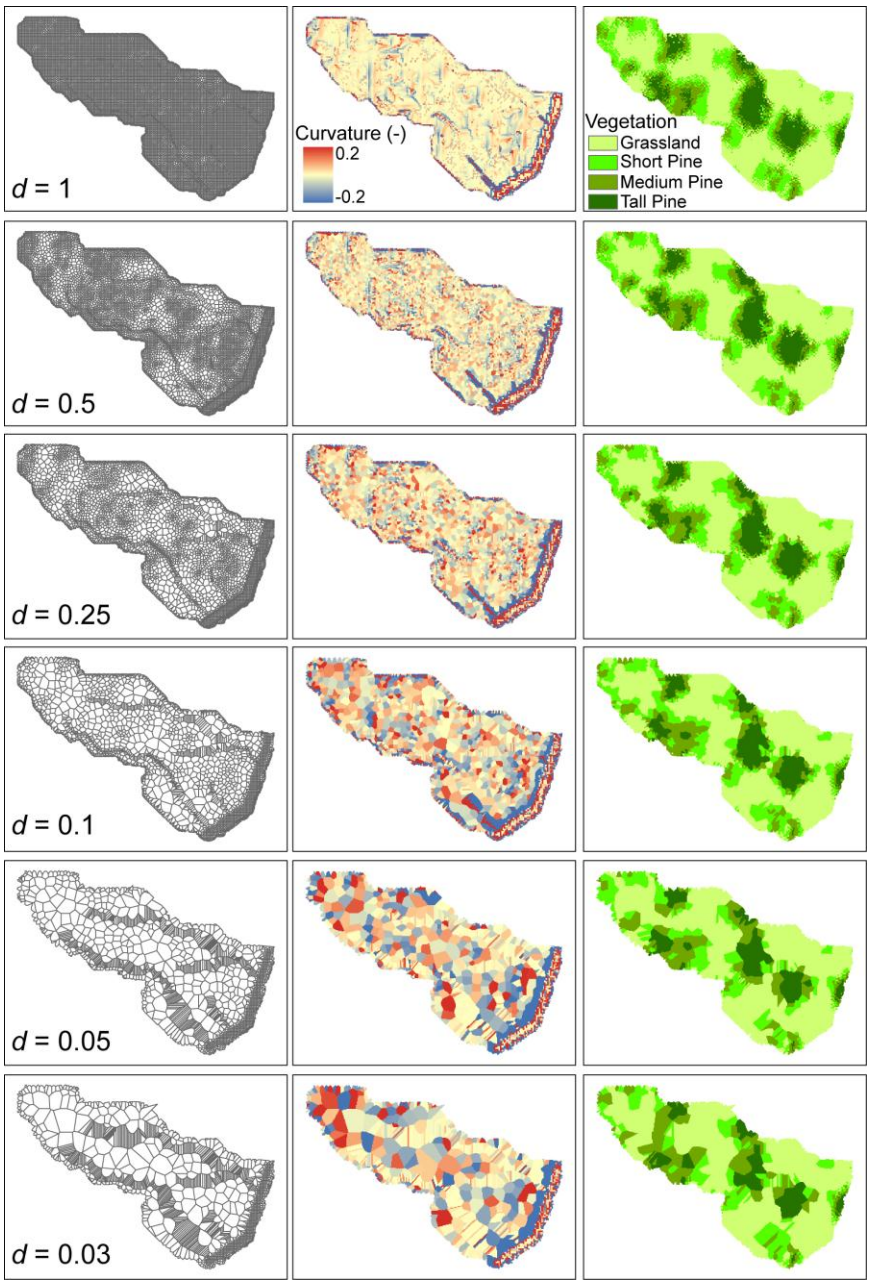

Figure 3.3. Impacts of model coarsening on hillslope discretization, curvature and vegetation classes from d = 1 (top) to d = 0.03 (bottom).

3.2.4. Spatial metrics to assess model coarsening

We used a range of quantitative metrics to identify the impact of model coarsening on the spatiotemporal patterns of soil moisture and runoff production.

An initial evaluation consisted of assessing the spatial probability density function (pdf) of temporally-averaged surface ($\bar{\theta}_{10cm}$) and root zone ($\bar{\theta}_{1m}$) soil moisture over three periods in 1997 (Figure 3.2). Then, we used the fraction homogeneity cover (f_c) and Pearson correlation coefficient (ρ) to compare spatial soil moisture and runoff fields between model resolutions. f_c indicates the degree of homogeneity of a spatial field and is based on a terrain index derived by *Gallant and Dowling* [2003]. Both f_c and ρ are used to find a threshold resolution at which the fidelity of the simulated patterns breaks down.

The fraction homogeneity cover (f_c) is based on the areal fraction of a domain that is found to have a homogeneity index (F) above a certain threshold (F_o) as:

$$f_c = \frac{A_{F \geq F_o}}{A} \quad , \qquad (2)$$

where A is the total area and $A_{F \geq Fo}$ is the area having $F \geq F_o$. Appendix A presents details on the estimation of F for a spatial field. In general, a low F value indicates that a field exhibits strong heterogeneity, while high F indicates homogeneity or smoothness of variation of the spatial field. Preliminary analyses of the homogeneity of soil moisture, runoff and curvature fields indicated that a threshold of F_o = 1.9 was appropriate for determining spatial homogeneity in this study.

3.2.5. Spatial error measures between model resolutions

Model coarsening causes spatial errors in simulated patterns of soil moisture, relative to the fine resolution (d = 1) fields. We identified zones with large errors in θ_{10cm} by using the root mean squared error (RMSE) between d = 1 and the coarser resolutions, as:

$$\theta_{RMSE} = \sqrt{\frac{\sum_{n=1}^{N}\left(\{\theta\}_{10cm}{}^{d<1} - \{\theta\}_{10cm}{}^{d=1}\right)^2}{N}} \quad , \quad (3)$$

where $\{\theta\}_{10cm}$ is the set of Voronoi polygons over which errors are calculated and N is the number of hourly time steps (N = 3744 for 1997). To compute θ_{RMSE}, we resampled model resolutions to a 0.17 m grid (or 0.5r) to capture sharp changes and boundary features, such that the set was ~42,379 pixels. We also derived curvature (c_{diff}) and vegetation height difference (H_{diff}) fields as:

$$c_{diff} = c^{d<1} - c^{d=1} \quad \text{and} \quad (4)$$

$$H_{diff} = H^{d<1} - H^{d=1} \quad . \quad (5)$$

Positive c_{diff} indicates an increase in concavity, while a positive H_{diff} occurs for increased tree height due to coarsening (and vice versa).

We are interested in identifying locations that induce high spatial error and linking these to curvature and vegetation differences across resolutions. To so do, we utilized thresholds in θ_{RMSE}, c_{diff} and H_{diff} consisting of exceedences of the spatial mean (μ) ± 1 standard deviation (σ). Areas (denoted θ_τ, c_τ and H_τ) were identified where the errors exceeded the threshold values as:

$$\theta_\tau : \theta_{RMSE} > \theta_{t1} \qquad \theta_{t1} = \mu(\theta_{RMSE}) + \sigma(\theta_{RMSE}) \ , \tag{6}$$

$$c_\tau : \begin{matrix} c_{diff} > c_{t1} & c_{t1} = \mu(c_{diff}) + \sigma(c_{diff}) \\ c_{diff} < c_{t2} & c_{t2} = \mu(c_{diff}) - \sigma(c_{diff}) \end{matrix} \quad \text{and} \tag{7}$$

$$H_\tau : \begin{matrix} H_{diff} > H_{t1} & H_{t1} = \mu(H_{diff}) + \sigma(H_{diff}) \\ H_{diff} < H_{t2} & H_{t2} = \mu(H_{diff}) - \sigma(H_{diff}) \end{matrix} \ . \tag{8}$$

To assess error sources, an intersection of areas with high soil moisture errors (θ_τ) with those exhibiting high errors in curvature (c_τ) and vegetation height (H_τ) was carried out. Intersections, $\theta_\tau \cap c_\tau$ and $\theta_\tau \cap H_\tau$, were determined between soil moisture errors and c_{diff} and H_{diff} that are +1 and -1 standard deviations away from the spatial mean value.

3.3. Results and Discussion

3.3.1. Coarsening impacts on soil moisture patterns

Figure 3.4 presents the impacts of model coarsening on $\bar{\theta}_{10cm}$ during the 1996, 1997 and 1998 periods. Spatially-averaged soil moisture (μ) follows the accumulated rainfall in each season: 1996 (358 mm, μ = 0.13 m^3/m^3), 1997 (423 mm, μ = 0.23 m^3/m^3), and 1998 (167 mm, μ = 0.10 m^3/m^3). Heterogeneous soil moisture patterns occur during each season at d = 1, with a stronger control exerted by ponderosa patches (Figure 3.3) in 1996 and 1998. As model resolution coarsens during the drier seasons, $\bar{\theta}_{10cm}$ patterns undergo minor distortions due to the larger scale of the vegetation features. For the wetter 1997 season, however, both curvature and vegetation control the spatial distribution of $\bar{\theta}_{10cm}$. *Mahmood*

and Vivoni, [2011a] attributed this to the effects of lateral redistribution during wet days and of pine transpiration during drier days. As a result, spatial soil moisture patterns are more sensitive to coarsening in 1997, as small scale terrain curvature features are readily eliminated upon aggregation. Resolutions coarser than d = 0.1 no longer exhibit terrain-mediated patterns. Based on this visual comparison, we infer that the drier 1996 and 1998 simulations show relatively low spatial sensitivity, whereas the wet 1997 season has a strong dependence on model resolution. Thus, we focus on this season for further analysis.

We analyzed the impact of coarsening on the pdf of temporally-averaged root zone soil moisture, $p(\bar{\theta}_{lm})$, during three periods: summer, transition and monsoon (Figure 3.5). For clarity, only three model resolutions are shown (d = 1, 0.25 and 0.03). In each case, we classify $p(\bar{\theta}_{lm})$ according to the vegetation type to investigate spatial sensitivities for each class. Note that the summer and transition periods exhibit limited variations with resolution, but show a partitioning into dry ponderosa patches and wet grassland areas. This is most clearly seen in the transition period, where $\bar{\theta}_{lm}$ = 0.25 m^3/m^3 divides dry pine and wet grass regions, leading to bimodality in $p(\bar{\theta}_{lm})$. During the monsoon period, the pdfs for d = 1 and 0.25 are normally-distributed, an indication of the curvature control on the spatial distribution, as all vegetation types experience a broader range of $\bar{\theta}_{lm}$. At d = 0.03, however, the shape of the pdf becomes distorted and exhibits characteristics that suggest a weakening of the curvature control and strengthening of vegetation effects. This analysis reveals that the spatial

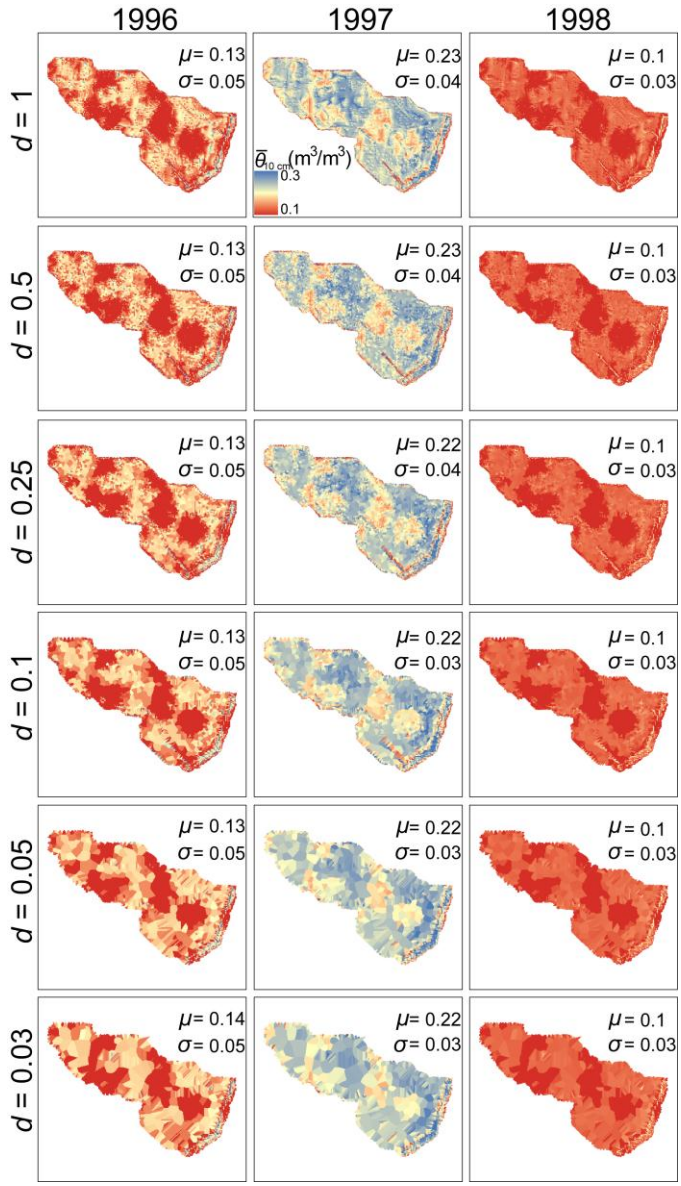

Figure 3.4. Coarsening of temporally-averaged shallow soil moisture ($\bar{\theta}_{10cm}$) during 1996, 1997 and 1998 periods. Spatial mean (μ) and standard deviation (σ) are shown for each map. Temporal averaging performed over May 15 to September 30 (1996), May 10 to October 12 (1997), and May 15 to August 12 (1998).

sensitivity is primarily concentrated in the monsoon period, where lateral fluxes

redistribute root zone moisture following small-scale terrain features.

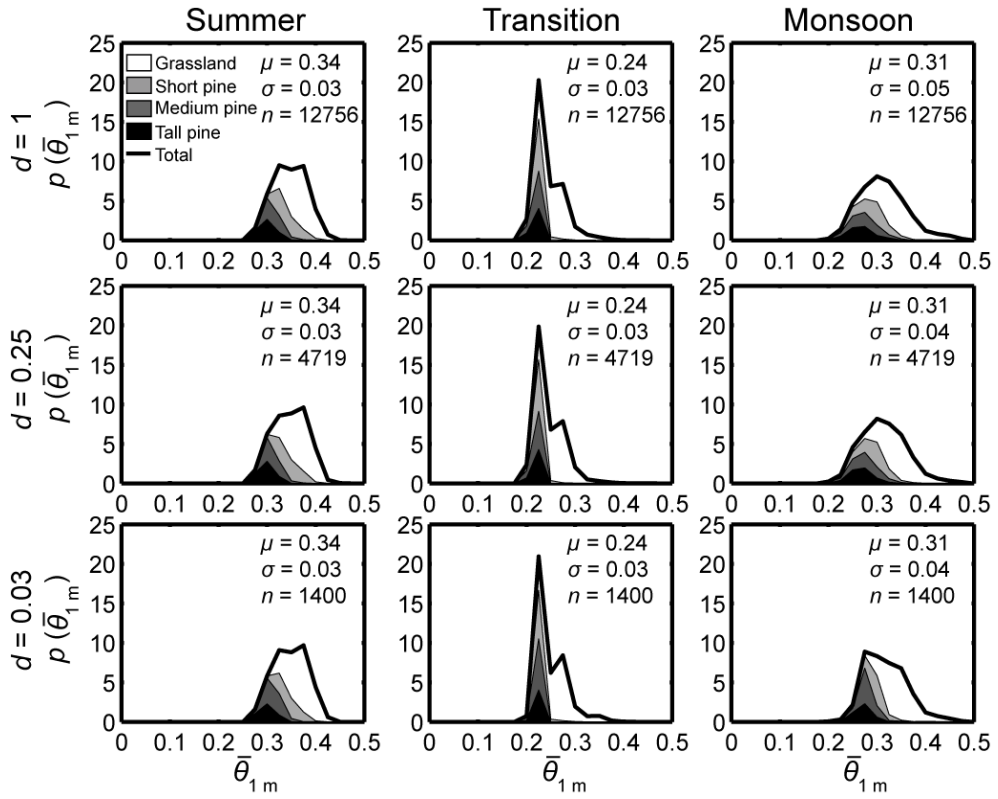

Figure 3.5. Coarsening of temporally-averaged shallow soil moisture ($\bar{\theta}_{1m}$) during 1996, 1997 and 1998 periods. Spatial mean (μ) and standard deviation (σ) are shown for each map. Temporal averaging performed over May 15 to September 30 (1996), May 10 to October 12 (1997), and May 15 to August 12 (1998).

To explore the impacts of coarsening on the curvature-mediated lateral fluxes, we present the pdf of temporally-averaged surface soil moisture, $p(\bar{\theta}_{10cm})$, for the monsoon period in Figure 3.6. Surface soil moisture in the monsoon period is expected to be more sensitive to the aggregation of the terrain field due to the greater wetness at shallower depth [e.g. *Western et al.*, 1999]. In this case, we classify the pdfs according to curvature (c) in three categories: Convex ($c < -0.01$), Planar ($-0.01 \leq c \leq 0.01$) and Concave ($c > 0.01$). As expected, concave areas exhibit higher soil moisture values than convex regions at all resolutions, with planar sites having intermediate values. While the total $p(\bar{\theta}_{10cm})$ only varies

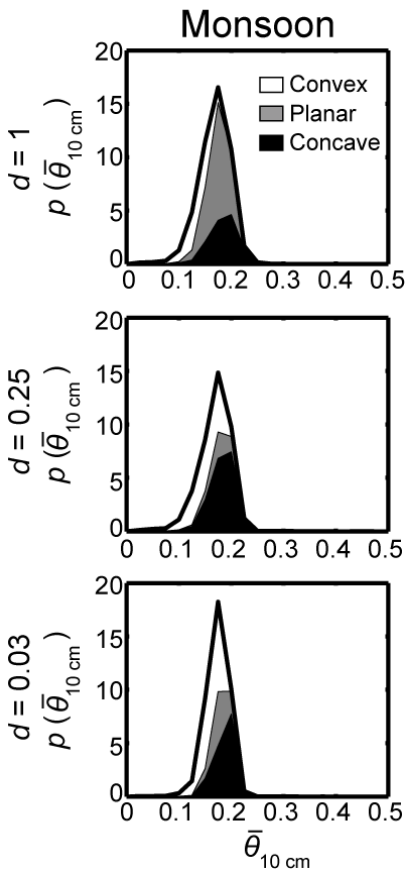

Figure 3.6. Probability density functions of temporally-averaged surface soil moisture, $p(\bar{\theta}_{10cm})$, with contributions by convex, planar and concave areas for entire 1997 period. The thick black lines represent the total distributions.

slightly with *d*, the proportion of convex and concave sites grows substantially due to a reduction of planar sites (also see Figure 3.3). As a result, coarsening distorts the curvature field, leading to large variations in the proportion of wet concave areas and dry convex sites, with impacts on lateral redistribution during wet periods.

3.3.2. Identifying a threshold resolution through spatial metrics

Figure 3.7 shows the homogeneity (*F*) field of the curvature, vegetation height, temporally-averaged $\bar{\theta}_{10cm}$ and infiltration-excess runoff rate (R_i) at d = 1,

0.25 and 0.03, along with the fraction homogeneity cover (f_c). Red (blue) areas representing homogeneous (heterogeneous) regions around a location increase (decrease) with model coarsening. As a result, f_c increases with the aggregation of each spatial field. Vegetation distributions are more homogenous (higher F) than the curvature field and undergo a lower change due to coarsening (smaller increase in f_c across d). Thus, the impact of aggregation is more prominent on curvature as small-scale features (convex, planar, concave) are quickly merged into larger patches. The time-averaged responses, $\bar{\theta}_{10cm}$ and R_i, exhibit low fractions of homogeneity cover ($f_c < 0.1$) at $d = 1$, with the signature of curvature on the homogeneity (F) of $\bar{\theta}_{10cm}$. Upon coarsening, f_c increases dramatically (by factors of ~100 and 1000), suggesting a stronger spatial sensitivity than experienced by the underlying vegetation and curvature fields. At $d = 0.03$, the homogeneity of $\bar{\theta}_{10cm}$ resembles a hybrid of the curvature and vegetation F fields, while F for R_i is similar to the curvature homogeneity field.

To further explore the homogenization with model coarsening, Figure 3.8 presents variations of f_c with d for curvature, vegetation height, $\bar{\theta}_{10cm}$, $\bar{\theta}_{1m}$, R_i and the frequency of occurrence of infiltration-excess runoff (T_{R_i}). Coarsening ($d = 1$ to 0.03) clearly increases f_c in all cases. For surface and root zone soil moisture ($\bar{\theta}_{10cm}$ and $\bar{\theta}_{1m}$), f_c exhibits an asymptotic behavior bounded by the vegetation f_c at low d and by curvature f_c at high d. Thus, the fractional homogeneity indicates small-scale curvature controls at fine resolutions and larger-scale vegetation controls at coarser resolutions. On the other hand, the variation of runoff f_c with coarsening (R_i and T_{R_i}) does not exhibit the same switching of spatial controls,

more closely resembling the curvature f_c pattern at all resolutions. The variation of f_c with d for all hydrologic responses can also be used to identify a threshold resolution upon which the spatial patterns are significantly impacted. For this case, d = 0.1 (10% of the original DEM) marks the transition between small-scale curvature controls on the f_c of $\bar{\theta}_{10cm}$ and $\bar{\theta}_{1m}$ and the larger-scale vegetation height controls at coarser resolutions. This threshold resolution corresponds to an equivalent cell size, $r_e \sim 1$ m, such that aggregations that surpass a 1 m resolution grid impact the hillslope hydrologic response in this study. Below d = 0.1, soil moisture f_c is more distant from the curvature f_c, suggesting a breakdown of curvature effects on soil moisture patterns.

To confirm this finding, we show the linear correlation coefficient (ρ) between landscape properties and the spatial hydrologic responses in Figure 3.9. ρ between soil moisture variables ($\bar{\theta}_{10cm}$ and $\bar{\theta}_{1m}$) and curvature are invariant between d =1 and the identified threshold resolution (d = 0.1). Below d = 0.1, the correlation weakens significantly (i.e. closer to zero), an indication of the breakdown of curvature controls on soil moisture. As a consequence, ρ between vegetation height and $\bar{\theta}_{10cm}$ exhibits a stronger negative correlation below d = 0.1 (i.e. further from zero), confirming an increase in vegetation controls at coarser resolutions. Note, however, that the correlation of vegetation height and $\bar{\theta}_{1m}$ increases slightly (more negative) with lower d due to the higher impact of evapotranspiration on root zone soil moisture [*Mahmood and Vivoni*, 2011a]. ρ between the runoff variables (R_i *and* T_{R_i}) and landscape properties exhibit consistent patterns. As resolution is coarsened below d = 0.1, runoff spatial

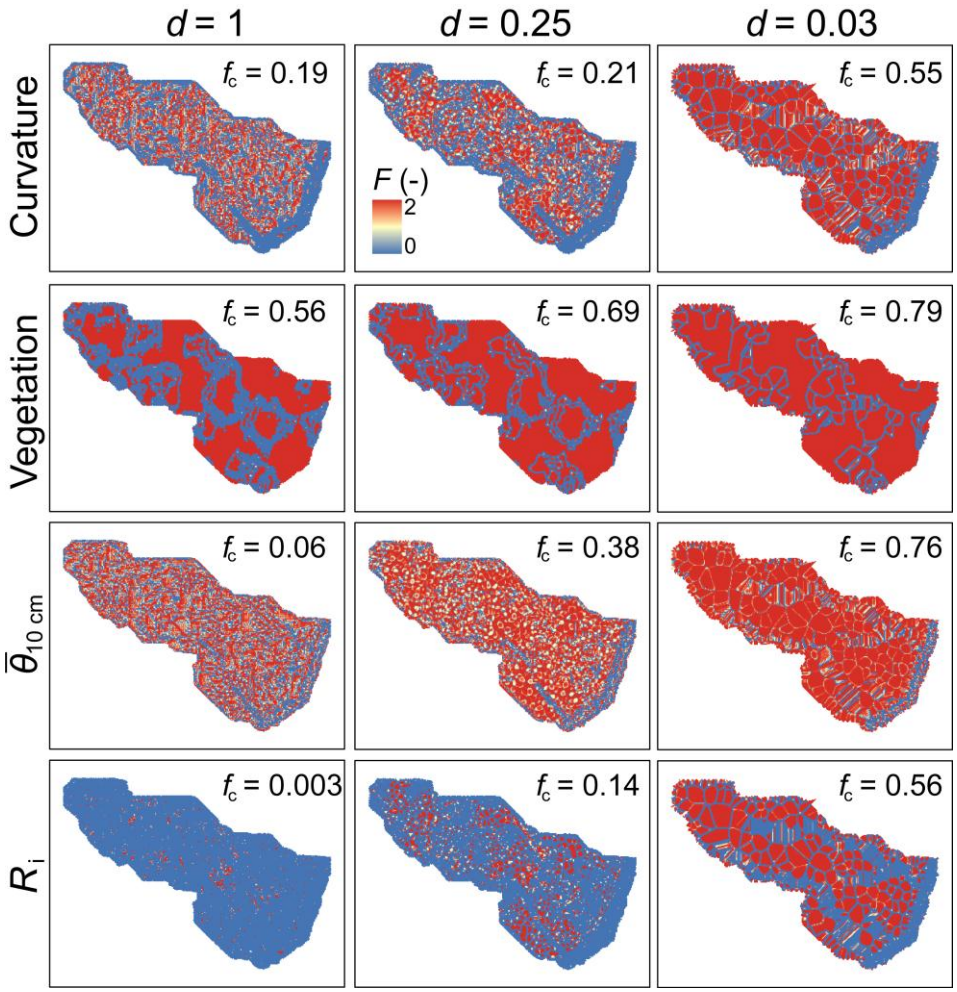

Figure 3.7. Spatial maps of homogeneity (F) of curvature, vegetation height, temporally-averaged surface soil moisture ($\bar{\theta}_{10cm}$) and temporally-averaged runoff rate (R_i) for three resolutions.

patterns exhibit greater correlation (i.e. higher absolute ρ) with vegetation and

lower correlation with curvature.

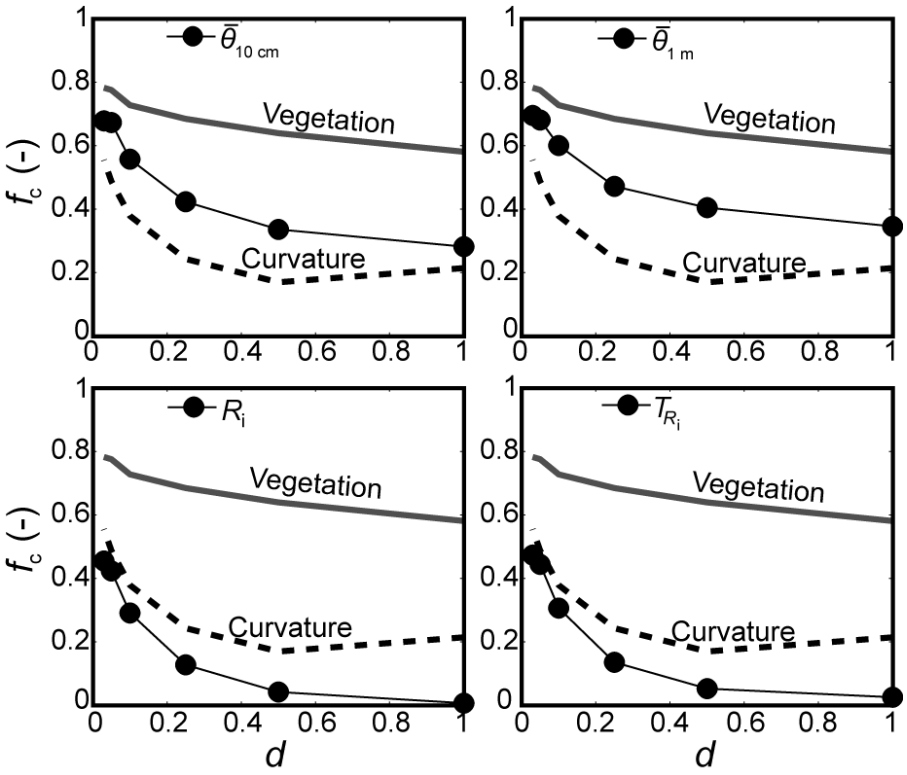

Figure 3.8. Variation of fraction homogeneity cover (f_c) with model resolution (d) for temporally-averaged surface ($\bar{\theta}_{10cm}$), root zone soil moisture ($\bar{\theta}_{1m}$), runoff rate (R_i) and runoff frequency (T_{R_i}). For reference, the variations of f_c with d for vegetation height and curvature are shown.

3.3.3. Spatial errors and the implications for experimental design

We utilize spatial error fields to identify hillslope areas exhibiting significant changes upon model coarsening with respect to d = 1. Figure 3.10 presents the spatial error metrics c_τ, H_τ, and θ_τ, as well as, the spatial intersections of $\theta_\tau \cap c_\tau$ and $\theta_\tau \cap H_\tau$ at resolutions of d = 0.5 and 0.03. c_τ shows high errors in small, linear patches for d = 0.5, whereas these error areas grow at d = 0.03 due to coarsening effects. Areas of increased concavity ($c_{diff} > c_{t1}$) and convexity ($c_{diff} < c_{t2}$) appear as large error patches for d = 0.03. In contrast, H_τ exhibits similar areas with high errors, increased height ($H_{diff} > H_{t1}$) and decreased height ($H_{diff} < H_{t2}$),

with respect to $d = 1$ for both resolutions, indicating more limited spatial sensitivity. Interestingly, the spatial errors for soil moisture (θ_τ) have patterns that reflect many processes, including infiltration, evapotranspiration and lateral redistribution [*Noto et al.*, 2008; *Mahmood and Vivoni*, 2011a]. At $d = 0.5$, many small and widespread areas with high errors occur in the hillslope. For $d = 0.03$, however, high error pixels organize into larger patches. Intersection maps aid in the interpretations of spatial error patterns in soil moisture. $\theta_\tau \cap c_\tau$ indicates that small, widespread errors at $d = 0.5$ and larger patches at $d = 0.03$ are due to equivalent curvature errors occurring when small-scale features are aggregated. $\theta_\tau \cap H_\tau$ suggests a smaller contribution of vegetation on soil moisture errors, specifically along ponderosa patch edges. While this method is useful, a large area of soil moisture error near the trench is not captured by the intersections, suggesting that it arises from the propagation of upstream (non-local) modifications induced by model coarsening.

Spatial error fields also allow a careful examination of the value of soil moisture observations in hillslope experiments. We evaluated the model performance for all resolutions with respect to the surface soil moisture at the fourteen sampling locations shown in Figure 3.1 [*Wilcox et al.*, 1997]. θ_{RMSE} values between each simulation ($d < 1$) and the finest resolution ($d = 1$) were computed using (3) for the limited set $\{\theta\}_{10cm}$ consisting of 14 sites. In addition, θ_{RMSE} was computed using all of the locations in the model hillslope (the set of 42,379 pixels at 0.17 m resolution). Based upon this analysis, it is possible to suggest alternative sampling locations that either minimize or maximize model-

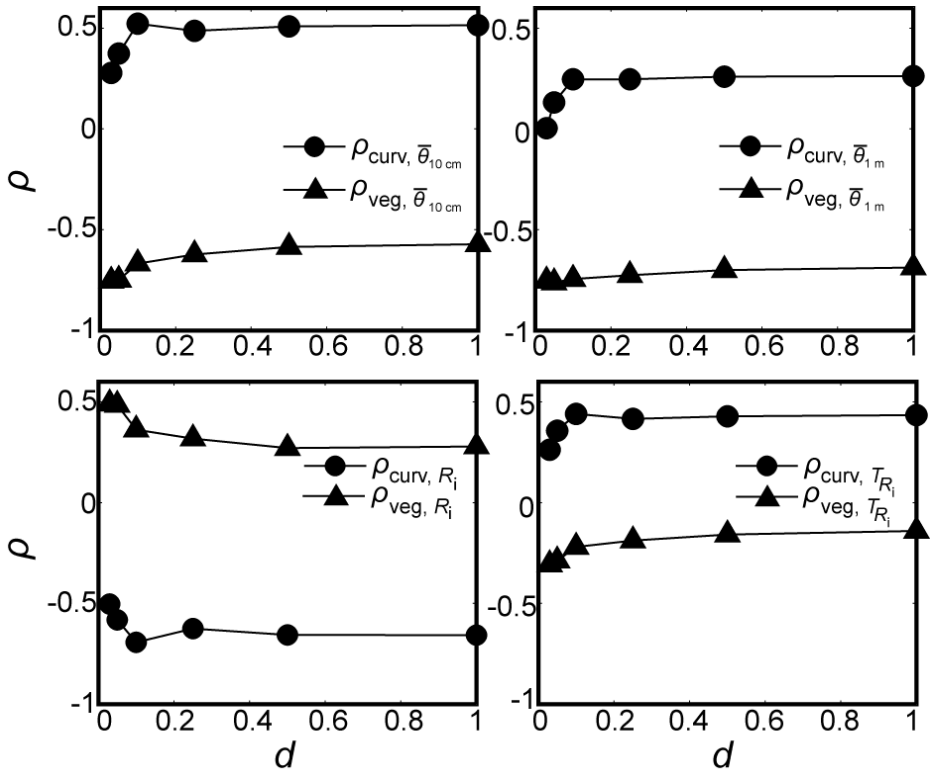

Figure 3.9. Variation of correlation coefficient (ρ) between land surface property (vegetation height and curvature) and hydrologic response with model resolution (d).

estimated θ_{RMSE}, while also impacting the model sensitivity to resolution. We limited our analysis to two alternative deployments with an identical number of sampling sites (14) near the current locations, as shown in Figure 3.11. We selected sites with a low θ_{RMSE} ($\theta_{RMSE} < \theta_{t1}$) in convex locations or a high θ_{RMSE} ($\theta_{RMSE} > \theta_{t1}$) in concave sites, respectively.

Figure 3.11 also presents θ_{RMSE} between $d = 1$ and $d < 1$ at the current location, low θ_{RMSE} locations, high θ_{RMSE} sites and all hillslope locations. Note that θ_{RMSE} for the entire hillslope is invariant with respect to model coarsening. This indicates that if all the information content of the model is preserved through

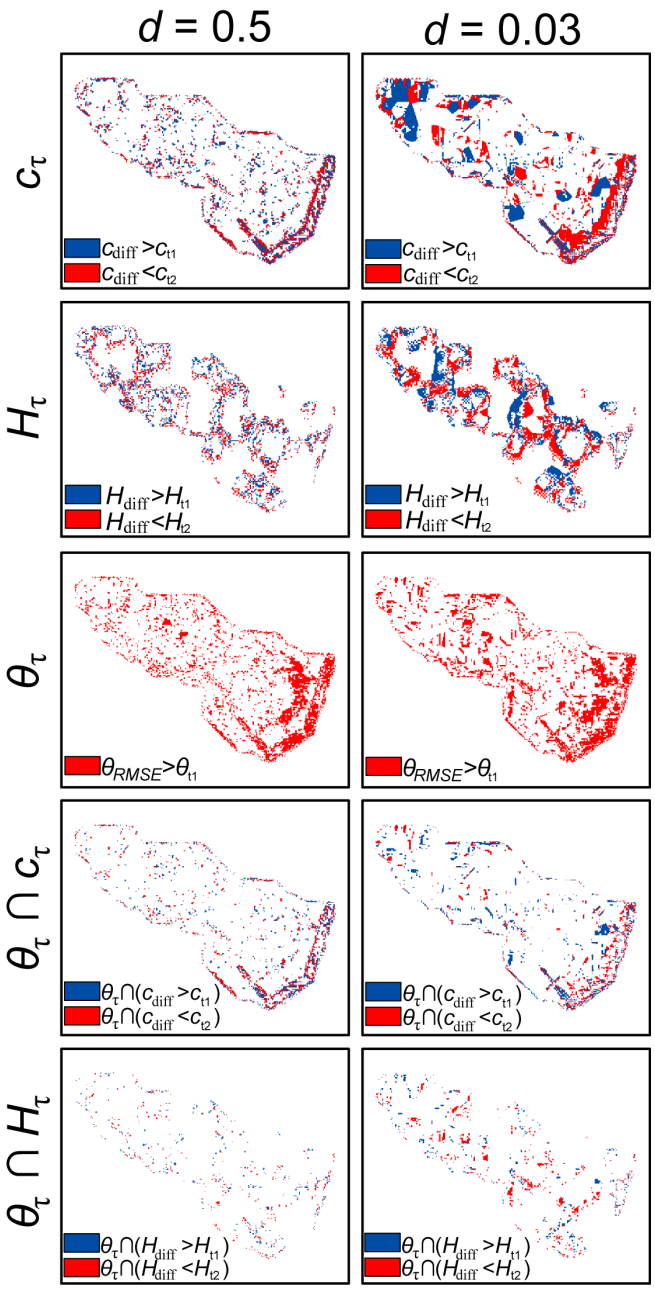

Figure 3.10. Spatial error maps between coarse (d = 0.5 and 0.03) and the finest (d = 1) resolution simulations. Error maps shown for curvature (cτ), vegetation height (H_τ), and surface soil moisture (θ_τ). Intersection maps $\theta_\tau \cap c_\tau$ (soil moisture and curvatur errors) and $\theta_\tau \cap H_\tau$ (soil moisture and vegetation height errors) are also shown.

sampling all locations, model aggregation can be conducted with a limited loss of accuracy for the selected performance metric. This is not the case for the cases

with only 14 sampling sites. In each case (high θ_{RMSE}, current, low θ_{RMSE}), spatial sensitivity in soil moisture is observed for model resolutions $d < 0.1$. Model coarsening beyond the threshold resolution ($d = 0.1$) introduces significant errors in the soil moisture simulations when these are tracked at a limited number of sampling locations. As expected, higher (lower) overall errors are found for high θ_{RMSE} (low θ_{RMSE}) deployments as compared to the current locations. Interestingly, a more limited spatial sensitivity to d is observed for the high θ_{RMSE} case, suggesting that this deployment minimizes concern over model resolution at the expense of accepting larger overall errors (~0.07 m^3/m^3). Selecting the low θ_{RMSE} deployment reduces the overall error (~0.03 m^3/m^3), but implies that the distributed model application needs to be aware of the sensitivity to coarsening. The current sites selected in the field experiment of *Wilcox et al.* [1997] have lower overall errors as compared to the entire hillslope, but exhibit stronger sensitivity to resolution.

3.4. Discussion and Conclusions

In this study, we investigated the breakdown of hydrologic patterns due to the coarsening of model resolution at the hillslope scale. Our findings show that model coarsening distorts small-scale curvature features and modifies, to some extent, the larger-scale vegetation patches. As a result, the highest spatial sensitivity was observed in the hydrologic patterns and processes, such as lateral soil moisture redistribution, that depend strongly on terrain curvature. A threshold resolution of ~10% ($d = 0.1$) of the original domain was also identified through

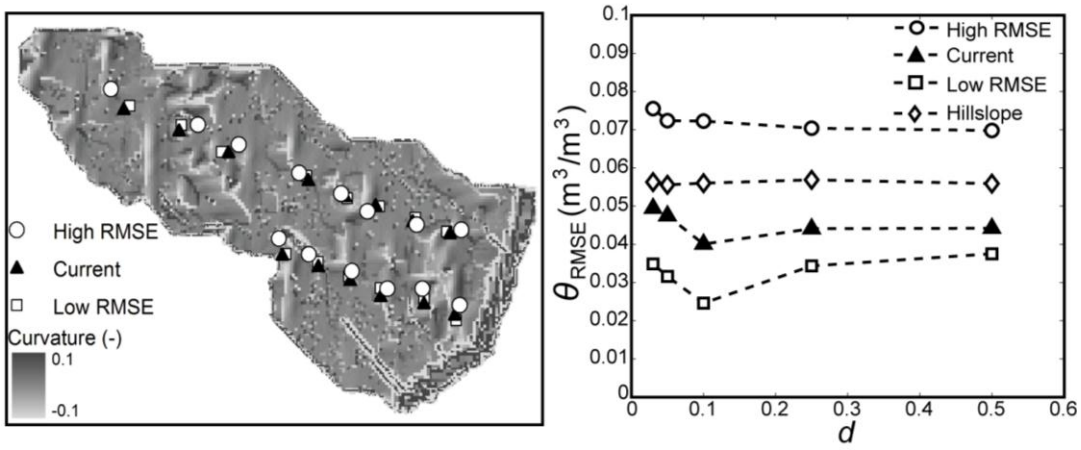

Figure 3.11. Location of current soil moisture sensors along with alternative deployments with low ($\theta_{RMSE} < \theta_{t1}$) and high ($\theta_{RMSE} > \theta_{t1}$) RMSE. Variation of surface soil moisture RMSE between fine ($d = 1$) and coarser resolution ($d < 1$) simulations at current and alternative deployments.

analyses of the fraction homogeneity cover and correlation coefficients. Below this threshold resolution, significant artifacts are introduced into the soil moisture and runoff patterns. Areas with high spatial errors in soil moisture were then associated with locations that experienced coarsening of the curvature and vegetation height fields. We found good correspondence between the spatial errors in soil moisture and the landscape properties, except for a region that demonstrated how model coarsening can also have downstream effects. Based on this analysis, we utilize the model to evaluate two alternative sampling designs for the hillslope instrumentation. We identified an interesting trade-off between the overall simulation errors and the sensitivity to model resolution. This example illustrates the usefulness of a distributed hydrologic model in the selection of sampling sites within hillslope experiments [e.g. *Anderson et al.,* 2008; *Hopp et al.,* 2009].

Prior studies on the effects of model resolution have typically focused on large river basins and on the integrated hydrologic response such as the outlet discharge [e.g. *Molnar and Julien,* 2000; *Haddeland et al.,* 2002; *Vázquez et al.,* 2002). *Kuo et al.* (2002] also inspected the impact of curvature on simulated soil moisture patterns in a set of large basins (6.5 to 24 km^2) and at coarse resolutions (10 to 400 m). To our knowledge, this study is the first to identify the impacts of model coarsening at the hillslope scale with a focus on the spatial sensitivity in soil moisture and runoff. This was only possible through the use of a distributed model that was tested against observations throughout the hillslope domain [*Mahmood and Vivoni,* 2011a]. Thus, the realism of the spatial simulations could be evaluated at fine resolutions prior to conducting the spatial sensitivity study. It is noteworthy that the distributed modeling was facilitated by the availability of high-resolution topographic and vegetation fields obtained from LIDAR. Fine-resolution representations of terrain, soil and vegetation properties are deemed essential for the success of distributed modeling in identifying threshold behaviors in hydrologic systems [*Seyfried and Wilcox,* 1995; *Grayson et al.,* 2002; *Rößler and Löffler,* 2010]. As LIDAR datasets become widely available for hydrologic studies [e.g. *Tarolli et al.,* 2009], distributed model applications need to place more emphasis on the simulation of realistic hydrologic patterns.

The spatial sensitivity analyses conducted here provide insights that can be generalized to other studies. In the ponderosa pine hillslope, the topographic features, in particular the curvature distribution, exhibited spatial variations that were smaller in scale than the vegetation patches. As result, the coarsening of the

domain first distorted the curvature features at low levels of aggregation, while the vegetation patches were preserved until large reductions in model resolution were made. Thus, hydrologic processes tied to curvature, specifically the lateral redistribution of soil moisture, exhibited a stronger sensitivity to model coarsening than the vegetation-mediated processes. In other studies, small-scale features may consist of vegetation or soil textural differences, rather than topographic attributes [e.g., *Crave and Gascuel-Odoux,* 1997; *Gomez-Plaza et al.,* 2001]. In these cases, model applications at hillslope scales should be cautious about the aggregation of the features exhibiting the smallest scale of variability as the processes linked to these attributes will have more significant sensitivity to model resolution. Another consideration is the potential for model aggregation to impact subsurface transport when heterogeneities exist in soil hydraulic properties or thickness. Geochemical and stratigraphic observations at the ponderosa pine hillslope suggest a relatively low amount of spatial variability in subsurface properties [*Newman et al.,* 1998; 2004]. Nevertheless, modeling studies in other forested catchments may require consideration of the horizontal soil properties and thickness, as these have been shown to exert significant controls on runoff response [e.g. *Freer et al.,* 2002].

Our study also highlights the ability of a distributed hydrologic model to evaluate design alternatives in hillslope experiments. The full information content of the distributed simulations at fine-resolution provides a benchmark upon which a limited number of sampling sites can be evaluated. We found that integrated spatiotemporal errors (θ_{RMSE}) computed for the entire hillslope were insensitive to

model coarsening, but that sampling at a subset of locations exhibited spatial sensitivity. Current sites [*Wilcox et al.,* 1997] had substantial sensitivity to model resolution, but lower overall errors than the full hillslope model. By sampling in nearby convex (concave) sites, the spatiotemporal errors can be decreased (increased), with the resulting increase (decrease) in the spatial sensitivity. As a result, a distributed model can potentially aid in hillslope experimental design by identifying locations that should be sampled due to their ability to capture the signature of spatial controls or to minimize the sensitivity to the resolution of a hydrologic model applied at the hillslope scale.

4. Forest Ecohydrologic Response to Bimodal Precipitation during Contrasting Winter to Summer Transitions

4.1. Introduction

Precipitation in the southwestern United States is characterized by a bimodal regime consisting of winter frontal storms and summer convective rainfall [e.g. *Mock,* 1996; *Sheppard et al.,* 2002]. The relative amount and timing of precipitation in each season varies from year to year in response to several synoptic scale mechanisms that control winter-time Pacific storms and the summer-time North American monsoon [e.g. *Cayan,* 1996; *Higgins and Shi,* 2000]. The proportion of annual precipitation falling within each season also varies geographically with a general increase of winter precipitation at higher latitudes and elevations [e.g. *Douglas et al.,* 1993; *Vivoni et al.,* 2008a; *Forzieri et al.,* 2011]. Interestingly, several studies have identified an inverse relation between the relative magnitudes of precipitation in each season and explored the potential mechanisms or teleconnections underlying the observations [e.g. *Gutzler and Preston,* 1997; *Gutzler,* 2000; *Ellis and Hawkins,* 2001; *Zhu et al.,* 2005; *McCabe and Clark,* 2006; *Mo,* 2008; *Notaro and Zarrin,* 2011]. In these studies, the snow amount and duration in the Rocky Mountains is considered to alter surface albedo, temperature and moisture which affects the land-ocean thermal gradient with the East Pacific and the strength of the North American monsoon.

As noted by *Notaro and Zarrin* [2011], the existence of and predictability derived from the snow-monsoon inverse relation have broad implications for

water resources and ecosystem productivity. Essentially, when the spatial extent and duration of winter snow cover is high, the amount of summer precipitation is lower, and vice-versa, thus providing a prediction on summer conditions a few months in advance [*Gutlzer and Preston,* 1997]. To our knowledge, limited attention has been paid to the ecohydrological consequences of the inverse relation by analyzing how landscapes respond to contrasting sequences of winter and summer precipitation. Most studies have focused on precipitation and its associated ecohydrological response within single seasons [e.g. *Seth et al.,* 1999; *Kurc and Small,* 2004; *Molotch et al.,* 2009; *Vivoni et al.,* 2008b]. Despite that, *Notaro et al.* [2010] attribute the bimodal growth of ecosystems in the southwestern US to seasonal precipitation inputs, while *Ogle and Reynolds* [2004] indicate the need to assess the effects of winter and summer precipitation on plant responses across the region. An example of these interactions was discussed by *Jenerette et al.* [2010] who report that increases in winter precipitation negatively impacted maximum vegetation growth in the summer.

In addition to effects on ecosystem productivity, relative amounts of winter and summer precipitation have important consequences on hydrologic systems in the southwestern US since: (1) soil moisture is replenished through snow melt inputs and summer convective storms [e.g. *Ogle and Reynolds,* 2004], (2) streamflow generation can have the signature of spring snow melt and summer storms [e.g. *Newman et al.,* 2006], and [3) evapotranspiration is affected by storm frequency through cloud cover [e.g. *Mahmood and Vivoni,* 2011a]. Thus, a wet winter followed by a dry summer is hypothesized to lead to the drying of a

hydrologic system as greater energy is added during the winter to summer transition. Prior studies have shown how wet conditions from snow melt inputs are followed by gradual drying during the summer when evapotranspiration is higher [e.g. *Newman et al.,* 1998; *Molotch et al.,* 2009; *Bales et al.,* 2011]. Fewer efforts have documented the hydrologic dynamics occurring when a dry winter is followed by a wet summer as a relatively lower amount of energy is inputted during the transition [*Newman et al.,* 1998]. A particular interesting outcome of the inverse relation is the potential to alter soil moisture patterns and their underlying local and nonlocal controls as described by *Grayson et al.* [1997].

Detecting the ecohydrological consequences of the inverse relation in a comprehensive fashion from field studies alone is difficult due to the need for coordinated winter and summer observations. Distributed hydrologic models evaluated against field data can be a useful means to depict ecohydrological processes, to extrapolate limited field data over broader spatiotemporal scales and to track the underlying physical mechanisms of the winter to summer transition. To do so, a numerical model should represent cold and warm season processes, and their interaction, in a continuous and reliable manner relative to site observations. In this study, we use a distributed hydrologic model with a snow component in a ponderosa pine field site to study the hydrologic dynamics of the winter to summer transition during two contrasting water years that represent well the inverse relation. Since the site is representative of ponderosa pine hillslope areas in southwestern US [*Brandes and Wilcox,* 2000] and selected water years depict well the snow-monsoon inverse relation [*McCabe and Clark,* 2006], the

ecohydrological insights gained from the modeling study are relevant to forests throughout the region and for other years. Moreover, our focus on spatial patterns during the winter to summer transition shed light on the controlling factors and thresholds for runoff production and lateral connectivity in forested hillslopes.

4.2. Methods

4.2.1. Study area and hydrologic observations

The study area, a ponderosa pine (*Pinus ponderosa*) hillslope (35° 53′ N, 106° 17′ W, elevation of ~2315 m) is located in the Los Alamos National Laboratory (LANL), New Mexico, USA (Figure 4.1). A series of studies at the site between 1993 and 1998 collected a set of hydrologic datasets, including snow depth, soil moisture and surface runoff [*Newman et al.,* 1997, 1998; *Wilcox et al.,* 1997]. Snow depth (cm) and volumetric soil moisture (m^3/m^3) estimates are available at 11 sampling locations within the hillslope at variable intervals in time. Soil moisture was measured manually using a neutron probe (NP) at a 22 cm soil depth through access tubes, while snow depth was visually read from meter sticks at these sites. In addition, snow depth was inspected at 28 snow meter posts distributed throughout the hillslope. Here, we used the snow depth, soil moisture at 22 cm and hillslope outlet runoff (mm/hr) obtained during the 1992-93 and 1993-94 water years (October to September) that constituted the most complete dataset for studying the winter to summer transition. Additional data include hourly meteorological data (i.e. precipitation, air temperature, relative humidity, wind speed, solar radiation). Unfortunately, there were large

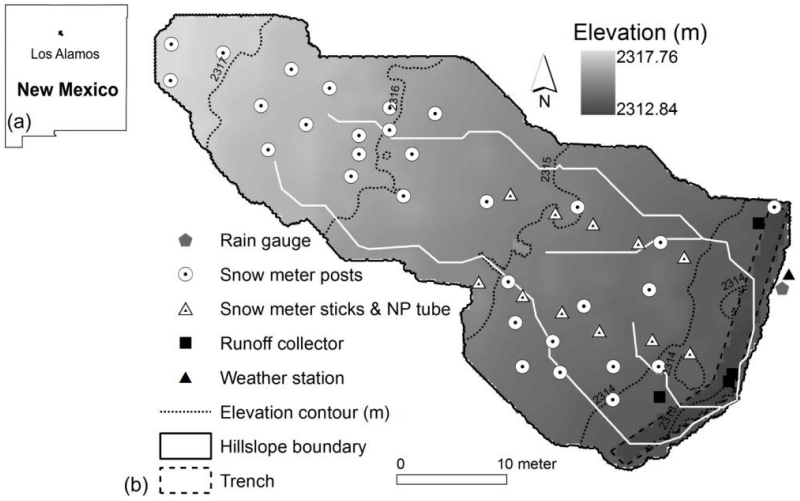

Figure 4.1. (a) Los Alamos county, New Mexico, USA. (b) Digital elevation model (DEM at 0.305 m resolution from LIDAR), boundary of the ponderosa pine hillslope and instrument sites.

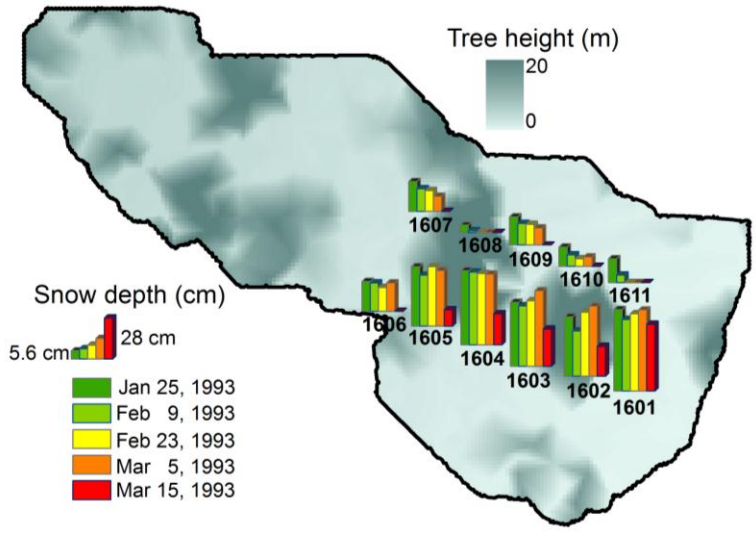

Figure 4.2. Spatiotemporal dynamics of snow depth during 1992-93 winter period.

meteorological data gaps from October 1992 to February 1993, requiring the use of data from the TA-6 site at LANL, ~2 km to the east and at a lower elevation (2263 m).

In addition to hydrologic observations in the hillslope, we obtained a high-resolution (0.305 m) digital elevation model (DEM) and canopy height model from an aircraft survey using LIght Detection And Ranging (LIDAR). These landscape datasets allowed deriving the hillslope domain (~1280 m^2 in size), including the boundary upstream of the runoff trench, flow network and the local slope, aspect and curvature [*Mahmood and Vivoni*, 2011a]. Overall, the hillslope has a low relief (~6 m) and a gentle slope from west to east following the general features of the Pajarito Plateau. The canopy height model allowed identifying the spatial locations of the open ponderosa pine stands (1 to 20 m in height, Figure 4.2) and their intercanopy grasses (0 to 1 m), that are characteristic of this region [e.g. *McDowell et al.*, 2008]. Soil stratigraphy is characterized as A and Bw horizons (loess deposit, sandy loam texture), a Bt horizon (alluvium), a clay-rich CB horizon (weathered tuff, clay texture), and an R horizon of Bandelier Tuff, with soil hydraulic properties and their variation with depth available at one location [*Wilcox et al.*, 1997].

As an example of the distributed observations, Figure 4.2 presents the variation of snow depth for the five available dates in the 1992-1993 water year at the NP tubes (snow meter sticks). The spatial patterns show noteworthy differences in snow accumulation and melt between northern (1607-1611) and southern (1601-1606) sites in the hillslope. Southern sites are in intercanopy grasses and receive more snow with delayed melting, while northern locations receive less snow and exhibit earlier melting. One northern site (1608) is located underneath a ponderosa pine and accumulates almost no snow. Thus, the

distributed observations provide insights into the processes leading to spatial variations in snow depth, as discussed in section 4.2.4. Unfortunately, there were no equivalent data collected for the 1993-1994 water year at the NP tubes. The snow depths at the 28 snow meter posts (Figure 4.1) during both water years lacked information relating the site location to the observed values, restricting their use as a hillslope-averaged quantity.

To summarize the site data, Figure 4.3 shows the available observations for the study period (October 1992 to September 1994) including precipitation, air temperature, hillslope-averaged soil moisture at 22 cm depth and hillslope-averaged snow depth (i.e. symbols with ±1 spatial standard deviation as vertical bars). For clarity, the runoff estimates are omitted. Note that colder conditions (air temperature below 0° C) during storms in 1992-1993 lead to greater snowfall and higher snow accumulation, while warmer conditions in 1993-1994 lead to lower snow depths overall. During 1992-1993, the hillslope snow cover begins in early January, peaks in late January, and melts by the end of March due to higher air temperatures. In contrast, snow cover in 1993-1994 is infrequent and of short duration. The contrasting periods allow investigating the hillslope response for varying winter to summer transitions: a wet winter followed by a dry summer (1992-1993) and dry winter followed by a wet summer (1993-1994).

4.2.2. Distributed hydrologic modeling with a snow component

We used the Triangulated Irregular Network (TIN)-based Real-time Integrated Basin Simulator (tRIBS) model for the hillslope simulations. tRIBS is a

distributed hydrologic model with a snow component [*Ivanov et al.,* 2004a,b; *Vivoni et al.,* 2007; *Rinehart et al.,* 2008]. The physical processes in the model include rainfall interception, infiltration, evapotranspiration, water table fluctuations, lateral subsurface transport and runoff production and routing. Cold season processes include snow interception and unloading, sublimation of intercepted and on-the-ground snow, snow accumulation and melt, and infiltration of melt water [*Rinehart et al.,* 2008]. The distributed model incorporates hillslope descriptors of topography, vegetation and soil properties in the simulation at high-resolution, when available. Here, we utilized the LIDAR DEM to generate a TIN at the finest possible resolution (0.305 m). While coarser resolutions are possible without significant loss of hydrologic information [*Vivoni et al.,* 2005; *Mahmood and Vivoni,* 2011b), this selection was made to represent the sampling sites with high fidelity.

Ivanov et al. [2004a,b] and *Vivoni et al.* [2007, 2011] present a detailed description of the model domain, physical processes, parameterization and initialization, as well as the model capabilities to produce spatiotemporal estimates of hydrologic variables. Furthermore, the model application to the ponderosa pine hillslope has been fully documented in *Mahmood and Vivoni* [2011a,b] for summer conditions, with a focus on reproducing observed soil moisture and runoff for three periods (1996-1998). As a result, we limit the following discussion of the model to the cold season processes initially described in *Rinehart et al.* [2008] and updated in this study. The snow component is a single-layer, coupled energy and mass balance approach that accounts for direct

and diffuse solar (shortwave) radiation and the age-dependant albedo effects of snow; incoming and outgoing longwave radiation; precipitation heat flux; and latent and sensible heat flux from the snow pack, including sublimation [e.g. *Tarboton and Luce*, 1996; *Wigmosta et al.*, 1994; *Wilson and Gallant*, 2000]. Incoming precipitation is linearly partitioned between liquid and solid phases using air temperature [*Wigmosta et al.*, 1994] and used to estimate precipitation heat flux. When falling in solid form, vegetation intercepts snow based on the leaf area index, unloads snow in relation to air temperature, and sublimates snow using the absorbed shortwave radiation and relative humidity [*Pomeroy et al.*, 1998; *Liston and Elder*, 2006].

The snow pack internal energy at each time step (U) determines the snow temperature (T_{sn}) and how liquid and solid phases are partitioned within the snow pack [see *Rinehart et al.*, 2008 for details]. We modified the original model to account for the latent heat leaving the snow pack upon melt by adding a term [see *Rinehart et al.*, 2008, equation A2]:

$$L_m = \lambda_j \rho_j M_{ij} \quad , \tag{1}$$

where L_m is the latent heat flux, j indicates liquid water, λ_j is the latent of freezing, ρ_j is the density of water and M_{ji} is the amount of phase change from ice (i) to liquid water (j). Overall, a positive U indicates the presence of liquid water in the snow pack, which can be held internally up to a fraction 0.35 of the snow water equivalent (SWE) [modified from a fraction of 0.06 in *Rinehart et al.*, 2008], with the remaining routed to the soil surface. Currently, the snow model neglects: (1) shallow ground heat flux, (2) wind redistribution of snow, (3) local differences in

meteorology from wind sheltering, (4) the effects of unstable temperature profiles on turbulent exchanges, and (5) the effects of vegetation or topography on the incoming longwave radiation.

Rinehart et al. [2008] also describe the model approaches to account for the impacts of topography and vegetation on the incoming solar radiation for both direct and diffuse terms. Topographic effects include both local controls of slope, aspect and plant canopies as well as remote controls from the surrounding landscape (e.g. distant mountains and their shading and reflection of light). For the hillslope application, we redefined the remote controls by using a simpler approach for the remote sky-view factor (v_{remote}) following *Dozier et al.* [1981]:

$$v_{remote} = \frac{1}{m}\sum_{d=1}^{m} \cos HA_m \quad , \qquad (2)$$

where HA_m is the horizon angle measured from the vertical in the azimuth direction m (16 total directions), instead of *Rinehart et al.* [2008, equation 2]. Furthermore, we utilized the LIDAR canopy height model to determine the remote controls, as the gentle relief of the hillslope made the effects of distant mountains negligible. This allowed for a more detailed treatment of vegetation effects on sky-view for the ponderosa pine hillslope. Other aspects of the shortwave radiation, including the treatment of albedo effects, remain as reported in *Rinehart et al.* [2008].

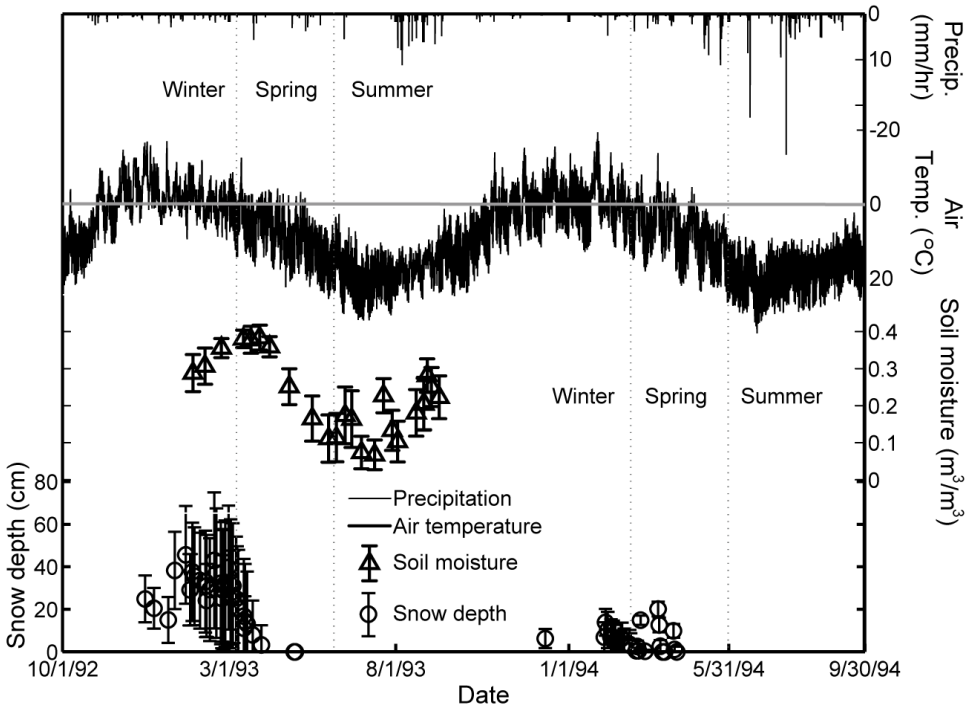

Figure 4.3. Hydrometeorological observations between October 1992 and September 1994 including precipitation, air temperature, hillslope-averaged snow depths (black circles with ± 1 standard deviation as bars) and hillslope-averaged soil moisture at 22 cm depth.

4.2.3. Snow model evaluation at the Quemazon SNOTEL site

To test the revised snow model physics, we carried out simulations at the Quemazon SNOTEL station (35° 55′ N, 106° 24′ W, Los Alamos, New Mexico) for multiple winter seasons with nearly complete meteorological and snow data (2004-2005, 2006-2007, 2008-2009 and 2009-2010). The Quemazon location is ~7 km northwest of the ponderosa pine hillslope and at a higher elevation of ~2900 m [*Rinehart et al.*, 2008]. The site is in a small meadow that is sheltered from winds by the surrounding forest such that snow interception processes or wind-induced undercatch of snow are considered negligible. Available data included hourly air temperature, precipitation and snow water equivalent (SWE)

measured by a snow pillow. We found that the cumulative precipitation data from the site weighing gauge could introduce some uncertainty to the total water input, in particular for the 2006-2007 winter season. Other meteorological variables, such as solar radiation, relative humidity and pressure, were obtained from the Los Posos weather station, located ~2 km west of Quemazon at a similar elevation, an improvement over the model forcing used in *Rinehart et al.* [2008] from a farther and lower site.

Figure 4.4 compares the observed SWE at the Quemazon SNOTEL site with simulated values at the co-located Voronoi polygon with the station for each winter season. Since a small domain was constructed around the station (1427 m^2 with 1495 Voronoi polygons derived from the LIDAR DEM), we are able to present the spatial variability around the station through the gray shading (±1 standard deviation of 8 neighboring polygons). Good model agreement is obtained for all winter seasons across a range of different seasonal precipitation and temperature conditions (Table 4.1). The model captures the snow accumulation and melt processes for each season and performs well in mimicking the peak SWE, ranging from ~20 to 38 cm. Overall, the Root Mean Square Error (RMSE) of the SWE is low (Table 1.1) and the performance is superior to *Rinehart et al.* [2008, their Figure 4.1]. This is attributed primarily to an improved model forcing and the effects of the revised snow physics. As expected, the seasonal weather plays a dominant role in the snow accumulation and melt for each period, with more snow in 2004-2005 and 2009-2010 due to the higher precipitation and lower mean air temperatures. For these wetter seasons, the snow

duration extends into late May, while the drier winters have snow cover until late April. The snow model performance for multiple seasons builds confidence in the simulated processes for conducting spatially-explicit snow simulations, as discussed in the following.

4.2.4. Distributed model application in ponderosa pine hillslope

Simulations in the ponderosa pine hillslope are based on a model domain with 12,755 Voronoi polygons, each characterized by elevation, soil and vegetation properties. Using the LIDAR-derived canopy heights, four vegetation classes were mapped: grassland (< 1 m height) and short (1-5 m), medium (5-10 m) and tall ponderosa pines (10-20 m). *Mahmood and Vivoni* [2011a] calibrated vegetation parameters for summer conditions in each class, finding a good match between simulated and observed soil moisture during recession periods. Due to a lack of distributed data, soil hydraulic properties and depth were assumed spatially-uniform in the hillslope (sandy loam texture and 1.06 m depth) following *Wilcox et al.* [1997]. Certain soil properties were also adjusted to match the observed soil moisture at distributed locations. Table 2 lists the vegetation and soil parameter values and describes whether these were obtained from field measurements, literature values or model calibration. Here, we relied on the calibration and testing of *Mahmood and Vivoni* [2011a] and did not further alter soil or vegetation parameters with one exception: grassland vegetation fraction and height were reduced when covered by snow. This important change allowed

capturing the appropriate heat fluxes when a snow pack developed in the intercanopy areas during the two winter-to-summer transition periods.

The distributed simulations for the two water years were conducted as a single model run (October 1992 to September 1994) at an hourly time step. A lack of soil moisture observations prior to the simulation period prevented a distributed initialization as in *Mahmood and Vivoni* [2011a]. Thus, a moderately wet, spatially-uniform initial condition was assumed for October 1, 1992 as this followed the summer season. Any potential errors introduced by this assumption were minimized by the fall season evapotranspiration that reduced soil moisture in the hillslope prior to the onset of winter snowfall. Over the simulation period, spatially-uniform forcing was applied for air temperature, relative humidity, wind speed, and solar radiation above the canopy (after which modifications were made due to local and remote shading, section 2.2). During the winter, however, the differential accumulation of snow in the northern and southern grassland areas of the hillslope (Figure 4.2) could not be simulated with uniform forcing. Thus, we explored several alternative hypotheses (e.g. spatial variation of air temperature due to wind sheltering) and found evidence for the effect of wind redistribution of snow, as shown in Figure 4.5a. During snowfall events, winds in the hillslope were primarily from the southerly direction leading to higher accumulation in the open southern sites and tree-sheltering in the northern sites.

Since wind-driven snow redistribution is not currently simulated [*Rinehart et al.*, 2008], we developed an obstruction map derived from the LIDAR canopy height model. For each pixel, we estimated the presence of an obstruction to wind

in the eight surrounding directions by comparing the elevation of the selected pixel and its neighbors within a 3 m radial distance. If the elevation difference was greater than 5 m, we assigned 1 for that pixel and zero otherwise, as:

$$O_{i,j}^{d} = \begin{cases} 1, & \text{if } (z^{d,r<3m} - z_{i,j}) > 5\,\text{m} \\ 0, & \text{if } (z^{d,r<3m} - z_{i,j}) < 5\,\text{m} \end{cases}, \qquad (3)$$

where $O_{i,j}^{d}$ is the obstruction index at site *i, j* in a direction *d*, $z^{d,\,r<3m}$ are all pixel elevations within a 3 m radius (*r*) and $z_{i,j}$ is the given pixel elevation. Each binary map for a direction *d* was then multiplied by the fraction of time that wind blows from that direction (p^d) during winter storms (Figure 5a) as: $B_{i,j}^{d} = p^{d} O_{i,j}^{d}$. The summation of $B_{i,j}^{d}$ over all directions leads to the final obstruction fraction map shown in Figure 5b with values ranging from 0 (no obstructions) to 1 (high obstructions) in the dominant wind direction. The sensitivity of the approach to changes in the radius and threshold elevation was minimal. Thus, to account for wind redistribution of snow during storm events, we moved snow precipitation from sheltered areas (e.g. north of the ponderosa pine patches in Figure 5b) into open areas (e.g. south of the pine patches) following the obstruction fraction, while conserving the total snow mass input to the hillslope. The spatially-variable precipitation forcing was utilized only during snowfall events in winter and early spring. Such spatially variable precipitation surfaces are considered only for the winter season and we assume uniform precipitation surface during summer season.

Two additional changes were made to the model to account for the patchy ponderosa stands and the relatively thin snow packs as compared to the Quemazon SNOTEL site (note that peak SWE of 40 cm in Figure 4.4a is equivalent to a snow depth of 400 cm for snow density, ρ_s = 0.1, roughly 10 times the peak snow depth in Figure 4.3). First, the minimum snow temperature (T_{min}) in the single layer model [*Rinehart et al.,* 2008] was replaced by the snow temperature (T_{sn}) occurring for SWE equal to 10 cm when the internal energy (U) was less than zero. This allowed for a more stable T_{sn} during a rapidly melting snow pack. Second, the snow melt water in the hillslope was retained on the soil surface until SWE was equal to zero for each melt period. Subsequently, snow melt was allowed to slowly infiltrate into the soil at a rate of 0.25 mm/hr, allowing soil absorption rather than runoff generation, consistent with the low runoff observations in the trench during the winter [*Newman et al.,* 2004]. We also neglect the topographic affects of the neighboring mountains due to low horizon angle as major neighboring mountain ranges are ~7 km far from our site. Instead we consider the effect of pine patches due to high horizon angle.

4.3. Results and Discussion

In the following, we describe the simulated ponderosa pine hillslope response to the two contrasting winter to summer transition periods. Comparisons with snow, soil moisture and runoff observations allow for a detailed evaluation of the modeled spatiotemporal patterns which reveal stark differences between the two water years. Finally, a detailed analysis tracks how precipitation input during

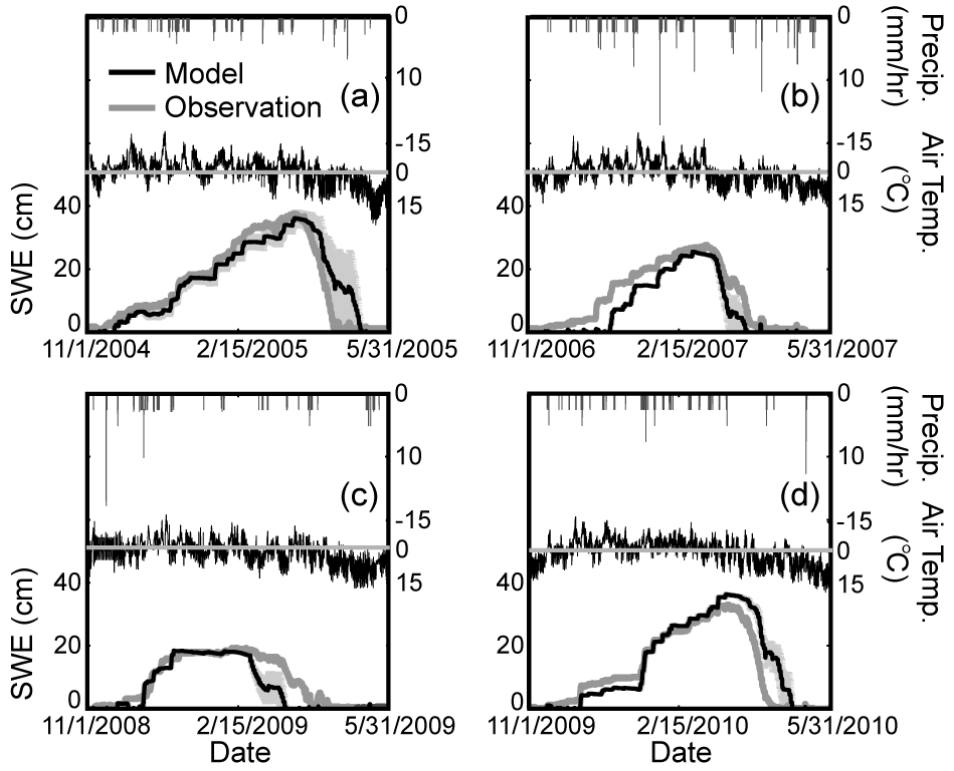

Figure 4.4. Comparisons of snow water equivalent (SWE) observations and simulations at the Quemazon SNOTEL station for multiple years: (a) 2004-2005, (b) 2007-2008, (c) 2008-2009, and (d) 2009-2010.

Year	Total Precipitation (mm)	Mean Temperature (°C)	Quemazon SWE RMSE (cm)	
			Entire Winter	Snow Period
2004-2005	481	-1.10	2.2	2.5 (Nov 20 –Apr 22)
2006-2007	428	0.70	5.7	6.8 (Nov 28 – Mar 27)
2008-2009	437	1.05	3.6	4.8 (Dec 10 – Mar 22)
2009-2010	479	-0.05	4.9	5.9 (Dec 7 – Apr 22)

Table 4.1. Total precipitation (mm) and mean air temperature (°C) along with the temporal RMSE between observed and simulated (Voronoi polygon average) SWE at Quemazon SNOTEL site.

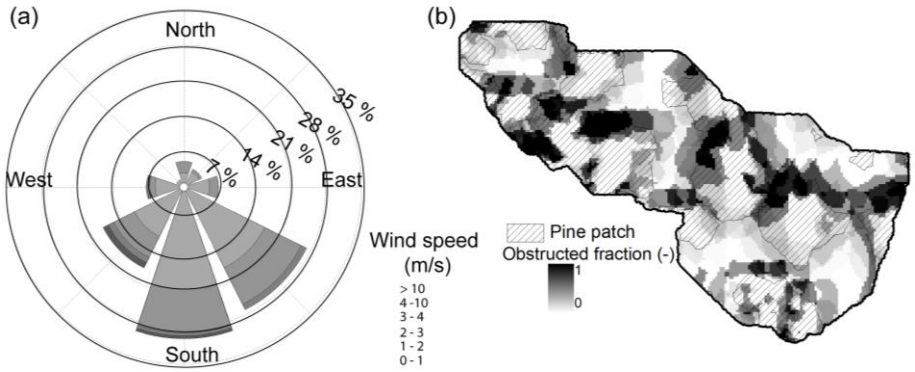

Figure 4.5. (a) Wind rose diagram for 1992-93 winter precipitation events. (b) Obstruction fraction map based on wind rose diagram and proximity to ponderosa pine patches.

each season influence the hillslope patterns of hydrologic response and how these are linked to landscape properties including terrain curvature and vegetation.

4.3.1. Distributed snow conditions for contrasting winter seasons

Figure 4.6 presents the observed and simulated snow depth at a selected number of snow meter sticks (at NP tube locations) for the 1992-1993 winter season. Visual measurements for five dates (black circles) are compared to the continuous snow depth simulations, presented as an average of the co-located Voronoi polygon with the site and its neighboring polygons (shading represents ± 1 standard deviation among the polygons). The sites depict the general behavior in the southern portion of the hillslope (1602, 1604, 1606) with higher snow accumulation (peak snow depth of 25 to 70 cm) and the northern grassland areas (1607, 1609, 1611) with a thinner snow pack (peak depths of 20 to 30 cm). Note that the model is able to reproduce the snow observations well at the selected sites, with an RMSE ranging from 2.3 to 16.4 cm, as presented in Table 3. Large spatial variations of snow depth (e.g. shading in 1602 and 1606) are found for

Vegetation Units	Vegetation Parameter									
	Area (%)	*p* (-)	*S* (mm)	*K* (mm/hr)	*g* (mm^{-1})	*A* (-)	H_v (m)	K_t (-)	r_s (s/m)	*v* (-)
Grassland (0-1 m)	52	0.9%	1.0%	0.12%	4.7%	0.28%	1*	0.9%	40%	0.8+
Short pine (1-5 m)	20	0.4%	1.5%	0.12%	4.7%	0.2%	5*	0.5%	10%	0.85+
Medium pine (6-10 m)	15	0.4%	1.5%	0.12%	4.7%	0.1%	10*	0.5%	10%	0.95+
Tall pine (10-20 m)	13	0.4%	1.5%	0.12%	4.7%	0.1%	20*	0.5%	10%	0.95+

Soil Unit	Soil Parameter							
	K_o (mm/hr)	θ_s (m^3/m^3)	θ_r (m^3/m^3)	θ^* (m^3/m^3)	λ (-)	Ψ (mm)	f (mm^{-1})	A_s (-)
Sandy loam	0.29*	0.45*	0.01%	0.18+	1.9+	-250+	0.007*	40+

Table 4.2. Vegetation and soil parameter values from field observations (*), literature (%), or manual calibration (+), including percentage of hillslope area (Area), throughfall coefficient (*p*), albedo (*A*) [*Iziomon and Mayer*, 2002], canopy water storage capacity (*S*), drainage rate from canopy (*K*), drainage exponential parameter (*g*) [*Rutter et al.*, 1971], vegetation height (H_v), optical transmission coefficient (K_t) [*Zou et al.*, 2007], minimum stomatal resistance (r_s) [*Karlson and Assmann*, 1990; *McDowell et al.*, 2008], vegetation fraction (*v*), hydraulic conductivity at surface (K_o), saturated (θ_s) and residual (θ_r) soil moisture [*Rawls et al.*, 1983], soil moisture stress threshold (θ^*), pore size distribution index (λ), air entry bubbling pressure (ψ), conductivity decay parameter (*f*), and soil anisotropy ratio (A_s).

sites at the edge of a ponderosa pine patch due to the impact of snow interception by the canopy. Model performance at other locations is also adequate, including for 1608 under a ponderosa pine where little snow accumulates, except at 1601

(RMSE = 31.5 cm) where the simulated snow depth underestimates the wind-driven redistribution at this exposed (unobstructed) site.

The simulated snow accumulation and ablation at the southern (sublimation is 35% and 17% during 1992-93 and 1993-94 respectively) and northern sites (sublimation is 56% and 36% during 1992-93 and 1993-94 respectively) helps to interpret the contrasting field observations. At the southern locations (1602, 1604, 1606), snow depth peaks in January and persists for 60 days due to the constant input of wind-redistributed snow. Snow ablation in southern grassland sites occurs rapidly in March due to increases in air temperature and the relatively high amount of incoming shortwave radiation at these exposed sites. In contrast, the northern grassland sites (1607, 1609, 1611) exhibit a lower maximum snow depth due to the obstructed nature of these locations (note the lower precipitation input) that persists for a shorter time, ranging from 30 to 60 days. The snow ablation characteristics are fundamentally different among the sites, with a more gradual decrease in snow depth at northern locations that are less exposed to incoming solar radiation, as further explored in section 3.3.

Due to data limitations, the winter simulations in the two water years are compared only in terms of the spatially-averaged snow depth across all available sites (both snow meter sticks and snow posts). Figure 4.7 presents the mean observed (black circles) and simulated (black lines) snow depth, along with measures of the spatial variability (± 1 spatial standard deviation) at the sampling sites. In addition, the spatially-averaged snow depth simulated over the entire

hillslope is presented (gray lines). The similarity between the spatial averages of snow depth over the hillslope and sampling sites indicates these are representative of the entire domain. Clearly, the model is able to reproduce well the contrasting snow pack development in each winter season, with an RMSE of 18.3 and 9 cm (Table 4.3). In 1992-1993, a sequence of snow storms under cooler weather during November leads to snow accumulation throughout the winter, resulting in a temporally continuous and thick snow pack. Conversely, the infrequent, precipitation events in 1993-1994 arrived during February under warmer weather conditions, leading to a late snow pack development that was thinner and temporally discontinuous. Under these drier and warmer conditions, the snow pack spent less time exposed to the atmosphere, thus experiencing lower sublimation, and also was subject to numerous snow melt periods.

To further compare the winter seasons, Figure 4.8 presents the spatial distribution of time-averaged snow depth, snow cover duration (T_d), total snowmelt and total canopy sublimation (S). As expected, snow depth is higher in open grassland areas as compared to the ponderosa pine patches, though the spatial variations are minimal for 1993-1994. T_d resembles the spatial pattern of snow depth, with longer time periods in intercanopy grassland sites, in particular for 1992-1993. The northern sampling sites can be distinguished well from other grassland areas by lower T_d for both seasons due to the effects of sheltering from wind-redistribution of snow. Differences between each season are pronounced in terms of the magnitudes of snow melt and canopy sublimation, though the spatial patterns are similar in each winter. Interestingly, the snow melt delivered to the

soil surface is higher for the drier and warmer 1993-1994 period. This can be attributed to: (1) the lower canopy sublimation due to the shorter T_d, and (2) the warmer temperatures that lead to more frequent snow melt periods. In contrast, the wetter and colder 1992-1993 winter has a higher *S* due to a greater snow cover duration promoting losses to the atmosphere rather than snow melt. Note the more complex spatial patterns of snow melt, as compared to sublimation, indicate this flux is dependent on several interacting processes, leading to spatially-variable water inputs to the hillslope soil surface, as discussed in the following.

4.3.2. Distributed soil moisture and runoff generation in contrasting water years

Figure 4.9 compares observed and simulated soil moisture at selected southern and northern sites during the two water years, with performance statistics presented in Table 3. Overall, the model captures well the soil moisture dynamics during winter, spring and summer seasons in 1992-1993 (RMSE of 0.02 to 0.12 m^3/m^3), despite no further calibration beyond *Mahmood and Vivoni* [2011a]. This is complemented with a comparison of spatially-averaged soil moisture at all sites and the hillslope domain in Figure 4.7. Note that there were no soil moisture observations in the 1993-1994 water year, limiting the capacity to further test the model. Despite this, the model helps to identify the hillslope response to the variable snow melt and rainfall inputs during the contrasting periods. Note the soil moisture initial condition is quickly dissipated by the first winter. In 1992-1993,

Stations	Temporal RMSE		
	1992-1993 Snow depth (cm)	1993-1994 Snow depth (cm)	1992-1993 Soil moisture (m^3/m^3)
1601	31.5	–	0.11
1602	16.4	–	0.06
1603	23.1	–	0.12
1604	14.5	–	0.08
1605	24.8	–	0.13
1606	7.4	–	0.11
1607	11.1	–	0.07
1608	2.3	–	0.15
1609	7.0	–	0.04
1610	7.5	–	0.10
1611	6.6	–	0.07
Hillslope	18.3	9.0	0.09
R^2	0.5	0.55	0.51

Table 4.3. Temporal RMSE between observed and simulated (Voronoi polygon average) snow depth and soil moisture. Distributed snow observations are not available during 1993-1994. The RMSE and R^2 are also shown for all sites (labeled Hillslope).

soil moisture exhibits a strong seasonality with a wet winter followed by drying during the spring due to elevated evapotranspiration caused by high solar radiation and air temperatures (see section 3.3). In the summer, the drying trend is briefly interrupted by small rainfall pulses that rapidly increase soil moisture, but these amounts quick recess due to high *ET* [*Mahmood and Vivoni*, 2011a]. In contrast, the 1993-1994 water year consists of relatively drier winter soils that experience brief episodes of wetting from snow melt inputs that are triggered by warmer temperatures. The spring and summer experience a sequence of frequent, large storms that induce higher soil moistures, aided by high cloud cover during

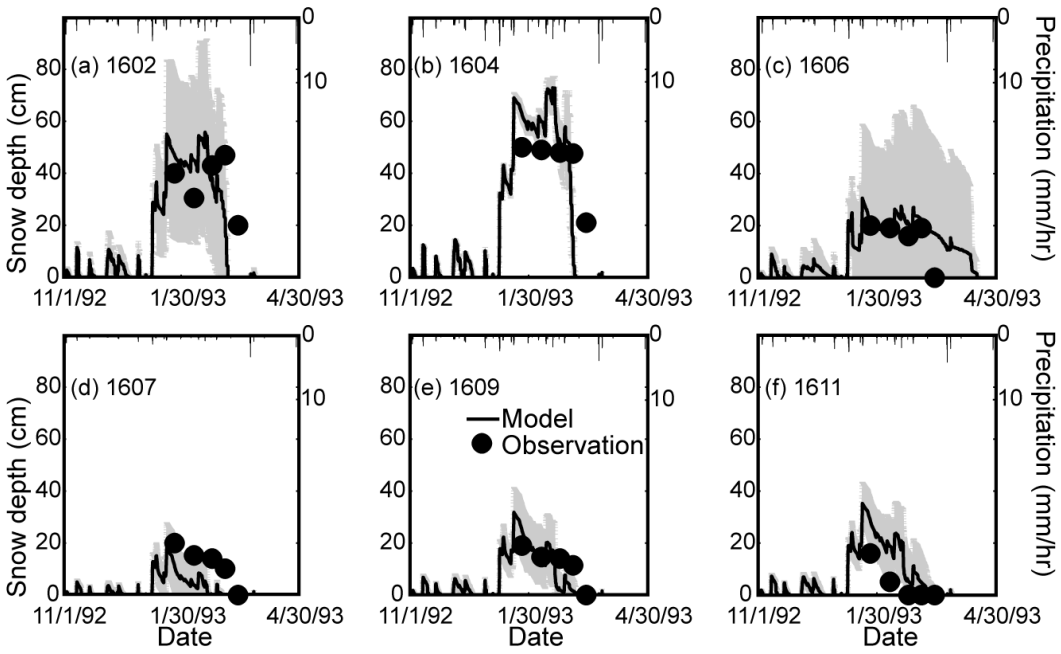

Figure 4.6. Comparisons of observed and simulated snow depth at distributed locations during the 1992-93 winter period. Top row represents sites located in the southern part of hillslope and bottom row are sites in the northern part. Simulated values are spatial averages of the Voronoi polygon co-located with the sampling location and its neighboring elements (black lines). Spatial uncertainties are shown as ± 1 standard deviation (gray shading).

induced low evapotranspiration rates. As a result, a strong seasonality is observed with relatively wetter soils during the North American monsoon.

Contrasts between the two water years are shown in terms of the spatial distribution of soil moisture during winter, spring and summer seasons in Figure 4.10. Soil moisture is a good indicator of the hillslope hydrologic processes as it responds to atmospheric inputs and losses. For example, the winter soil moisture in 1992-1993 has wet grassland areas and dry ponderosa pine patches induced by differences in snow melt. In the spring, grasslands dry at faster rate than ponderosa pines, leading to a nearly uniform and dry summer soil. Spatial maps of the temporal standard deviations in 1992-1993 show higher variability in

grassland areas, consistent with the patterns described by *Mahmood and Vivoni* [2011a] for the drier summers of 1996 and 1998. In contrast, a uniformly dry soil condition is observed during the winter in 1993-1994, with low temporal variations throughout the hillslope. This is followed by a wetting period during the spring and summer resulting in a progressively wetter soil moisture distribution that resembles the vegetation pattern, with wetter grassland sites as compared to ponderosa pine patches. The spatial distribution of the standard deviation in the summer of 1993-1994, however, obtains the signature of the terrain curvature, as shown by *Mahmood and Vivoni* [2011b] for the wetter summer of 1997. As a result, differences in the winter to summer transition can lead to substantially different controls on hillslope soil moisture patterns.

Snow melt or rainfall events can induce runoff generation in the hillslope [*Wilcox et al.*, 1997; *Newman et al.*, 2004]. Figure 4.11 compares trench runoff observations to simulated values at the hillslope outlet with no additional calibration. The overall performance is adequate, in particular during the 1993-1994 summer season where the major events are captured well [see *Guan et al.*, 2010 for a similar comparison]. However, the model overestimates runoff during the 1992-1993 water year (with a potential reason being inaccurate runoff data transcription). The model also provides insight into the fraction of hillslope runoff contributed by different runoff mechanism during each event. In 1992-1993, winter and early spring runoff is dominated by the saturation excess mechanism due to the wet soil moisture condition. As the hillsope dries out in spring and summer, the dominant mechanism switches to infiltration excess runoff. Thus, a

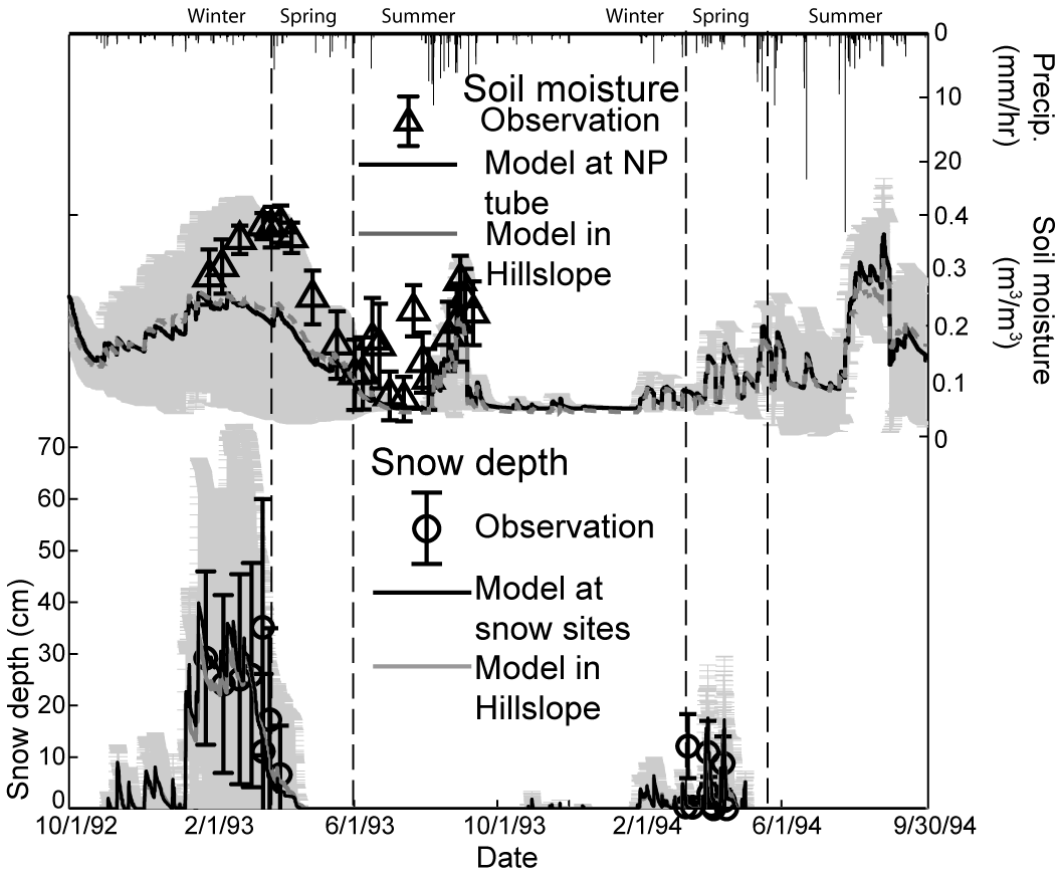

Figure 4.7. Comparison between observed and simulated spatially-averaged snow depth and soil moisture at the distributed locations between October 1992 and September 1994.

transition in runoff generation is detected in the model when a wet winter is followed by a dry summer. The opposite behavior is simulated during the 1993-1994 water year, with a transition from infiltration excess runoff in the early spring to saturation excess runoff in the summer. As a result, the relative wetness conditions in each season and their sequencing lead to significantly different switching of runoff generation mechanisms at the hillslope scale.

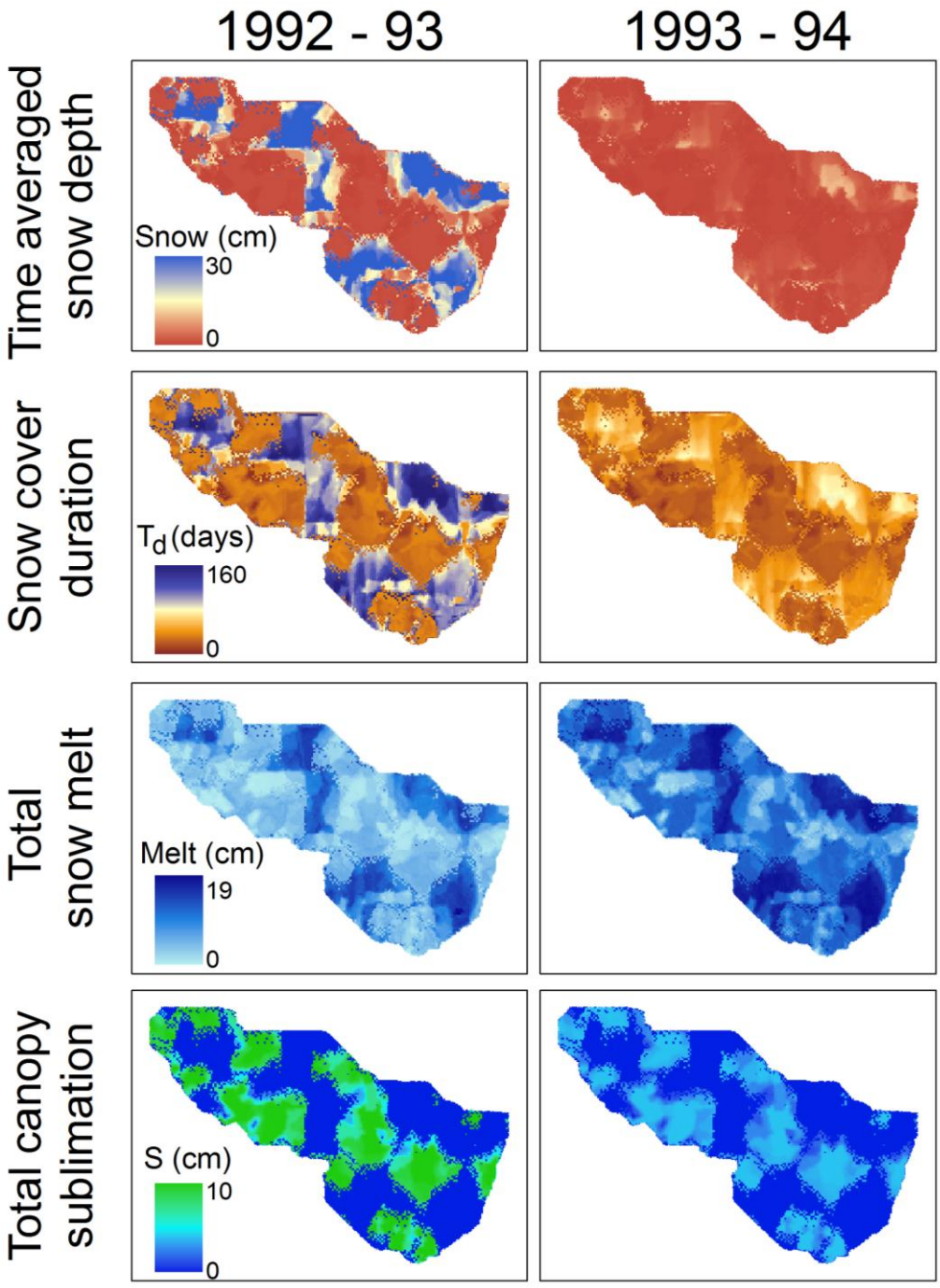

Figure 4.8. Spatial patterns of simulated time-averaged snow depth, snow cover duration, total snow melt and total canopy sublimation during the 1992-93 and 1993-94 winters.

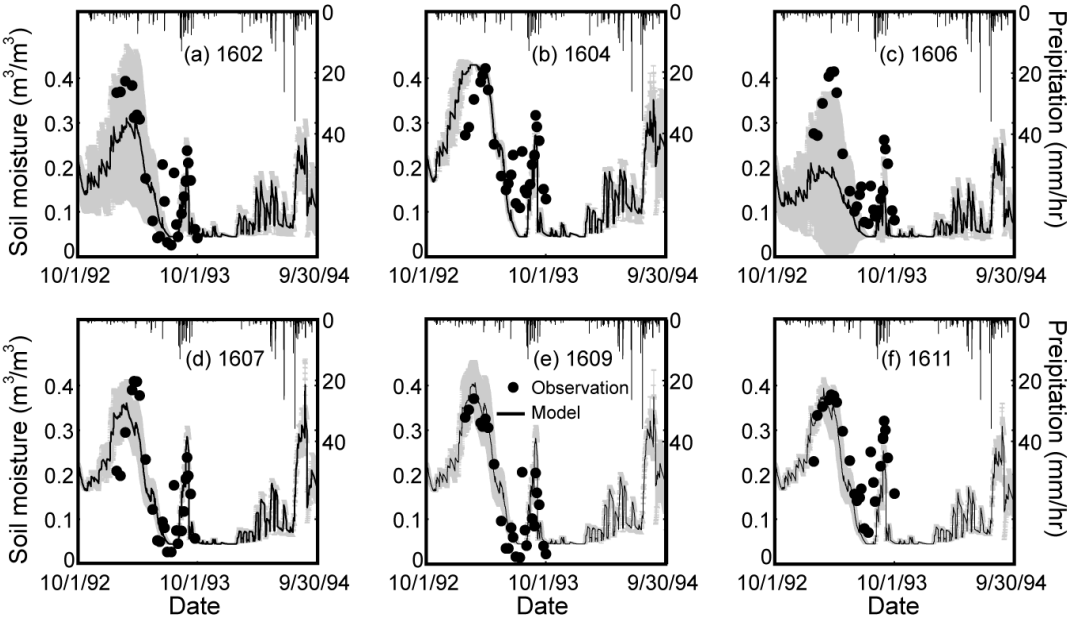

Figure 4.9. Comparisons between observed and simulated soil moisture at distributed locations during 1992-1994. Top row represents sites located in the southern part of hillslope and bottom row are sites in the northern part. Simulated values are spatial averages of the Voronoi polygon co-located with the sampling location and its neighboring elements (black lines). Spatial uncertainties are shown as ± 1 standard deviation (gray shading).

4.3.3. Contrasting hydrologic responses at site to hillslope scales

A detailed analysis of the hydrologic response in the hillslope for the contrasting water years can reveal how the bimodal precipitation regime influences the underlying mechanisms at scales ranging from single sites to the entire domain. Figure 4.12 presents the hydrologic dynamics at southern (1604) and northern (1611) grassland sites, including snow depth, soil moisture, latent heat flux from the land surface (evapotranspiration) and snow surface (sublimation), runoff, lateral transport and depth to groundwater. The southern grassland site receives more snow during both winters, though the difference with

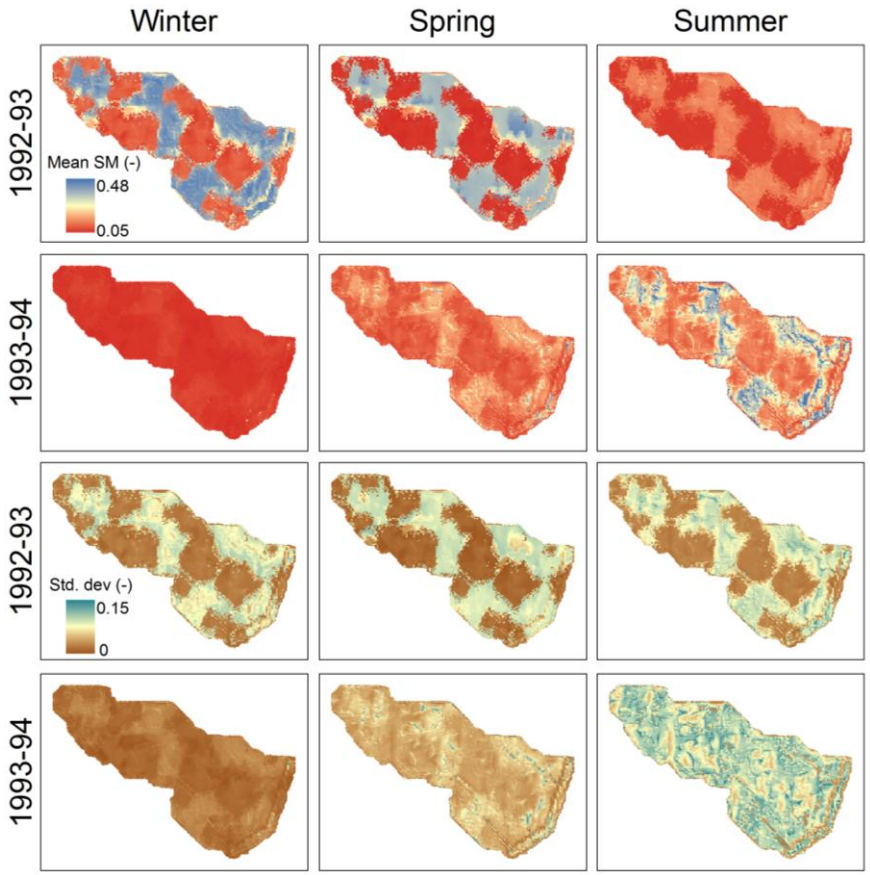

Figure 4.10. Spatial patterns of simulated soil moisture (25 cm depth-averaged) during the 1992-93 and 1993-94 periods for winter, spring and summer seasons. Top two rows depict the temporal mean soil moisture, while bottom two rows are the 1 temporal standard deviation.

the northern site is greater for 1992-1993. The larger snow depth at the southern site is subject to higher winter sublimation. Snow melt from the southern site leads to a saturated soil profile and groundwater depth near the surface for the wet winter in 1992-1993 that is not present at the northern site. Wetter soils at the southern grassland also induce more runoff generation through the saturation-excess mechanism during the winter and spring of 1992-1993. In contrast, winter wetting at the northern site elevates soil moisture more moderately, thus reducing runoff generation and promoting lateral transport away from the site. During the

drier 1993-1994 winter season, marked spatial differences in hydrologic dynamics are not observed. The reduced snow packs at both sites have lower sublimation, while the warmer temperatures in the spring lead to snow melt-induced soil moisture increases and lateral transport. Soil water availability in the 1993-1994 water year is also attributed to lower evapotranspiration from more frequent cloud-cover days in the spring and summer.

Figure 4.13 presents a summary of the hydrologic contrasts between the two water years based on the spatially-averaged water balance, $\Delta S/\Delta t = P - ET - Q$ for each season, where ΔS is the total change in storage (snow and soil moisture), P is the total precipitation (snow and rain), ET is the total losses to the atmosphere (sublimation and evapotranspiration) and Q is the total runoff (omitted due to its low values). In all cases, the water balance components are presented as mean seasonal quantities (symbols) with their ±1 spatial standard deviations (vertical bars). Clearly, the two water years exhibit opposing behavior during the winter to summer transition: (1) 1992-1993 has a decreasing ΔS in time resulting from an increasing ET that exceeds P, thus depleting both the snow pack and the soil water storage, and (2) 1993-1994 has an increase in ΔS in time, primarily due to soil water availability from periods of higher P than ET. This summary highlights how the differential sequencing of precipitation during winter and summer seasons (wet-to-dry or dry-to-wet) impact the hydrologic response of a forested hillslope, leading to either land surface water depletions to the atmosphere or water inputs from the atmosphere that remain in storage and may be redistributed internally as lateral transport or runoff.

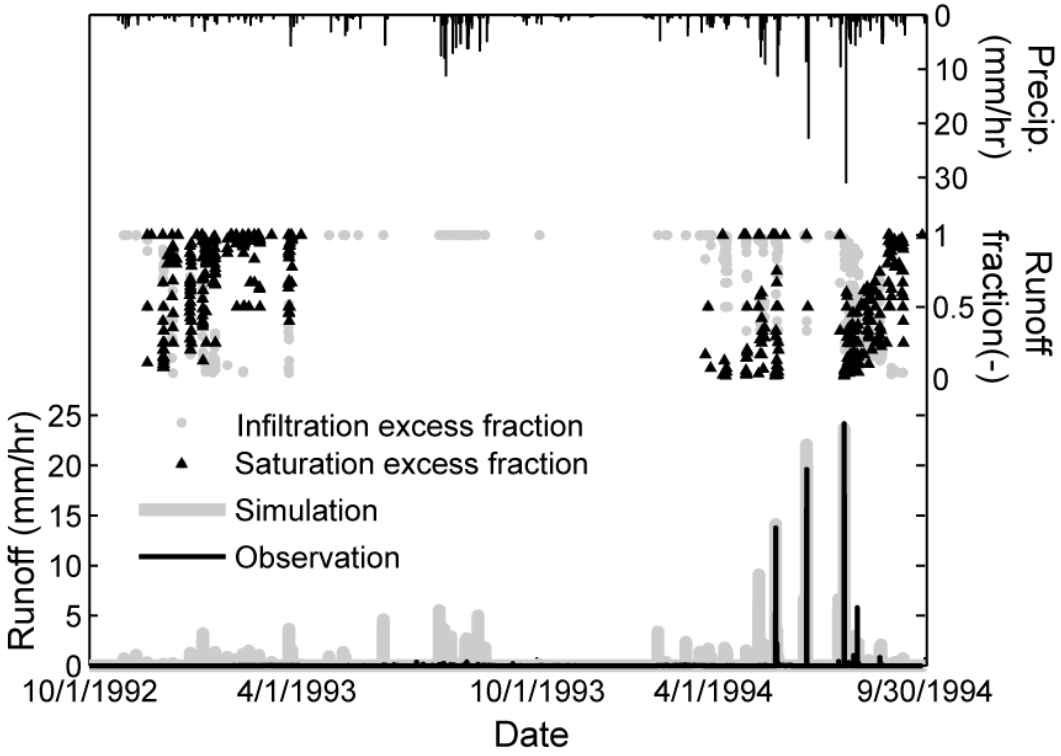

Figure 4.11. Comparison of observed and simulated runoff at the hillslope outlet and the fraction of total runoff from infiltration excess and saturation excess mechanisms during 1992-1994.

To investigate if the winter-to-summer transitions impact lateral transport, we derived an index of hydrologic connectivity. This dimensionless index was obtained as the hillslope areal fraction with root zone (top 1 m) soil moisture above a certain threshold. Three thresholds were based on the work of Newman et al. (2004) who found that beyond a root zone moisture of 0.33 m^3/m^3, a lateral connection was established in subsurface macropores (represented in the model by the anisotropy of saturated hydraulic conductivity, *Mahmood and Vivoni*, [2011a]. Two other thresholds (0.28 and 0.38 m^3/m^3) are used to test the sensitivity of the connectivity, which ranges from 0 (disconnected) to 1 (fully

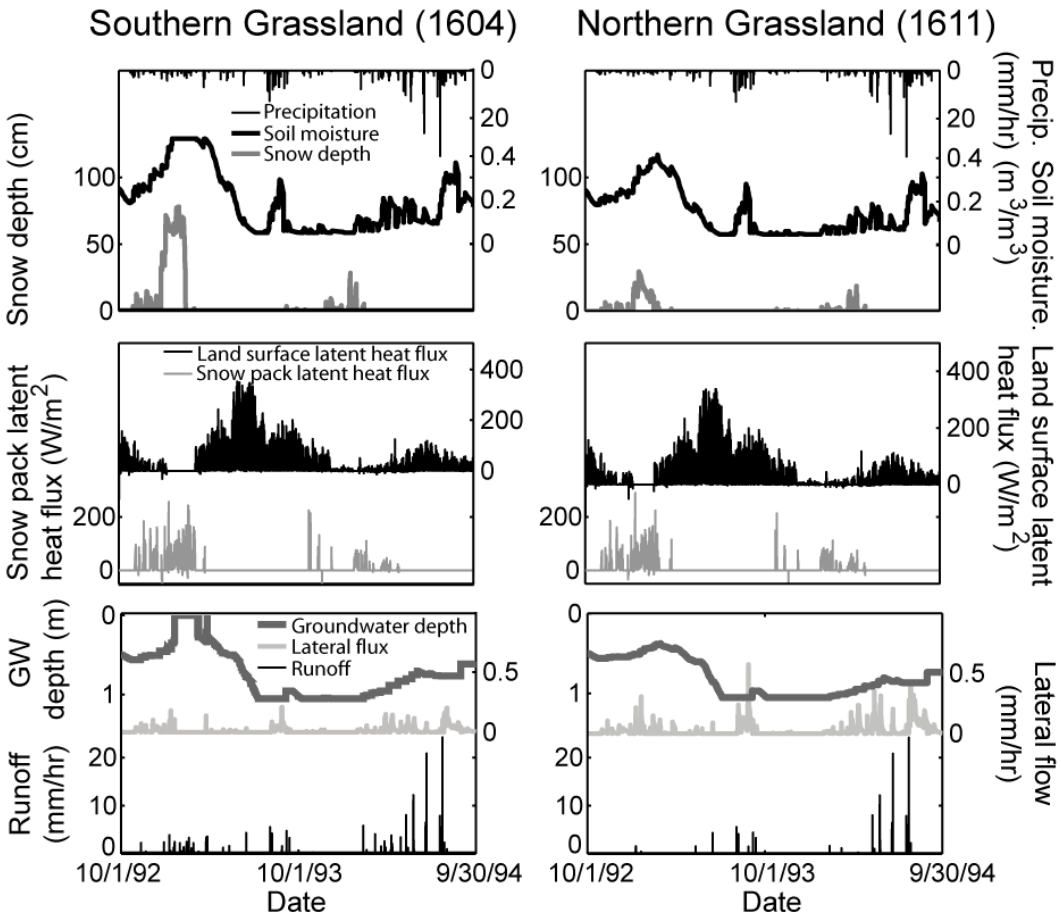

Figure 4.12. Hydrologic processes in southern (1604) and northern (1611) grassland sites, including 25 cm depth-average soil moisture, snow depth, land surface latent heat flux, snow surface latent heat flux, runoff, lateral flow and groundwater depth.

connected). Figure 4.14 presents the hydrologic connectivity for each water year, along with spatially-averaged hillslope conditions for reference. In 1992-1993, the hillslope is well-connected (index values greater than 0.5 for all thresholds) during the winter season due to moderately wet initial conditions and snow melt-induced infiltration. During the spring, lateral connectivity remains constant followed by a sudden decrease (index values fall to zero) in early summer due to

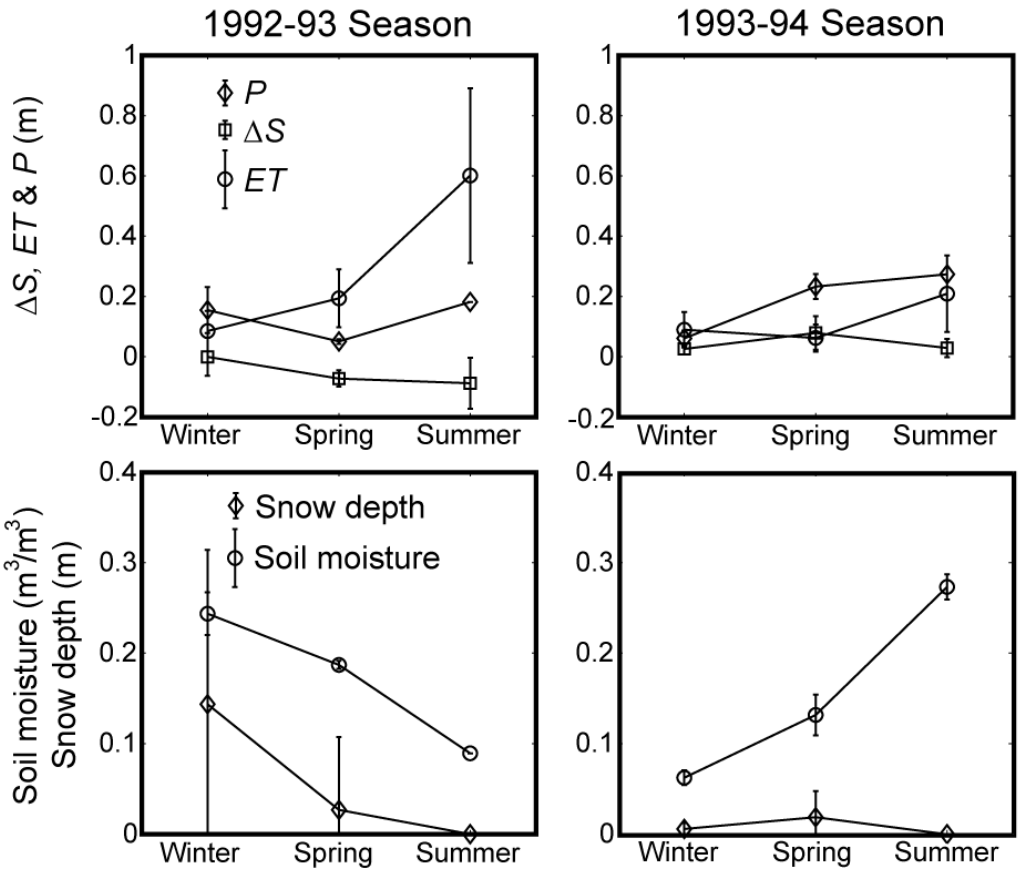

Figure 4.13. Seasonality in hillslope averaged hydrologic responses during 1992-93 and 1993-94 seasons. Note that we represent hydrologic responses from winter, spring and summer season. Hydrologic responses include season total evapotranspiration (*ET*), storage change (Δ*S*), precipitation (*P*), seasonal mean snow depth and soil moisture. Vertical bars represent ±1 spatial standard deviation within hillslope.

the coincident rise in evapotranspiration. This is consistent with the soil moisture pattern resembling the vegetation distribution for the dry summer. A contrasting behavior is observed in the hydrologic connectivity of the 1993-1994 water year. During the dry winter, the hillslope is disconnected in terms of lateral fluxes for all thresholds. As hillslope wets up with a series of rain and snow events in the spring, connectivity increases to values above 0.4 for all thresholds. Consistent with prior analyses, the wet summer in 1993-1994 increases the lateral connectivity due to high rainfall and low evapotranspiration, leading to soil

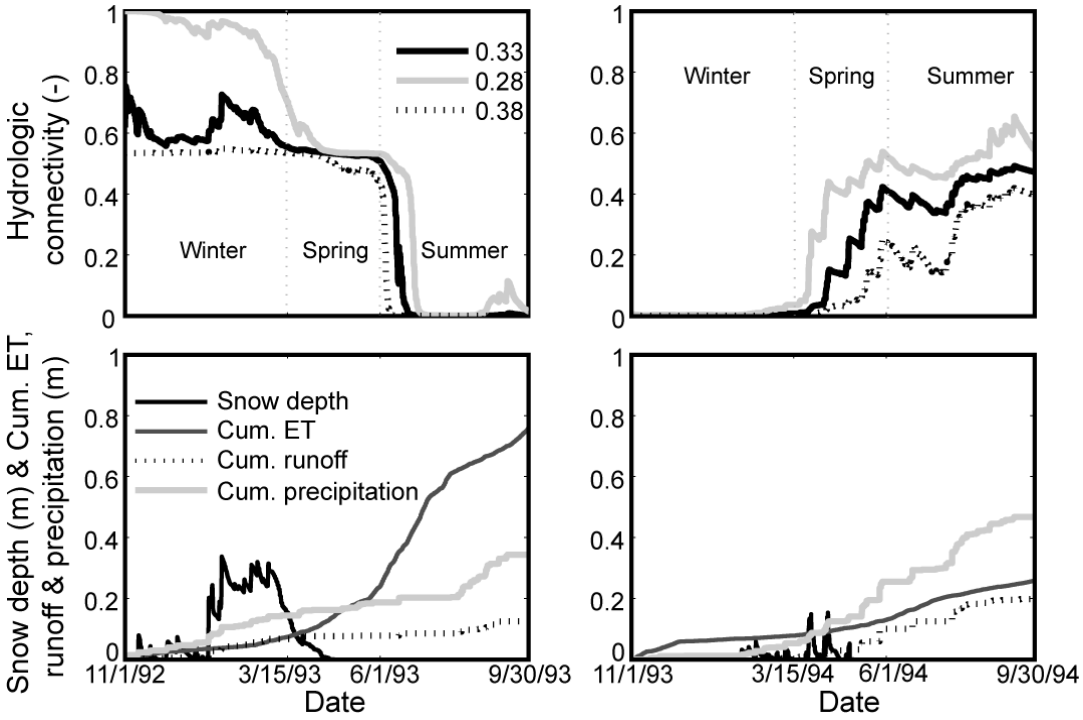

Figure 4.14. Temporal dynamics of hillslope connectivity during 1992-93 and 1993-94 season. Note that top row represents hillslope connectivity and bottom row represents temporal dynamics of hillslope snow depth and cumulative precipitation, evapotranspiration and runoff.

moisture patterns that resemble the terrain curvature distribution [*Mahmood and Vivoni*, 2011a].

4.4. Synthesis and Conclusions

Bimodal precipitation in the winter and summer seasons is an important climate feature of the southwestern United States. Precipitation amounts in each season have been hypothesized to be physically-linked through several proposed pathways [e.g. *Gutzler and Preston*, 1997; *Gutzler*, 2000; *Small*, 2001; *Zhu et al.*, 2005; *McCabe and Clark*, 2006; *Mo*, 2008; *Notaro and Zarrin*, 2011). In this study, we analyze the hydrologic response in a ponderosa pine hillslope during

two contrasting winter to summer transitions: a wet winter followed by a dry summer (1992-1993) and dry winter followed by a wet summer (1993-1994). These water years represent well the inverse relation between winter and summer precipitation found in prior studies. We use a distributed hydrologic model tested against field observations to provide spatiotemporal estimates of hillslope states and fluxes, including snow cover, soil moisture and runoff. Used in this way, the model is a tool for interpreting the plausible physical mechanisms that underlie the contrasting responses to the seasonal precipitation and as a means for generating a consistent set of spatially-distributed hydrologic estimates (see *Vivoni*, 2012, for further discussion).

Winter to summer season simulations at the hillslope scale are challenging due to the high number of process representations and the hydrologic variations found over short distances. For example, accounting for the role of wind-redistribution on snow through a simplified tree sheltering was essential for reproducing the available snow depth measurements [*Wilcox et al.,* 1997]. For wet winters, spatial differences in snow depth induced by tree sheltering propagated to melt water infiltration and soil moisture patterns during the spring. For dry winters, spatial variations are muted and the role of vegetation on soil moisture patterns is limited to effects on summer interception and evapotranspiration. Given the number of interacting processes, the model performance is considered to be good as compared to the snow depth, soil moisture and runoff observations for the purposes of outlined above. The spatiotemporal simulations for the two water years are consistent with summer simulations (1996-1998) conducted by

Mahmood and Vivoni [2011a] in several ways: (1) the same set of model parameter reproduced available data, (2) similar vegetation and terrain curvature controls were identified on soil moisture patterns, and (3) model performance relative to observations was similar. As a result, including the winter period in the continuous simulation allowed a detailed investigation of the winter to summer transition. Furthermore, we found the dry summer in 1996 was preceded by a wet winter (160 mm), while the wet summer in 1997 had a dry (14 mm) antecedent winter, supporting that the inverse relation could be applicable over other years, as shown by *McCabe and Clark* [2006].

The impact of the contrasting winter to summer transitions on the hillslope hydrologic response can be summarized as follows. (1) Wet winters lead to a substantial snow pack in ponderosa pine forests which increases snow melt input into soils throughout the winter and spring, despite the high sublimation losses. When followed by a dry summer, evapotranspiration increases substantially leading to drier soils, a switch occurs from saturation excess to infiltration excess runoff mechanisms, lateral transports diminish such that hydrologic connectivity is reduced, and the drier soil moisture pattern in the summer resembles vegetation patches. (2) Dry winters lead to a reduced snow pack in the forested landscape that is exposed to less sublimation and yields higher proportional snow melt inputs into the soil during the spring. When followed by a wet summer with frequent cloud cover, soil moisture is preserved in the subsurface due to lower evapotranspiration rates, runoff generation progressively favors the saturation excess mechanism, and a lateral connection is established in the hillslope such

that the wetter soil moisture patterns contain the signature of the terrain curvature distribution.

To our knowledge, this is the first attempt to compare the hydrologic consequences of the contrasting winter to summer transition at hillslope or watershed scales in the southwestern US. At regional scales, however, several studies have used hydrologic models to study the land influence on the inverse relation [*Zhu et al.,* 2005, 2007; *Notaro and Zarrin,* 2011]. Our modeling approach complements these regional efforts by: (1) providing spatial details on snow and soil moisture distributions and the influence of vegetation and topography [*Rinehart et al.,* 2008], (2) revealing the underlying physical processes involved in the link between winter and summer seasons, and (3) predicting the consequences on runoff production and hydrologic connectivity in the subsurface. Thus, the use of a distributed model over continuous periods can be useful for understanding site-specific responses to changes in seasonal precipitation distribution for bimodal climate regimes. Furthermore, the contrasting winter to summer transitions should have implications on vegetation phenology [*Jenerette et al.,* 2010], groundwater recharge [*Small,* 2005] and geomorphic development [*Etheredge et al.,* 2004] that merit additional attention.

5. Conclusion and Future Work

5.1. Conclusion

This dissertation represents the hillslopes scale quantitative analyses of distributed hydrologic processes using the tRIBS model which performs adequately against multiple hydrologic variables such as soil moisture, snow depth and runoff. Such performance allows us to answer hydrologic science questions under different seasons described in Chapters 2, 3 and 4.

Chapter 2 utilized the tRIBS model to answer the following science questions:

1. What are the spatial controls on hydrologic patterns during the NAM?
2. Are these controls static or evolve with seasonality? What are the processes and physical mechanisms responsible for the temporal evolutions of spatial controls?

First, we have built confidence on the model by manually calibrating the model to soil moisture and runoff simultaneously for the 1997 NAM and tested our calibrated parameter for the 1996 and 1998 NAMs. Model performance is adequate based on a visual inspection and the RMSE metric between observation and simulation. Based on good model performance, we explore the spatial controls on simulated soil moisture and runoff patterns. Overall, vegetation and topographic curvature are major spatial controls in the study site under uniform soil condition (Answer of question 1). During the 1996 and 1998 NAMs, vegetation exerts controls on soil moisture, runoff and storage spatial patterns. However, during the 1997 NAM, vegetation exerts controls during dry summer

period resulting in a patchy soil moisture pattern with dry soil underneath ponderosa pine patches and wetter soil in inter-patch grassland areas. Vegetation controlled spatial patterns during the dry summer transitions to a topographic controlled system during the NAM. Our investigations also indicate that a climate threshold involving the NAM rainfall amount (total august, 1997 rainfall = 146 mm) and cloud cover duration (~42 % day time is cloudy during August, 1997) are responsible for switching the spatial controls from vegetation to topographic curvature. Thus, the system transitions from an ET dominated system to s lateral flux dominated system as heavy rainfall infiltrate abundant moisture in the vadose zone for lateral transport and longer cloudy condition reduces ET during the NAM. Thus, the answer of question # 2 is that local spatial control such as vegetation is static when NAM climatic condition stays below the detected threshold. However, local (vegetation) spatial control switches to the nonlocal control (topographic curvature), when the detected climate threshold is exceeded during the NAM. The nonlocal to local spatial control switch was previously observed during the winter to summer transitional period in Australia [*Grayson et al.,* 1997]. As of our knowledge, our study first reveals such a spatial switch during NAM in the semiarid region. In summary, Chapter 2 improves our understanding about the spatial controls on the hydrologic patterns and the temporal evolution of these spatial controls with underlying physical mechanism.

Chapter 3 is an extension of Chapter 2 in the line of investigating model coarsening on simulated soil moisture response. Science questions of the Chapter 3 are given below:

1. What are the impacts of model coarsening on land surface characteristics and simulated hydrologic patterns?
2. Is there any threshold model resolution beyond which the reliability of simulated hydrologic patterns is no longer reliable?
3. What are implications for selecting future sampling site if the finest resolution model simulations are representations of real world hydrologic patterns?

In Chapter 3, we have explored the impacts of spatial sensitivity on the reliability of simulated soil moisture pattern and threshold model resolution beyond which soil moisture pattern is no longer reliable. Chapter 3 clearly has demonstrated that the model coarsening significantly impacts topographic curvature and slightly distorts ponderosa pine patches. Thus, model coarsening eradicates fine resolution curvature controlled soil moisture pattern and slightly distorts vegetation controlled soil moisture patterns (Answer of question # 1). We also have detected a threshold model resolution which is ~10% of original LIDAR topographic field for the reliable soil moisture simulation using multiple spatial metrics such as homogeneity indices, correlation coefficient and spatial error (Answer of Question # 2). Using the spatial error map, we have conducted experiments of designing future sensor network by moving current sensor network to the nearest convex and concave areas. Here we assume that the finest resolution soil moisture pattern represents real world pattern. Our experimental designs in model domain suggest the highest error in the concave sites and the lowest error in the convex site due to model coarsening demonstrating the

importance of sampling in the concave areas for the future hillslope sensor network design. The answer of question # 3 is that we have indentified future sampling sites based on our findings.

In Chapter 4, we have investigated the hydrologic responses of two years having sequence winter and summer seasons with contrasting wetness. Science question for the Chapter 4 is given below:

1. What are impacts on hydrologic responses during contrasting winter to summer transitions (spring season)?

We utilize the tRIBS model evaluated concurrently against the snow depth, soil moisture at 22 cm depth and hillslope outlet runoff for two water years having contrasting winter and summer wetness to answer this question. During a water year having a wet winter followed by a dry summer, generally ET induced hillslope drying is observed. Thick snowpack develops and soil saturation occurs in the inter-canopy grassland areas due to the snow albedo induced very low radiation in soil and the infiltration of initial melts during the wet winter period. However, due to lack of precipitation and high evapotranspiration, very wet soil dries out during the spring season. During the dry summer season, soil drying continues due to high evapotranspiration and low precipitation and lowers the soil moisture content to the residual soil moisture content. Thus, during a sequence having wet winter and dry summer, very wet soil condition dries out due to uptake of moisture via outgoing vertical flux from the soil resulting in the hillslope disconnection and vegetation controlled hydrologic pattern during summer period. In contrast, generally soil wetting is observed during a water year

having a dry winter prior to wet summer. Soil is very dry during dry the winter period, soil wets up during the spring season due to early spring snow event with subsequent melts and high rainfall amount. Soil wetting further continues during the wet summer period due to the infiltration of high rainfall amount and low evapotranspiration caused by frequent cloud cover. Thus, hillslope wetting is observed during a transition from dry winter to wet summer periods activating hillslope lateral connectivity and resulting topographic curvature controlled soil moisture pattern. Our findings suggests that the contrasting hydrologic responses are resulted due to inverse relationship between the winter and summer wetness. Thus, the inverse relation has strong influence on the hillslope connectivity, wetting, and drying and spatial soil moisture pattern with implications on other ecohydrologic processes including tree phenology, recharge and geomorphic development.

Finally, this dissertation clearly improves our knowledge about the spatial controls on hydrologic patterns, seasonal evolution of the spatial controls during NAM, the threshold model resolution to simulate this ecosystem and the winter to summer transitional hydrologic responses during a sequence of the winter and summer having contrasting wetness.

5.2. Future work and recommendation

Hillslope scale distributed modeling of patchy ponderosa pine ecosystems and the analyses of distributed model results provide a strong basis for further observation and modeling based studies in the large watershed and landscape

scale in the southwestern U.S. Since the study site is representative of the ponderosa pine areas in Arizona, New Mexico and Colorado, the hydrologic knowledge gained from our modeling effort are relevant to forested watershed throughout the southwestern U.S. In following, I would like to recommend the future observation and modeling based studies in the ponderosa pine forest ecosystem:

- **Testing current findings:** Future studies can utilize current model set up to simulate ponderosa pine hillslope for multiple years (1993-98) to assess our current findings. Such studies are useful for determining the frequency of spatial control switch, assessing and refining the currently detected climate threshold, validating the currently detected threshold model resolution and finally assessing current findings about the impacts inverse relationship between the winter and summer wetness on hydrologic responses. Similar studies should be carried out in large watershed scale particularly in the Pajarito Plateau and the Jemez River Basin for assessing and improving our current findings. In our sensor network design, we considered only the summer simulations which lack hydrologic insights of winter and spring season. Future study should consider the simulations for the full year weather conditions and redesign sensor network which can provide new information.
- **Future observation and modeling based study:** Our current findings can be useful for designing and planning for future zero order basin studies. Such study requires selection of a site, designing instrumentation networks for flux measurement and modeling of the site. Our current findings can be useful for

all of these requirements. We selected the current site based on its land cover type (Patchy ponderosa pine forest) and data availability. However, we did not have opportunity to consider other land surface properties and hydrologic considerations for selecting our site. Future study can utilize the currently available high resolution geospatial datasets involving vegetation, vegetation dynamics (forest regeneration and deforestation), topography, geophysical maps, soil maps and geological maps for selecting future sites and formulating science questions. Instrumentation of a future site should consider the deployment of soil moisture sensors for continuous measurements at topographically and land cover sensitive areas, measuring evapotranspiration using eddy-covariance tower at footprint scale and sap-flow measurement rings for individual tree (current study lacks such measurement), measuring ground, sensible and latent heat flux and finally deployment of SNOTEL site for continuous SWE measurements and distributed snow depth measurement tools for capturing spatial snow depth variation. In addition to these direct observations, future works should consider the shallow geophysical techniques such as resistivity tomography during the wet winter and summer period to map 3D soil moisture variability. Such estimates will be helpful to evaluate the spatial soil moisture patterns simulated by the model. Further, future study can contemplate their findings from direct observation by indirect inference made from cation, anion and isotopic composition of soil water. Such hydrogeochemical approach also can be helpful to determine the transit time of the system, evapotranspiration and downward vertical flux. Advanced

ecohydrological model (e.g. tRIBS+VEGGIE) is also recommended for future modeling studies to advance our standing about the biophysical and hydrological processes in the ponderosa pine ecosystem. In addition, further model development such as addition of ground heat flux component from snowpack, representation of macropore in subsurface soil for capturing lateral transport and incorporation wind-blown snow component are also recommended.

- **Future studies under climate change and land cover change scenario:** Land cover like ponderosa pine at the mid-altitude semiarid environment is of particular importance since this land cover is highly susceptible to climate change [e.g., *Woodhouse et al*., 2010]. Current climate predictions estimate the drier semiarid southwest with the flashy precipitation pulses. On the other hand, the snowpack of the southern Rocky Mountain will be thinner as warming continues in the future. Lack of snow in the Rocky Mountain may lead to the wetter summer as seen in previous studies [e.g. *Gutzler and Preston*, 1997]. In addition, warming also may increase the amount of liquid precipitation and decrease the snowfall amount during the winter. Therefore, we can use our current model set up or any future model set up at other sites under these climatic scenarios (using current climate prediction or stochastic weather generator) to predict future hydrologic responses of the ponderosa pine ecosystem. In addition to climate change, ponderosa pine land cover type was deforested and regenerated during last 100 years. It was also impacted by the forest fire occurring at the frequent interval. Finally, the investigations for

exploring the impacts of such land cover change on hydrologic responses are also recommended for future study.

I have found that the combination of the distributed observations and modeling are very useful for deciphering the hydrologic patterns, spatial controls and hydrologic processes. Although, our modeling effort is limited to a hillslope and few year simulations, findings of our study can help to advance our understanding for the ponderosa pine forest hydrology in the semiarid southwest by testing current findings for other years in the current site and also at larger watershed scales throughout the region. Our findings have multiple implications on the future field and modeling studies in the ponderosa pine ecosystems. Further, the dual use of the distributed modeling and field observations studies in ponderosa pine forests can help to improve prediction capability under important climate and land cover change scenario that are widely anticipated for the southwestern United States.

References

Anderson, S. A., R. C. Bales and C. J. Duffy, Critical Zone Observatories: Building a network to advance interdisciplinary study of Earth surface processes, *Mineral. Mag.*, 72(1): 7-10, 2008.

Anderson, J., J. C. Refsgaard and K. H. Jensen, Distributed hydrologic modeling of the Senegal River Basin- model construction and validation, *J. Hydrol.*, 247(3-4), 200-214, 2001.

Bales, R. C., J. W. Hopmans, A. T. O'Geen, M. Meadows, P. C. Hartsough, P. Kirchner, C. T. Hunsaker and D. Beaudette, Soil moisture response to snowmelt and rainfall in a Sierra Nevada Mixed-Conifer forest, *Vadose Zone Journal*, 10: 786-799, 2011.

Balmat, J., Assessment of timber resources and logging history of the Valles Caldera National Preserve. MS Thesis. University of Arizona, Tucson, AZ, 2004.

Bertoldi, G., C. Notarnicola, G. Leitinger., S. Endrizzi, M. Zebisch, S. Della Chiesa, and U. Tappeiner, Topographical and ecohydrological controls on land surface temperature in an alpine catchment, *Ecohydrol.* 3(2): 189-204, 2010.

Beven, K., Prophecy, reality and uncertainty in distributed hydrological modeling, *Advances in Water Resour.*, 16: 41-51, 1993.

Bi, H., J. Zhang, L. Lin, C. Guo, Y. Ren, L. Yun and N. Ma, Spatial dynamics of soil moisture in a complex terrain in the semi-arid loess plateau region, China, *J. Amer. Water Resour. Assoc*., 44 (5): 1121-1131, 2008.

Bowen, B. M., Rainfall and climate variation over a sloping New Mexico plateau during the North American Monsoon, *J. Climate*, 9: 3432-3442, 1996.

Brandes, D. and B. P. Wilcox, Evapotranspiration and soil moisture dynamics on a semiarid ponderosa pine hillslope, *J. Amer. Water Resour. Assoc.*, 36 (5): 965-974, 2000.

Broxton, P. D., P. A. Troch and S. W. Lyon, On the role of aspect to quantify water transit times in small mountainous catchments, *Water Resour. Res.* 45: W08427, doi:10.1029/2008WR007438, 2009.

Brooks, P. D., and M. W. Williams, Snowpack controls on nitrogen cycling and export in seasonality snow-covered catchments, *Hydrol. Process*., 13: 2177-2190, 1999.

Bruneau, P., C. Gascuel-Odoux, P. Robin, P. Merot, K. Beven, Sensitivity to space and time resolution of a hydrologic model using digital elevation data, *Hydrol. Process.* 9: 69-81, 1995.

Burt, T. P. and D. P. Butcher, Topographic controls on soil moisture distributions, *European J. Soil Sci.*, 36 (3): 469-486, 2006.

Cabral, M. C., L. Garrote, R. L. Bras and D. Entekhabi, Kinematic infiltration in vertically heterogeneous, anisotropic and sloped soils, *Adv. Water Resour.*, 15: 311-324, 1999.

Cayan, D. R., Interannual climate variability and snowpack in the western United States, *J. Climate* 9: 928-948, 1996.

Canfield, H. E., C. J. Wilson, L. J. Lane, K. J. Crowell, W. A. Thomas, Modeling scour and deposition in ephemeral channels after wildfire. *Catena*. 61: 273-291, 2005.

Carey, S. K. and M. Woo, Spatial variability of hillslope water balance, Wolf Creek basin, subarctic Yukon, *Hydrol. Process*., 15 (16): 3113-3132, 2001.

Cayan, D. R., T. Das, D. W. Pierce, T. P. Barnett, M. Tyree and A. Gershunov, Future dryness in the southwest US and the hydrology of the early 21st century drought. *Proc. Natl. Acad. Sci.* USA. 107: 21271-21276, 2010.

Caylor, K. K., S. Manfreda and I. Rodriguez-Iturbe, On the coupled geomorphological and ecohydrological organization of river basins, *Adv. Water Resour.*, 28: 69-45, 2005.

Chamran, F., P. E. Gessler and O. A. Chadwick, Spatially explicit treatment of soil-water dynamics along a semiarid catena, *Soil Sci. Soc. Amer. J.*, 66: 1571-1583, 2002.

Chaubey, I., A. S. Cotter, T. A. Costello, T. S. Soerens, Effect of DEM data resolution on SWAT output uncertainty, *Hydrol. Process.* 19: 621-628, 2005.

Cho, S., M. Lee, Sensitivity considerations when modeling hydrologic processes with digital elevation model, J. Am. Water Resour. Assoc. 37: 931-934, 2007.

Chochrane, T. A., and D. C. Flanagan, Effect of DEM resolutions in the runoff and soil loss predictions of the WEPP watershed model, *Trans. of the ASAE,* 48: 109-120, 2005.

Coop, J.D., and T. J. Givnish,. Spatial and temporal patterns of recent forest encroachment in montane grasslands of the Valles Caldera, New Mexico, USA. *Journal of Biogeography* 34: 914–927, 2007.

Crave, A., and C. Gascuel-Odoux, The influence of topography on time and space distribution of soil surface water content, *Hydrol. Process.* 11: 203-210, 1997.

Crockford, R.H., and D. P. Richardson, Partitioning rainfall into throughfall, stemflow and interception: effect of forest type, ground cover and climate, *Hydrological Processes* 14: 2903-2920, 2002.

Cuo, L., D. P. Lettenmaier, B. V. Mattheussen, P. Storck, P and M. Wiley, Hydrologic prediction for urban watersheds with the Distributed Hydrology-Soil-Vegetation Model, *Hydrol. Process.* 22(21): 4205-4213, 2008.

Dixon, B., and J. Earls, Resample or not? Effects of resolution of DEMs in watershed modeling, *Hydrol. Process.* 23: 1714-1724, 2009.

Douglas M. W., R. A. Maddox, K. Howard, S. Reyes, The Mexican monsoon, *J. Climate* 6: 1665-1677, 1993.

Dozier, J., A method for satellite identification of surface temperature fields of subpixel resolution, *Remote Sensing of Environmen*t 11 (3), 221–229, 1981.

Ellis, A. W., and T. W. Hawkins, An apparent teleconnection between snow cover and the North American monsoon, *Geophys. Res. Lett.,* 28 (13): 2653-2656, 2001.

Etheredge, D., D. S. Gutzler, F. J. Pazzaglia, Geomorphic response to seasonal variations in rainfall in the Southwest United States, *Geological Society of America Bulletin* 116: 606-618, 2004.

Evett, S. R., J. A. Tolk and T. A. Howell, A depth control stand for improved accuracy with the neutron probe, *Vadose Zone Journal,* 2: 642-649, 2003.

Famiglietti, J. S and E. F. Wood, Multiscale modeling of spatially variable water and energy balance processes, *Water Resour. Res.* 30(11): 3061-3078, 1994.

Forzieri G, F. Castelli, E. R. Vivoni, Vegetation dynamics within the North American monsoon region, *J. Climate* 24(6): 1763-1783, 2011.

Freer, J., McDonnell, J. J., Beven, K. J., Peters, N. E., Burns, D. A., Hooper, R. P., B. Aulenbach and C. Kendall, The role of bedrock topography on subsurface storm flow, *Water Resour. Res.* 38(12): 1269, doi:10.1029/2001WR000872, 2002

Gallant, J. C., and T. I. Dowling, A multiresolution index of valley bottom flatness for mapping depositional areas, *Water Resour. Res.* 39(12): 1347, doi:10.1029/2002WR001426, 2003.

Georgakakos, K. P., and K. M. Carpenter, Potential value of operationally available and spatially distributed ensemble soil water estimates for agriculture, *J. Hydrol.* 328(1-2): 177-191, 2006.

Gomez-Plaza, A., M. Martinez-Mesa, J. Albaladejo and V. M. Castillo, Factor regulating spatial distribution of soil water content in small semiarid catchments, *J. Hydrol.* 253:211-226, 2001.

Goodrich, D. C., C. L. Unkrich, T. O. Keefer, M. H. Nichols, J. J. Stone, L. R. Levick and R. L. Scott, Event to multidecadal persistence in rainfall and runoff in southeast Arizona, *Water Resour. Res.*, 44 (5): W05S14, 2008.

Grayson, R. B., A. W. Western, F. H. S. Chiew and G. Blöschl, Preferred states in spatial soil moisture patterns: local to nonlocal controls, *Water Resour. Res.*, 33 (12): 2897-2908, 1997.

Grayson, R. B., G. Bloschl, A. W. Western and T. McMahon, Advances in the use of observed spatial patterns of catchment hydrologic response, *Adv. Water Resour.* 25: 1313, 2002.

Guan, H., J. Simunek, B. D. Newman and J. L. Wilson, Modelling investigation of water partitioning at a semiarid ponderosa pine hillslope, *Hydrol. Process.*, 24: 1095-1105, 2010.

Gustafson, J. R., P. D. Brooks, N. P. Molotch and W. C. Veatch, Estimating snow sublimation across a gradient of solar radiation, *Water Resour. Res.* 46: W12511, doi:10.1029/2010WR009060, 2010.

Gutzler D.S., and J. W. Preston, Evidence for a relationship between spring snow cover in North America and summer rainfall in New Mexico, *Geophys. Res. Lett.*, 24: 2207-2210, 1997.

Guztler D.S., Covariability of spring snowpack and summer rainfall across the southwest United States, *J. Climate*, 13: 4018-4027, 2000.

Hedstorm, N.R. and J. W. Pomeroy, Measurements and modeling of snow interception in boreal forest, *Hydrological Processes* 12: 1611-1625, 1998.

Higgins R. W., and W. Shi, Dominant factors responsible for interannual variability of the summer monsoon in the Southwestern United States, *J. Climate* 13: 759-776, 2000.

Higy, C., A. Musy, Digital terrain analysis of the Haute-Mentue catchment and scale effect for hydrologic modeling with TOPMODEL, *Hydrol. Earth Syst. Sci.* 4(2): 225-237, 2000.

Hopp, L., C. Harman, C., S. L. E. Desilets, C. B. Graham, J. J. McDonnell and P. A. Troch, Hillslope hydrology under glass: confronting fundamental questions of soil-water-biota co-evolution at Biosphere 2, *Hydrol. Earth Sys. Sci.* 13(11): 2105-2118, 2009.

Horn, B. K. P., Hillshading and the reflectance map, *Proc. of the IEEE.* 69(1): 14-47, 1981.

Ivanov, V. Y., E. R. Vivoni, R. L. Bras and D. Entekhabi, Catchment hydrologic response with fully-distributed triangular irregular network model, *Water Resour. Res.,* 40: doi:10.1029/2004WR003218, 2004a.

Ivanov, V. Y., E. R. Vivoni, R. L. Bras and D. Entekhabi, Preserving high-resolution surface and rainfall data in operational-scale basin hydrology; a fully-distributed physically-based approach, *J. Hydrol.,* 298 (1-4): 80-11, 2004b.

Ivanov, V. Y., R. L. Bras and E. R. Vivoni, Vegetation-hydrology dynamics in complex terrain of semiarid areas: 2. Energy-water controls of vegetation spatiotemporal dynamics and topographic niches of favorability, *Water Resour. Res.,* 44: W03430, doi: 10.1029/2004WR003218, 2008.

Ivanov, V. Y., S. Fatichi, G. D. Jenerette, J. F. Espeleta, P. A. Troch and T. E. Huxman, Hysteresis of soil moisture spatial heterogeneity and the 'homogenizing' effect of vegetation, *Water Resour. Res*., 46: W09521, doi: 10.1029/2009WR008611, 2010.

Izioman, M. G. and H. Mayer, On the variability and modeling of surface albedo and long-wave radiation components, *Agri, Forest Meteorol.,* 111: 141-152, 2002.

Jenerette, G.D., R. L. Scott, A. R. Huete, Functional differences between summer and winter season rain assessed with MODIS-derived phenology in a semi-arid region, *J. Veg. Sci.* 21: 16-30, 2010.

Kalma, J. D., B. C. Bates and R. A. Woods, Predicting catchment-scale soil moisture status with limited field measurements, *Hydrol. Process.,* 9: 445-467, 1995.

Kavvas, M. L., On the coarse-graining of hydrologic processes with increasing scales, *J. Hydrol.* 217: 191-202, 1999.

Karlson, P. E. and S. M. Assmann, Rapid and specific modulation of stomatal conductance by Blue Light in Ivy (*Hedera helix*), *Plant Physiology*, 94: 440-447, 1990.

Kuo, W-L., T. S. Steenhuis, C. E. McCulloch, C. L. Mohler, D. A.Weinstein, S. D. DeGloria and D. P. Swaney, Effect of grid size on runoff and soil moisture for a variable-source area hydrology model, *Water Resour. Res.* 35(11): 3419-3428, 1999.

Kurc S. A., and E. E. Small, Dynamics of evapotranspiration in semiarid grassland and shrubland ecosystems during the summer monsoon season, central New Mexico, *Water Resour. Res.*, 40: W09305, doi:10.1029/2004WR003068, 2004.

Kwicklis, E., M. Witkowski, K. Birdsell, B. Newman and D. Walther, Development of an infiltration map for the Los Alamos Area, New Mexico, *Vadose Zone J.*, 4: 672-693, 2005.

Laio, F., A. Porporato, L. Ridolfi and I. Rodriguez-Iturbe, Plants in water-controlled ecosystems: active roles in hydrologic processes, *Adv. Water Resour*., 24: 707-723, 2001.

Lawrence, J. E. and G. M. Hornberger, Soil moisture variability across climate zones, *Geophys. Res. Lett.*, 34: L20402, 2007.

Litaor, M. I., M. Williams and T. R. Seastedt, Topographic controls on snow distribution, soil moisture and species diversity of herbaceous alpine plant vegetation, Niwot Ridge, Colorado, *J. Geophys. Res.*,113: doi:10.1029/2007JG000419, 2008.

Loague, K. M., Impact of rainfall and soil hydraulic property information on runoff predictions at the hillslope scale, *Water Resour. Res.*, 24: 1501-1510, 1988.

Mahmood, T. H. and E. R. Vivoni, Evaluation of distributed soil moisture simulations through field observations during the North American monsoon in Redondo Creek, New Mexico, *Ecohydrol.*, 1 (3): 271-287, 2008.

Mahmood, T. H, and E. R. Vivoni, A climate-induced threshold in hydrologic response in a semiarid ponderosa pine hillslope, *Water Resour. Res.* 47: W09529, doi:10.1029/2011WR010384, 2011a.

Mahmood, T. H, and E. R. Vivoni, Breakdown of hydrologic patterns upon model coarsening at hillslope scales and implications for experimental design, *J. Hydrol.*, 411: 309-321, 2011b.

McCabe, G. J, and M. P. Clark, Shifting covariability of North American summer monsoon precipitation with antecedent winter precipitation, *Int. J. Climatology* 26: 991-999, 2006.

McDowell, N. G., H. D. Adams, J. D. Bailey and T. E. Kolb, The role of stand density on growth efficiency, leaf area index and resin flow in southwestern ponderosa pine forests, *Canadian Journal Forest Research*, 37 (2): 343-355, 2007.

McDowell, N. G., S. White and W. T. Pockman, Transpiration and stomatal conductance across a steep climate gradient in the southern Rocky Mountains, *Ecohydrol.*, 1 (3): 193-204, 2008.

McNamara J.P., D. G. Chandler, M. Seyfried and S. Achet, Soil moisture states, lateral flow, and streamflow generation in a semi-arid, snowmeltdriven catchment, *Hydrological Processes* 19: 4023–4038, 2005.

Minet, J., E. Laloy, S. Lambot and M. Vanclooster, Effect of high-resolution spatial soil moisture variability on simulated runoff response using a distributed hydrologic model, *Hydrol. Earth Sys. Sci.* 15(4): 1323-1338, 2011.

Mo, K.C., Influence of sea surface temperature on soil moisture and precipitation interactions over the southwest, *J. Geophys. Res.*,113: D12116, doi:10.1029/2007JH009221, 2008.

Mock C. J., Cilmatic controls and spatial variations of precipitation in the western United States, *J. Climate* 9(5): 1111-1125, 1996.

Molotch, N. P., P. D., Brooks, S. P., Burns, M., Litvak, R. K., Monson, J. R. McConnell, and K. Musselman, Ecohydrological controls on snowmelt partitioning in mixed-conifer sub-alpine forests, *Ecohydrol.*, 2: 129-142, 2009.

Molnar, D. K., and P. Y. Julien, Grid-size effects on surface runoff modeling, *J. Hydrol. Eng.* 5(1): 8-16, 2000.

Motovilov, Y. G., L. Gottschalk, K. Engeland, and A. Rodhe, Validation of a distributed hydrologic model against spatial observations, *Agricultural and Forest Meteorol.,* 98-99 (31): 257-277, 1999.

Newman, B. D., A. R. Campbell and B. P. Wilcox, Tracer-based studies of soil water movement in semi-arid forests of New Mexico, *J. Hydrol.*, 196 (1-4): 251-270, 1997.

Newman, B. D., A. R. Campbell and B. P. Wilcox, Lateral subsurface flow pathways in a semiarid ponderosa pine hillslope, *Water Resour. Res.*, 34 (12): 3485-3496, 1998.

Newman, B. D., B. P. Wilcox and R. C. Graham, Snowmelt-driven macropore flow and soil saturation in a semiarid forest, *Hydrol. Process*., 18 (5): 1035-1042, 2004.

Newman B.D., E. R. Vivoni, and A. R. Groffman, Surface-groundwater interactions in semiarid drainages of the American southwest, *Hydrol. Process*., 20: 3371-3394, 2006.

Noto, L. V., V. Y. Ivanov, R. L. Bras and E. R. Vivoni, Effects of initialization on response of a fully-distributed hydrologic model, *J. Hydrol.* 352: 107-125, 2008.

Notaro, M., and A. Zarrin, Sensitivity of the north American monsoon to antecedent rocky mountain snowpack, *Geophys. Res. Lett.,* 38: L17403, 2011.

Ogle K., and J. F. Reynolds, Plant responses to precipitation in desert ecosystems: integrating functional types, pulses, thresholds and delays, *Oecologia* 141: 282-294, 2004.

Rawls, W.J., D. L. Brakensiek and N. Miller, Green-Ampt infiltration parameters from soil data, *J. Hydraulic Eng.,* 109 (1): 62-70, 1983.

Rinehart A.J., E. R. Vivoni and P. D. Brooks,. Effects of vegetation, albedo and solar radiation sheltering on the distribution of snow in the Valles Caldera, New Mexico. *Ecohydrol.* **1**: 253-270, 2008.

Röβler, O., and J. Löffler, Potentials and limitations of modeling spatio-temporal patterns of soil moisture in a high mountain catchment using WaSiM-ETH, *Hydrol. Process.* 24: 2182-2196, 2010.

Rutter, A. J., K. A. Kershaw, P. C. Robins and A. J. Morton, A predictive model of rainfall interception in forests. 1. Derivation of the model from observation in a plantation of Corsican pine, *Agric. Meteorol*., 9: 367-384, 1971.

Seth., A., R. C. Bales and R. E. Dickinson, A framework for the study of seasonal snow hydrology and its interannual variability in the alpine regions of the southwest, *J. Geophys. Res.* 104 (D18), 22117-22135, 1999.

Seyfried, M. S., and B. P. Wilcox, Scale and the nature of spatial variability: Field Examples having implications for hydrologic modeling, *Water Resour. Res.* 31(1): 173-184, 1995.

Small, E. E., The influence of soil moisture anomalies on variability of the North American monsoon system, *Geophys. Res. Lett.,* 28(1): 139-142, 2001.

Small, E. E., Climatic controls on diffuse groundwater recharge in semiarid environments of the southwestern United States. *Water Resour. Res.* 41(4): W04012, 2005.

Sheppard P. R., A. C. Comrie, G. D. Packin, K. Angersbach, M. K. Hughes, The climate of the US Southwest, *Climate Res.* **21**(3), 219-238, 2002.

Tarboton D. G., and C. H. Luce, Utah Energy Balance Snow Accumulation and Melt Model (UEB). Utan Water Research Laboratory and USDA Forest Sesvice, 82 p, 1996.

Tarolli, P., J. R. Arrowsmith and E. R. Vivoni, Understanding earth surface processes from remotely sensed digital terrain models, *Geomorphology.* 113: 1-3, 2009.

Teuling, A. J. and P. A. Troch, Improved understanding of soil moisture variability dynamics, *Geophys. Res. Lett.,* 32: L05404, 2005.

Teuling, A. J., F. Hupet, R. Uijlenhoet and P. A. Troch, Climate variability effects on spatial soil moisture dynamics, *Geophys. Res. Lett.,* 34: L06406, 2007.

Vázquez, R. F., L. Feyen, J. Feyen and J. C. Refsgaard, Effect of grid size on effective parameters and model performance, *Hydrol. Process.* 16: 355-372, 2002.

Vieux, B. E., DEM aggregation and smoothing effects on surface runoff modeling, *J. Computing in Civil Engr.* 7(3): 310-338, 1991.

Vivoni, E. R., V. Y. Ivanov, R. L. Bras and D. Entekhabi, Generation of triangulated irregular networks based on hydrological similarity, *J. Hydrol. Eng.,* 9 (4): 288-302, 2004.

Vivoni, E. R., V. Y. Ivanov, R. L. Bras and D. Entekhabi, On the effects of triangulated terrain resolution on distributed hydrologic model response, *Hydrol. Process.,* 19: 2101-2122, 2005.

Vivoni, E. R., D. Entekhabi, R. L. Bras and V. Ivanov, Controls on runoff generation and scale-dependence in a distributed hydrologic model, *Hydrol. Earth Sys. Sci.,* 11: 1683-1701, 2007.

Vivoni, E. R., A. J. Rinehart, L. A. Méndez-Barroso, C. A. Aragon, G. Bisht, M. B. Cardenas, E. Engle, B. A. Forman, M. D. Frisbee, H. A. Gutiérrez-Jurado, S. Hong, T. Mahmood, K. Tai and R. L. Wyckoff, Vegetation controls on soil

moisture distribution in the Valles Caldera, New Mexico, during the North American monsoon, *Ecohydrol.*, 1 (3): 225-238, 2008a.

Vivoni, E. R., F. Di Benedetto, S. Grimaldi and E. A. B. Eltahir, Hypsometric control on surface and subsurface runoff, *Water Resour. Res.*, 44: W12502, doi:10.1029/2008WR006931, 2008b.

Vivoni, E. R., J. C. Rodríguez and C. J. Watts, On the spatiotemporal variability of soil moisture and evapotranspiration in a mountainous basin within the North American monsoon region, *Water Resour. Res.*, 46: W02509, doi: 10.1029/2009WR008240, 2010.

Vivoni E. R., Spatial patterns, processes and predictions in ecohydrology: Integrating technologies to meet the challenge, *Ecohydrol.* doi:10.1002/eco.1248, 2012.

Wallace, W. C., P. Z. Fule, M. M. Moore, S. C. Hart, T. E. Kolb, J. N. Mast, S. S. Sacket and M. R. Wagner, Restoring ecosystem health in ponderosa pine forest in southwest, *J. Forestry.*, 95 (4): 23-29, 1997.

Western, A.W., R.B. Grayson, G. Bloschl, G.R. Willgoose and T.A. McMahon, Observed spatial organization of soil moisture and its relation to terrain indices, *Water Resour. Res*., 35 (3): 797-810, 1999.

Wechsler, S. P., Uncertainties associated with digital elevation models for hydrologic applications: a review, *Hydrol. Earth Syst. Sci.* 11: 1481-1500, 2007.

Wilcox, B. P., B. D. Newman, D. Brandes, D. Davenport and K. Reid, Runoff from a semiarid ponderosa pine hillslope in New Mexico, *Water Resour. Res.*, 33 (10): 2301-2314, 1997.

Wilson JP, Gallant JC (eds). *Terrain Analysis: Principles and Applications.* John Wiley and Son: New York; 91–106.

Wigmosta, M.S., L. W. Vail, and D. P. Lettenmaier, A distributed hydrology vegetation model for complex terrain, *Water Resour. Res.* 30(6):1665–1679, 1994.

Wolock, D. M., C. V. Price, Effects of digital elevation model map scale and data resolution on a topography-based watershed model, *Water Resour. Res.* 30(11): 3041-3052, 1994.

Williams, A. P., C. D. Allen, C. I. Millar, T. W. Swetnam, J. Michaelsen, C. J. Still and S. W. Leavitt, Forest responses to increasing aridity and warmth in the southwestern United States, *Proc. Natl. Acad. Sci.,* 107 (50): 21289-21294, 2010.

Woodhouse, C. A., D. M. Meko, G. M. MacDonald, D. W. Stahle and E. R. Cook, A 1200-year perspective of 21st century drought in southwestern North America, *Proc. Natl. Acad. Sci.,* 107 (50): 21283-21288, 2010.

Yildiz, O. and A. P. Barros, Elucidating vegetation controls on the hydroclimatology of a mid-latitude basin, *J. Hydrol*., 333: 431-448, 2007.

Zhang, W., D. R. Montgomery, Digital elevation model grid size, landscape representation, and hydrologic simulations, *Water Resour. Res.* 30(4): 1019-1028, 1994.

Zhao, G. J., G. Hörmann, N. Fohrer, J. F. Gao, Impacts of spatial data resolution on simulated discharge, a case study of Xitiaoxi catchment in south China. *Adv. Geosci.* 21: 131-137, 2009.

Zhu, C., D. P. Lettenmaier, and T. Cavazos, Role of antecedent land surface conditions on North American monsoon rainfall variability, *J. Climate* 18: 3104-3121, 2005.

Zou, C. B., G. A. Barron-Gafford and D. D. Breshears, Effects of topography and woody plant canopy cover on near-ground solar radiation: Relevant energy inputs for ecohydrology and hydropedology, *Geophys. Res. Lett.,*. 34: doi:10.1029/2007GL031484, 2007.

Zou, C. B., D. D. Breshears, B. D. Newman, B. P. Wilcox, M. O. Gard and P. M. Rich, Soil water dynamics under low-versus high-ponderosa pine tree density: ecohydrological functioning and restoration implications, *Ecohydrol.,* 1 (4): 309-315, 2008.

APPENDIX A

CHAPTER 3 SUPPLEMENTARY

A.1. Derivation of homogeneity index

The homogeneity index (F) for a spatial field is adapted from the multiresolution valley bottom flatness (MRVBF) developed by Gallant and Dowling (2003). It utilizes the flatness and lowness characteristics of a field. Flatness is the inverse of slope (S) of the spatial field, whereas lowness is the ratio of the number of neighboring pixels at a lower value to the total number of pixels in a circular window. Gallant and Dowling (2003) developed MRBVF to identify valley bottoms from a DEM using multiple spatial resolutions of the terrain slope field. We generalize the concept to handle any spatial field. F is mathematically equivalent to their $MRVBF_2$.

A two step process is used to compute flatness (F_1 and F_2) and local lowness (L_1 and L_2). In each step, a generic nonlinear function, $M(x, t, b)$, is used to transform positive ($x > 0$) input values into the 0 to 1 range (Gallant and Dowling, 2003) as:

$$M(x,t,b) = \frac{1}{1+\left(\frac{x}{t}\right)^b} \quad , \qquad \text{(A1)}$$

where t is a threshold parameter, x are input values of a spatial field and b is shape parameter. $M(x, t, b)$ is 1, when $x = 0$; and $M(x, t, b)$ is 0.5, when $x = 1$. Flatness (F_1) is obtained by applying A1 to the slope of the spatial field obtained using third-order finite differencing (Horn, 1981) as:

$$F_1 = M(S, t_{s1}, b_s) \quad , \qquad \text{(A2)}$$

where b_s is 4 and t_{s1} is 16% (Gallant and Dowling, 2003). Lowness (LO_1) is the ratio of the number of pixels having lower values than the center pixel to the total

number of pixels. It is applied using a circular window with radius of 3 pixels. Local lowness (L_1) is obtained as:

$$L_1 = M(LO_1, t_1, b_1) \quad , \quad \text{(A3)}$$

where t_1 is 0.4 and b_1 is 3 (Gallant and Dowling, 2003). We combined flatness (F_1) and local lowness (L_1) of step 1 to produce a preliminary homogeneity index, $QF_1 = F_1 L_1$.

As described by Gallant and Dowling (2003), the nonlinear transformation in A1 is applied to QF_1 to avoid biasing the results toward low values, as:

$$HF_1 = 1 - M(QF_1, t_{h1}, b_{h1}) \quad , \quad \text{(A4)}$$

where t_{h1} is 0.3 and b_{h1} is 4. High values of HF_1 indicate homogeneous areas obtained in this first step. The second step follows same procedures, but with changes in the threshold parameter for flatness and the window size for lowness. F_2 is obtained as $F_2 = M(S, t_{s2}, b_s)$, with $t_{s2} = 0.5\ t_{s1}$. LO_2 is obtained using a six-pixel radius and applied as $L_2 = M(LO_2, t_1, b_1)$. Subsequently, a second preliminary homogeneity index, $QF_2 = F_2 L_2$, is rescaled to HF_2 as:

$$HF_2 = 1 - M(QF_2, t_{h1}, b_{h1}) \quad . \quad \text{(A5)}$$

These results are used to produce a homogeneity index (F) varying from 0 to 2. HF_1 and HF_2 are weighted such that homogeneous areas identified using HF_2 occur from F = 1.5 to 2.0, and areas not detected by HF_2, but captured by HF_1, are in the 0.5 to 1 range. Thus, F is obtained as:

$$F = W_2(1 + HF_2) + (1 - W_2)HF_1 \quad , \quad \text{(A6)}$$

where the weight W_2 is derived using a nonlinear transformation of HF_2: $W_2 = 1 - M(HF_2, t_w, b_w)$, with t_w and p_w are 0.4 and 6.68, respectively (Gallant

and Dowling, 2003). Detailed analyses of the spatial fields used here revealed that the values of the threshold (t_{s1}, t_{s2}, t_1, t_{h1}) and shape (b_s, b_1, b_{h1}) parameters used by Gallant and Dowling (2003) for the elevation field were adequate to capture flatness and lowness characteristics. In addition, the majority of the homogenous areas were identified by HF_2, while the contribution of HF_1 to F was small.

REFERENCES

Gallant, J. C., and T. I. Dowling, A multiresolution index of valley bottom flatness for mapping depositional areas. *Water Resour. Res.* 39(12): 1347, doi:10.1029/2002WR001426, 2003.

APPENDIX B

PONDEROSA PINE HILLSLOPE AND QUEMAZON SNOTEL SITE HYDROMETEOROLOGICAL VARIABLES

B.1. Hydrometeorological datasets of the ponderosa pine and Quemazon sites

In this section, the hydrometeorological data of ponderosa pine and Quemazon snotel sites are presented in the folder “Appendix B”. During the 1992-1993 seasons, meteorological datasets of the ponderosa pine site are temporally discontinuous. To fill these data discontinuity, the weather station data between Oct 1, 1992 and Feb 3, 1993 (PA, US, RH, TA, XC and IS) are collected from the nearby TA 6 weather station. Rainfall data discontinuities are also filled by rainfall data between Oct 1, 1992 and Sep 30, 1993 from TA 6 site. Quemazon site weather station provides only air temperature and precipitation data. Other meteorological variable such as vapor pressure (VP), wind speed (US) and incoming solar radiation (IS) for the Quemazon site are used from the nearby Los Posos weather station.

Site	**Location** (F:\Appendices\Appendix B\Hydrometeorological Variable\) and **File Name**
Ponderosa pine	1992_1994_hourly_runoff.csv
Ponderosa pine	1992_94_seasons_meteorological_variable.csv
Ponderosa pine	Distributed_snow_depth_NP_Tube_1993winter.csv
Ponderosa pine	Distributed_snow_depth_Snow_Post_both_1993&1994_winter.csv
Ponderosa pine	Distributed_snow_soil_moisture_NP_Tube_1992_93winter_summer.csv
Ponderosa pine	1996_summer_hourly_runoff.csv
Ponderosa pine	1996_summer_hourly_soil_moisture_at10cm_depth.csv
Ponderosa pine	1996_summer_hourly_soil_moisture_at1m_depth_averaged.csv
Ponderosa pine	1996_summer_meterological_variable.csv
Ponderosa pine	1997_summer_hourly_runoff.csv
Ponderosa pine	1997_summer_hourly_soil_moisture_at10cm_depth.csv
Ponderosa pine	1997_summer_hourly_soil_moisture_at1m_depth_averaged.csv
Ponderosa pine	1997_summer_meterological_variable.csv
Ponderosa pine	1998_summer_hourly_runoff.csv
Ponderosa pine	1998_summer_hourly_soil_moisture_at10cm_depth.csv
Ponderosa pine	1998_summer_hourly_soil_moisture_at1m_depth_averaged.csv
Ponderosa pine	1998_summer_meterological_variable.csv
Quemazon	quemazon_observed_SWE_2004_2005winter.csv
Quemazon	quemazon_observed_meteorological_variable_2004_2005winter.csv
Quemazon	quemazon_observed_SWE_2006_2007winter.csv
Quemazon	quemazon_observed_meteorological_variable_2006_2007winter.csv
Quemazon	quemazon_observed_SWE_2008_2009winter.csv
Quemazon	quemazon_observed_meteorological_variable_2008_2009winter.csv
Quemazon	quemazon_observed_SWE_2009_2010winter.csv
Quemazon	quemazon_observed_meteorological_variable_2009_2010winter.csv
Variables and units	variable&units.csv

APPENDIX C

RASTER AND VECTOR DATASETS FOR PONDEROSA PINE AND QUEMAZON SNOTEL SITES

C.1. Raster and vector data used and produced in this study

Raster and vector data of this dissertation are provided in the folder "Appendix C". In the "Appendix C" folder, there are five sub folders; Vector_data, Raster, Chapter 2, Chapter 3 and Chapter 4.

Vector_data folder: This folder contains shape files. The lists and descriptions of these files are given below:

Flow_line.shp: Flow concentration lines derived by threshold method.

contour_1m_int.shp: Contour line at 1 m interval for hillslope topography.

Hillslope_boundary.shp: Hillslope boundary derived by model.

lanl_hill_boundary.shp: Field derived hillslope boundary.

Rain_gauge.shp: Location of rain gauge.

lanl_hill_line.shp: Field derived hillslope divide.

Snow_meter_stick_at_NP_tube.shp: Locations of snow meter sticks at neutron probe tube (NP tube) locations.

lanl_trench.shp: Field derived trench boundary.

Snow_meter_stick_at_post_locations.shp: Locations of snow meter sticks at snow post locations.

model_trench.shp: Trench boundary used in the model.

Weather_station.shp: Location of weather station.

Raster folder: This folder contains LIDAR canopy (grid site_canopy) and LIDAR bare earth surface (grid site_dem) for ponderosa pine site and its neighboring areas. It also contains hillslope canopy surface (grid hillsl_canopy) and bare earth surface (grid hillsl_dem).

Chapter 2 folder: This folder contains raster grid files for soil moisture maps (sub folder: Soil_moisture10cm_maps), runoff maps (sub folder: runoff_maps) and monthly storages maps (sub folder: Storage_maps) prepared and presented in Chapter 2.

Chapter 3 folder: This folder includes raster grid files used in Chapter 3. Raster grids of each model resolution are presented using separate sub folder. The name of the sub folders are d = 1, d = 0.5, d = 0.25, d = 0.1, d = 0.05, and d = 0.03. Sub folder for each model resolution contains the raster grid file for curvature (grid curvature), vegetation (grid vegetation), soil moisture at 10cm depth during 1996, 1997 and 1998 summer (grid sm_10cm_96, sm_10cm_97 & sm_10cm_98), root zone soil moisture for 1997 (grid root_sm), runoff rate (grid runoff_rate) and frequency (grid runoff_freq) for 1997 summer. Only three model resolution folders (*d*'=1, 0.25 and 0.03) contain homogeneity maps of curvature (grid patch_curv), vegetation (grid patch_veg), soil moisture at 10 cm depth (grid patch_sm_10cm) and runoff rate depth (grid patch_runoff). Chapter 3 sub folder also has "Future_instrumentation" folder where shape file for thr current (current_site.shp), convex (Convex_site.shp) and concave (Concave_site.shp) site sensors networks are provided.

Chapter 4 folder: This folder contains snow (Snow_maps sub folder) and soil moisture maps (Soil_moisture_maps sub folder) presented in the Chapter 4. Snow_maps sub folder includes 1992-93 and 1993-94 seasons snow maps which are average snow depth (grid avg_snowdpth), snow cover duration (grid

duration), total melt (grid total_melt) and sublimation from canopy (grid canopy_sublim).

Appendix D

MODEL SET UP FOR THE PONDEROSA PINE AND QUEMAZON SNOTEL SITE

D.1. Model set up for simulations for ponderosa pine and Quemazon snotel site

Model set up for ponderosa pine and Quemazon snotel site are shown in the folder Appendix D. Appendix D contains three sub folders: Ponderosa_snow, Quemazon and Ponderosa_summer.

Ponderosa_snow: This folder includes the model set up for ponderosa pine site during the period between Oct 1, 1992 and Sep 30, 1994. Note that the model snow module is activated during this model run. The *.in* file to run the model is ponderosa_sm44cm_n500.in.

The sub folder Shelter_belt contains ASCII file of precipitation surface at each hour. Note that precipitation spatially varies in those ASCII files only during winter period.

Model output are recorded at hourly interval at Output/voronoi/point1/ and Output/hyd/point1/ location. Base name for model output is sm25cm_hourly_temp. The sub folder input contains soil and land cover ASCII files (pp.soi and pp.lan), soil parameter file (psi50_2.sdt) and land cover (mod_dry5.ldt) tables. Weather condition forcing data are provided in Weather subfolder (new_ta6_wind.mdf).

Soil parameters for this simulation are given below:

Soil Parameter										
K_o (mm/hr)	*thetas* (m^3/m^3)	*thetaR* (m^3/m^3)	*m* (-)	*PsiB* (mm)	*f* (mm^{-1})	*As* (-)	*Au* (-)	*n* (m^3/m^3)	*ks* (J/m sK)	*Cs* (J/m^3K)
0.29	0.45	0.01	1.9	-250	0.0067	40	40	0.48	1	10e+6

Land cover parameters are given below:

Vegetation Units	Vegetation Parameter									
	p (-)	S (mm)	K (mm/hr)	g (mm^{-1})	A (-)	H_v (m)	K_t (-)	r_s (s/m)	v (-)	*ID*
Grassland (0-1 m)	0.9	1.0	0.12	4.7	0.28	1	0.9	40	0.8	4
Short ponderosa pine (1-5 m)	0.4	1.5	0.12	4.7	0.2	5	0.5	10	0.85	3
Medium ponderosa pine (6-10 m)	0.4	1.5	0.12	4.7	0.1	10	0.5	10	0.95	2
Tall ponderosa pine (10-20 m)	0.4	1.5	0.12	4.7	0.1	20	0.5	10	0.95	1

Quemazon: This folder includes the model set up for Quemazon snotel station for 2004-05, 2006-07, 2008-09 and 2009-10 winters. Simulation starts at Nov 1 and ends at May 31 for each year. The files for simulations of these years are given below:

Snow simulation for 2004-05 winter:

.*in* file: quemazon_snow_point_2005.in

Base name for spatial output: new2005e.

Output files locations: Output/snow/voronoi and Output/snow/hyd

Meteorological forcings: Weather/2005/ quem0405.mdf

Precipitation forcing: Weather/2005/ quemPrec0405.mdf

Snow simulation for 2006-07 winter:

.*in* file: quemazon_snow_point_2007.in

Base name for spatial output: new2007f.

Outputs file locations: Output/snow/voronoi and Output/snow/hyd

Meteorological forcings: Weather/2007/ quem0405.mdf

Precipitation forcing: Weather/2007/ quemPrec0405.mdf

Snow simulation for 2008-09 winter:

.*in* file: quemazon_snow_point_2009.in

Base name for spatial output: new2009e.

Outputs file locations: Output/snow/voronoi and Output/snow/hyd

Meteorological forcings: Weather/2009/ quem0405.mdf

Precipitation forcing: Weather/2009/ quemPrec0405.mdf

Snow simulation for 2009-10 winter:

.*in* file: quemazon_snow_point_2010.in

Base name for spatial output: new2010e.

Outputs file locations: Output/snow/voronoi and Output/snow/hyd

Meteorological forcings: Weather/2010/ quem0405.mdf

Precipitation forcing: Weather/2010/ quemPrec0405.mdf

Soil parameters for Quemazon simulations are given below:

Soil Parameter										
K_o (mm/hr)	*thetas* (m^3/m^3)	*thetaR* (m^3/m^3)	*m* (-)	*PsiB* (mm)	*f* (mm^{-1})	*As* (-)	*Au* (-)	*n* (m^3/m^3)	*ks* (J/msK)	*Cs* (J/m^3K)
5	0.4	0.03	0.47	-87	0.0001	1	1	0.43	2.6	1.2e+6

Vegetation parameters for Quemazon simulations are given below:

Vegetation Units	Vegetation Parameter									
	p (-)	*S* (mm)	*K* (mm/hr)	*g* (mm^{-1})	*A* (-)	H_v (m)	K_t (-)	r_s (s/m)	*v* (-)	*ID*
Grassland (0-1 m)	1	0.8	0.1	3.2	0.28	0.1	0.1	40	0.1	1

Ponderosa summer: Ponderosa summer folder presents model runs for 1996, 1997 and 1998 summer periods at multiple model resolutions. The model resolutions (*d*) used are 1, 0.5, 0.25, 0.1, 0.05 and 0.03. The finest resolution or *d*=1 model results are used for Chapter 2. The model results using all resolutions are used in Chapter 3.

in. file: Sub folders 1996_infile, 1997_infile and 1998_infile contain *in* files for six model resolutions. Each sub folder include following *in* files

d=0.5_8cm.in and d=0.5_12cm.in files simulate at model resolution *d* = 0.5 and output 8 cm depth averaged (d=0.5_8cm.in) and 12 cm depth averaged (d=0.5_12cm.in) soil moisture.

d=0.25_8cm.in and d=0.25_12cm.in files simulate at model resolution *d* = 0.25 and output 8 cm depth averaged (d=0.25_8cm.in) and 12 cm depth averaged (d=0.25_12cm.in) soil moisture.

d=0.1_8cm.in and d=0.1_12cm.in files simulate at model resolution *d* = 0.1 and output 8 cm depth averaged (d=0.1_8cm.in) and 12 cm depth averaged (d=0.1_12cm.in) soil moisture.

d=0.05_8cm.in and d=0.05_12cm.in files simulate at model resolution *d* = 0.05 and output 8 cm depth averaged (d=0.05_8cm.in) and 12 cm depth averaged (d=0.05_12cm.in) soil moisture.

d=0.03_8cm.in and d=0.03_12cm.in files simulate at model resolution *d* = 0.03 and output 8 cm depth averaged (d=0.03_8cm.in) and 12 cm depth averaged (d=0.03_12cm.in) soil moisture.

Output files:

1997 model runs for six model resolutions are outputted in following folders:

Output\voronoi\1997\d = 1, Output\voronoi\1997\d = 0.5,

Output\voronoi\1997\d = 0.25, Output\voronoi\1997\d = 0.1,

Output\voronoi\1997\d = 0.05 and Output\voronoi\1997\d = 0.03.

1996 model runs for six model resolutions are outputted in following folders:

Output\voronoi\1996\d = 1, Output\voronoi\1996\d = 0.5,

Output\voronoi\1996\d = 0.25, Output\voronoi\1996\d = 0.1,

Output\voronoi\1996\d = 0.05 and Output\voronoi\1996\d = 0.03.

1998 model runs for six model resolutions are outputted in following folders:

Output\voronoi\1998\d = 1, Output\voronoi\1998\d = 0.5,

Output\voronoi\1998\d = 0.25, Output\voronoi\1998\d = 0.1,

Output\voronoi\1998\d = 0.05 and Output\voronoi\1998\d = 0.03.

Meteorological data

1997 meteorological data: Weather/Station/may10weather.mdf

1997 precipitation data: /Rain/Gauges/may10rain.mdf

1996 meteorological data: Weather/Station/may15_96_weather1.mdf

1996 precipitation data: Rain/Gauges/may15_96rain.mdf

1998 meteorological data: Weather/Station/may15_98_weather.mdf

1998 precipitation data: Rain/Gauges/may15_98.mdf

APPENDIX E

SNOW MODEL IMPROVEMENTS AND UPDATES

Following changes were made in *tSnowPack* class:

1. Latent heat flux from snow pack: This change was made in *latentHFCalc()*

function of the *tSnowPack* class (line 1670)

Before code change

```
if (snTempC == 0.0)
   lhf = (-latVapkJ*0.622*rhoAir*Kaero*(vPress - vapPressSmb)/atmPress);
//evaporation
 else
   lhf = (-latSubkJ*0.622*rhoAir*Kaero*(vPress - vapPressSmb)/atmPress);
//sublimation
end
```

After code change

```
if (snTempC == 0.0)

   lhf = (latVapkJ*0.622*rhoAir*Kaero*(vPress - 6.111)/atmPress); //evaporation
 else
   lhf = (latSubkJ*0.622*rhoAir*Kaero*(vPress -
6.112*exp((17.67*snTempC)/(snTempC+243.5)))/atmPress);  //sublimation
end
```

2. Add latent heat leaving the snowpack due to melting of snow.

emelt=-latFreezekJ*rholiqkg*(Utot/(latFreezekJ*rholiqkg)); (line 2453)

The equation for above line (Latent heat transfer from melting) is given below:

$$Q_m = \lambda_j \rho_{water} M_{ji}$$

Where Q_m is the latent heat (W/m^2) leaving the snow pack, λ_j is latent of freezing, ρ_{water} is density of water (kg/m^3) and M_{ji} is the amount of water internally change from ice phase (j) to liquid phase (i).

3. Excess internal snowpack energy (U > 0), melt equivalent amount of ice into water.

liqWE += Uwat/(latFreezekJ*rholiqkg); line 1285

2. We assume that minimum SWE is 10 cm for snow temperature estimation. The minimum snow water equivalent (SWE) is 10 cm for simulating snow temperature when internal snow pack energy (*U*) is less than zero. This approach suggests that for given snowpack energy, the snow temperature for SWE less than 10 cm is equal to SWE of 10 cm. This approach was taken to avoid numerically very low snow temperature for very low SWE content as SWE content contribute in the equation as denominator (line: 1298).

5. We assume that vegetation fraction and height for grass is very low when snow occurs in the grassland areas (in *resFactCalc()* function of *tSnowPack* class).

6. The code releases the melted water as 0.25 mm/hr following complete removal of SWE from existing pack. Here we assume that melted water from pack is not available for infiltration and routing until the snow melts completely. Our code release melted water to hydrologic system at a rate of 0.25 mm/hr after SWE lowers to zero. The rate 0.25 mm/hr is set to force more infiltration in the system for lateral transport rather than routed as runoff (Very low runoff is observed during snowmelt period).